DYNAMIC ANALYSIS OF SANDWICH COMPOSITE BEAM WITH MAGNETORHEOLOGICAL FLUID CORE

Thesis

Submitted in partial fulfillment of the requirements for the degree of

DOCTOR OF PHILOSOPHY

by

VIPIN ALLIEN J

DEPARTMENT OF MECHANICAL ENGINEERING

NATIONAL INSTITUTE OF TECHNOLOGY KARNATAKA,

SURATHKAL, MANGALORE - 575025

AUGUST - 2020

DYNAMIC ANALYSIS OF SANDWICH COMPOSITE BEAM WITH MAGNETORHEOLOGICAL FLUID CORE

Thesis

Submitted in partial fulfillment of the requirements for the degree of

DOCTOR OF PHILOSOPHY

by

VIPIN ALLIEN J

Under the guidance of

Dr. Hemantha Kumar

Associate Professor

Prof. Vijay Desai

Professor

DEPARTMENT OF MECHANICAL ENGINEERING

NATIONAL INSTITUTE OF TECHNOLOGY KARNATAKA,

SURATHKAL, MANGALORE - 575025

AUGUST - 2020

DECLARATION

I hereby declare that the Research Thesis entitled **"DYNAMIC ANALYSIS OF SANDWICH COMPOSITE BEAM WITH MAGNETORHEOLOGICAL FLUID CORE"** which is being submitted to the **National Institute of Technology Karnataka, Surathkal** in partial fulfillment of the requirements for the award of the Degree of **Doctor of Philosophy** in **Mechanical Engineering** is a *bonafide report of the research work carried out by me*. The material contained in this Research Thesis has not been submitted to any other Universities or Institutes for the award of any degree.

Register Number: **148016 ME14F22**

Name of the Research Scholar: **VIPIN ALLIEN J**

Signature of the Research Scholar:

Department of Mechanical Engineering

Place: NITK, Surathkal

Date:

CERTIFICATE

This is to certify that the Research Thesis entitled **"DYNAMIC ANALYSIS OF SANDWICH COMPOSITE BEAM WITH MAGNETORHEOLOGICAL FLUID CORE"** submitted by **Mr. VIPIN ALLIEN J (Register Number: 148016 ME14F22)** as the record of the research work carried out by him, *is accepted as the Research Thesis submission* in partial fulfillment of the requirements for the award of the Degree of **Doctor of Philosophy.**

Research Guide(s)

Dr. Hemantha Kumar   **Prof. Vijay Desai**

Associate Professor   Professor

Department of Mechanical Engineering   Department of Mechanical Engineering

NITK, Surathkal   NITK, Surathkal

Chairman-DRPC

Department of Mechanical Engineering

Place: NITK, Surathkal

Date:

Dedication

This thesis work is dedicated to my parents and brother for their love support and encouragement

ACKNOWLEDGEMENT

<div align="right">**Vipin Allien J**</div>

ABSTRACT

Magnetorheological fluid (MRF) is a smart fluid which can change its rheological properties under the influence of an applied magnetic field. Sandwich structures with MRF as core have unique characteristics permitting to vary the stiffness and damping properties under the influence of the applied magnetic field. Hence, MRF core sandwich structures can be effectively utilized to suppress the vibration and enhance the life of the structures. This study, investigates the dynamic characterization of MRF core sandwich beams with two types of composite face layers viz. polymer matrix composite and metal matrix composite.

The two-layer, four-layer and six-layered chopped strand mat glass fiber reinforced unsaturated polyester resin polymer matrix composites (CGRP-PMC) were prepared by the hand layup method. The tensile, flexural, impact, inter-laminar shear strength (ILSS), fracture toughness properties were evaluated. The results have revealed that the four-layered CGRP-PMC material has high impact strength, ILSS and fracture toughness compared to two-layer and six-layered CGRP-PMC material. Free vibration analysis was carried out to determine the natural frequency and damping ratio of the CGRP-PMC materials. The result obtained from free vibration analysis indicated that the natural frequency of six-layered CGRP-PMC is higher than two-layer and four-layered CGRP-PMC materials. The density, tensile strength, flexural strength, impact strength, absorbed energy, ILSS, fracture toughness, and damping ratio results of the CGRP-PMC specimens were considered as attributes for the selection of the optimal composite using multi-attribute decision making (MADM) techniques. The six-layered CGRP-PMC material was selected as the optimal PMC based on the results of MADM techniques.

The Al6082 and Al7075 aluminum alloy reinforced with (0, 1, 2, 3, 4, 5, 7.5, 10, 15 and 20) different weight percentages (wt%) of silicon carbide particles (SiC_p) metal matrix composites (MMCs) were fabricated through stir casting method. The mechanical and dynamic properties such as density, hardness, tensile strength, impact strength, natural frequencies and damping ratio of the MMCs were determined. The

mechanical tests and free vibration analysis results revealed that the addition of SiC_p reinforcement increased the strength and stiffness of the MMCs. 15% SiC_p/Al7075 MMC was selected as the best MMC based on the results obtained from MADM techniques.

The MRF is prepared in-house at room temperature and contains 30% volume carbonyl iron powder and 70% volume silicone oil. The rheological properties of the MRF with and without the magnetic flux density were determined. The viscosity of MRF increased with an increase in magnetic flux density and saturated at 0.63 T. The shear stress of MRF increased and viscosity of MRF decreased with an increase in the shear rate at zero magnetic flux density. Since the MRF is used as the core for sandwich beams, the frequency sweep analysis was performed in the rheometer. The complex shear modulus, storage modulus, loss modulus, shear stress and complex viscosity properties of MRF increased with an increase in the applied magnetic flux densities. The loss factor of MRF decreased with an increase in the magnetic flux densities. The complex viscosity of MRF decreased with an increase in oscillatory frequency and increased with increase in the applied magnetic flux density.

The two-layer, four-layer and six-layered CGRP-PMC prepared using hand lay-up technique is used as top and bottom layers of the sandwich beams and the in-house prepared MRF is used as the middle core layer of the sandwich beams. The dynamic characterization of CGRP-PMC sandwich beams enclosed MRF core is experimentally investigated. The effect of various parameters such as magnetic flux density, the thickness of CGRP-PMC layers and MRF core layer on the natural frequencies, damping ratio and vibration amplitude suppressions of the CGRP-PMC-MRF core sandwich beams are examined. From free vibration analysis, it was observed that the natural frequency of the CGRP-PMC-MRF core sandwich beams decreases with increase in the thickness of the MRF core layer. However, the damping ratio of the CGRP-PMC-MRF core sandwich structure increased with increase in the thickness of the MRF core layer. Also, the experimental forced vibration results reveal that CGRP-PMC-MRF core sandwich beams have excellent vibration amplitude suppression capabilities.

Dynamic characterization of (0, 5, 10, 15 and 20%) SiC_p reinforced Al6082 alloy MMC sandwich beam with MRF core is experimentally investigated. The MRF core of the sandwich beam is activated using a non-homogeneous magnetic field using permanent magnets. The natural frequency, damping ratio and frequency amplitude response of the MMC-MRF core sandwich beams were determined through experimental free and forced vibration analysis at 0, 200, 400 and 600 gauss magnetic flux densities. Vibration amplitude suppression capabilities of the MMC-MRF core sandwich beams subjected to varying magnetic flux densities are determined. The experimental results revealed that the natural frequency, damping ratio and vibration amplitude suppression capabilities of the MMC-MRF core sandwich beams improved with the increase in the applied magnetic flux density. The experimental forced vibration results reveal that MMC-MRF core sandwich beams have excellent vibration amplitude suppression capabilities.

Keywords: Magnetorheological fluid, Polymer matrix composite, Metal matrix composite, Sandwich beam, Free and forced vibration analysis, Vibration damping

CONTENTS

LIST OF FIGURES

LIST OF TABLES

ABBREVIATIONS

AHP	Analytic Hierarchy Process
ASTM	American Society for Testing and Materials
CGRP	Chopped strand mat glass fiber reinforced polyester resin
CGRP-PMC	Chopped strand mat glass fiber reinforced polyester resin polymer matrix composite
CGRP- PMC-MRF core	Chopped strand mat glass fiber reinforced polyester resin polymer matrix composite beam with magnetorheological fluid core
CI_p	Carbonyl iron powders
CR	Consistency ratio
CSM	Chopped strand mat
EDS	Energy dispersive spectroscopy
ERF	Electrorheological fluid
FFT	Fast Fourier transform
FRF	Frequency response function
ILSS	Interlaminar shear strength
MADM	Multi Attribute Decision Making
MMC	Metal matrix composite
MMC-MRF core	Metal matrix composite beam with magnetorheological fluid core
MRF	Magneto rheological fluid
PMC	Polymer matrix composite
PROMETHEE	Preference Ranking Organisation Method for Enrichment Evaluations
PSD	Particle size distribution
RI	Relative index
RSM	Response surface methodology
SAW	Simple Additive Weighting
SEM	Scanning electron microscope

SiC$_p$	Silicon carbide particles
SR	Sedimentation ratio
TOPSIS	Technique for Order Preference by Similarity to Ideal Solution
UTM	Universal testing machine
UTS	Ultimate tensile strength
WEDM	Wire electro discharge machining
WPM	Weighted Product Model

CHAPTER 1

INTRODUCTION

1.1 INTRODUCTION

Vibration damping control is an important characteristic for all the dynamic structures when the structure is subjected to excitation due to an external force. The vibration damping control in a system can be achieved in three ways, such as passive, semi-active and active control devices. The passive vibration control device is an inexpensive device which mainly has spring or rubber to absorb the vibration and shock. The passive devices have low effectiveness in controlling the vibration when compared to the semi-active and active devices. The active vibration control devices are smart devices which have sensors, actuators, and control algorithm. The sensor is used to sense the vibration excitation, based on this excitation actuators is used to excite a counterforce to control the vibration excitation. The control algorithm gets feedback signals from the sensors and immediately actuates the actuator. The active devices have excellent vibration controlling capabilities. However, the affordability of the active devices is affected due to its high cost and complexity in its control algorithm. The semi-active vibration control devices are also smart devices without externally applied energy they behave as passive devices. When external energy is applied to this device, it changes the stiffness and damping behavior of the system. The magnetorheological fluid (MRF) is used in semi-active vibration control devices like dampers, brakes, clutches, beams, plates, rods, etc. In this study, the semi-active vibration control of MRF core composite sandwich beams dynamic characteristics are investigated.

1.2 COMPOSITE MATERIAL

Composite materials are finding increased usage in many applications mainly due to their high strength to weight ratio. Focused research and development are undertaken in developing high-performance composite materials for automobiles, buildings, construction works, railways, aerospace and biomedical applications. The

composite material consists of two constituents; the matrix and the reinforcement. When more than two constituents are used, it is termed as hybrid composites. The matrix phase is the continuous phase and the reinforcement phase is the discontinuous phase. In general, the matrix phase will be soft and continuous material and reinforcement phase will be hard and discontinuous material. The matrix material can be polymeric, metallic or ceramic. Polymer matrix composite (PMC) and metal matrix composite (MMC) are the most competent materials in replacing the conventional material such as aluminum and steel due to their improved performance.

1.2.1 Polymer matrix composite

The main advantage of using polymer resins is its low cost and density when compared to metals and ceramics. The polymer resins have low mechanical properties. However, when the polymer resin matrix is reinforced with the reinforcement, they had an enormous increase in mechanical properties. The polymer resins such as phenol, vinyl ester, polystyrene, polyester and epoxy are used as matrix phases. The PMC is classified based on the fiber reinforcement such as continuous long fiber-reinforced PMC, discontinuous chopped fiber-reinforced PMC, laminate PMC, particulate PMC and flake PMC. The fiber reinforcement can be of synthetic fiber and natural fiber. The synthetic fiber such as glass, carbon, graphite and aramid are widely used in PMC. The plant leaf, stem, seeds, wood, root, etc usually refers to natural fiber. The PMC can be fabricated mainly by four methods, they are hand layup method, spray-up method, autoclave molding method and filament winding method.

1.2.2 Metal matrix composite

The MMC has a matrix phase as the metal and reinforcement phase is a ceramic or organic compound. Hybrid MMC consists of a minimum of three constituents, one matrix phase and two or more reinforcement phase. The matrix phase is usually a metal such as aluminum, magnesium, titanium and copper. Magnesium is the lightest of all conventional material with average density of $(2/3)^{rd}$ of aluminum and has a good vibration damping property. The reinforcement phase is usually ceramic compounds such as silicon carbide (SiC), aluminum oxide (Al_2O_3), graphite (Gr), titanium diboride (TiB_2) and so on. The MMC can be fabricated by solid-state processing, liquid route

processing, and in-situ process. Comparing the properties of MMC's as compared to conventional metals, MMCs possess high specific strength, specific modulus, damping capacity and good wear resistance.

1.3 MAGNETORHEOLOGICAL FLUID

Magnetorheological fluid (MRF) is a smart fluid, it has the ability to change liquid-state to solid-state and vice versa when subjected to the magnetic field. The MRF rheological properties can be varied and controlled by varying the applied magnetic field. The fast response of the MRF subjected to the magnetic field is used in the reliable technology of sandwich structures to absorb vibration. MRF applications are categorized into two classes: controllable devices (dampers, brake and clutches) and adaptive structures (aircraft wings, ship and engine mounts). MRF is prepared by mixing magnetizable particles (mainly carbonyl iron or ferrous iron) as suspensions in a suitable carrier liquid such as silicone oil, mineral oil, synthetic oil, water or ethylene glycol. A small quantity of lithium grease is added as additives for reducing the magnetizable particle sedimentation. The sedimentation of the magnetizable particles in MRF is a serious problem that affects the rheological properties of MRF and requires attention (Kumbhar et al. 2015). MRF semi-active control devices are in use in many applications like vibration isolation of systems under harmonic or random force excitation, structural vibration control, transportation and automobiles. MRF core composite sandwich structures such as beams, plates, panels and bars are used to control the dynamic behaviour of the mechanical systems.

1.3.1 Operational modes of MRF

1.3.1.1 Flow mode

In flow mode, the movement of MRF is limited to the middle of the stationary plates by applying the magnetic field. Application of flow mode is evident mainly in damper, shock absorbers, actuators, servo valves and hydraulic controls. Figure 1.1 shows the flow mode operation of the MRF.
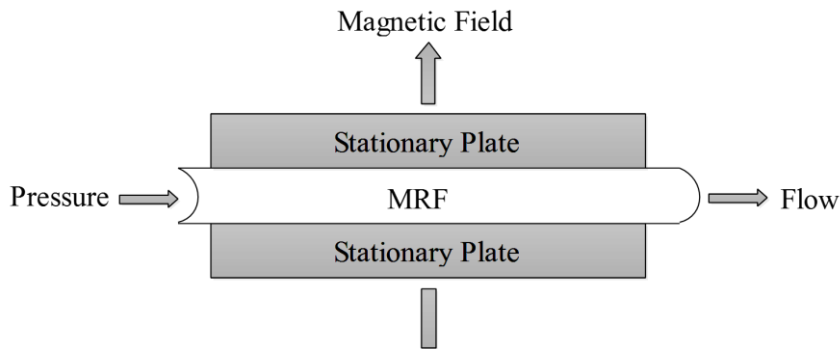
Figure 1.1 Flow mode

1.3.1.2 Shear mode

In shear mode, the MRF is operated between two plates moving in relation to each other and the magnetic field is applied perpendicular to the direction of motion of the shear plates. The shear stress of MRF could be changed by changing the magnetic field intensity. Application of MRF shear mode is seen mainly in brakes, clutches, locking devices, structural composites and dampers. Figure 1.2 shows the shear mode of MRF.
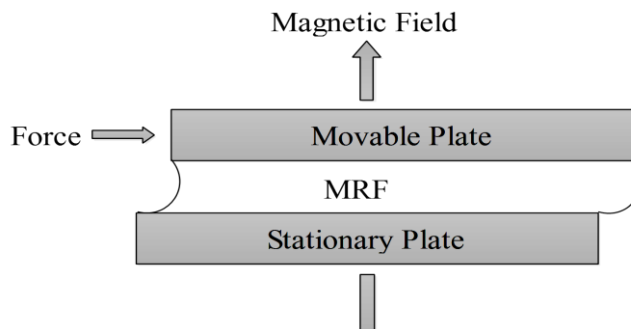
Figure 1.2 Shear Mode

1.3.1.3 Squeeze mode

In squeeze mode, the direction of the magnetic field and movement of the movable plate are parallel to the magnetic induction line. Hence the MRF attains stretches and compression during actuation, although the displacement of the magnetic poles is small, which produce high resistance force, it is usually used as vibration control in buildings. The MRF inside the dampers changes the building from a rigid structure to a smart structure by absorbing the shock waves. Figure 1.3 shows the squeeze mode of MRF.

4
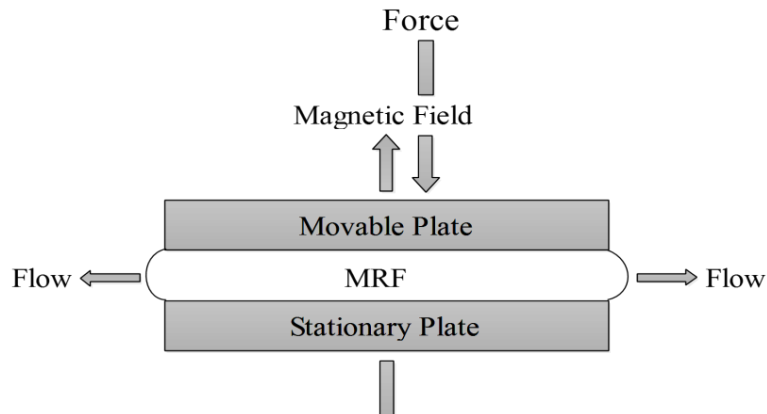
Figure 1.3 Squeeze mode

1.4 MRF CORE SANDWICH STRUCTURE

Every structure has its own stiffness and damping behavior. When an external force or excitation is applied beyond the structural resistance then the structure undergoes failure. MRF core sandwich structure is a smart structure. These sandwich structures can adjust their stiffness and damping characteristics by varying the applied magnetic flux density. Hence smart structures have the ability to protect from the structural resonance effect which is induced due to the external forces. The sandwich structure consists of three layers; top and bottom stiff layers (face plates) that bonded to the middle soft-core layer. MRF core sandwich structures are used to suppress harmful vibrations in the various structural appliances. Due to quick response and controllability, the MRF is very much preferred in the mechanical systems (Ahamed et al. (2018)). Sandwich structures are widely used in aerospace, automobiles and building structures to reduce the overall weight and improve the dynamic properties of the system. The MRF core smart sandwich structures will be an alternate for the conventional solid structures while considering their mechanical and dynamical properties.
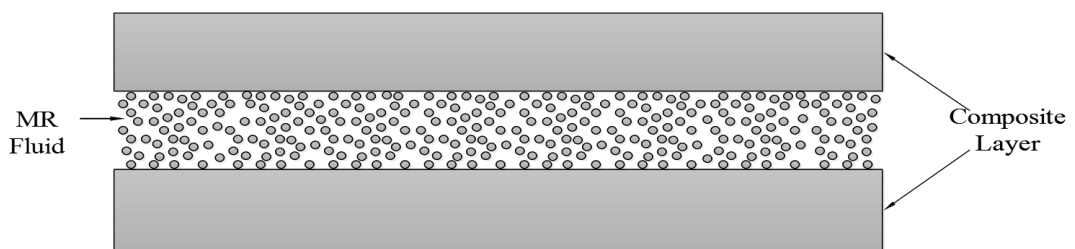
Figure 1.4 MRF core sandwich composite without magnetic field

5

The schematic view of the MRF core sandwich structure having randomly oriented magnetizable particles without the influence of the magnetic field is shown in figure 1.4. Figure 1.5 shows the schematic view of the actuation of magnetizable particles as a chain-like structure subjected to the influence of the magnetic field. Due to this chain-like structure of magnetizable particles, MRF layer attains increased stiffness, storage modulus and loss modulus.
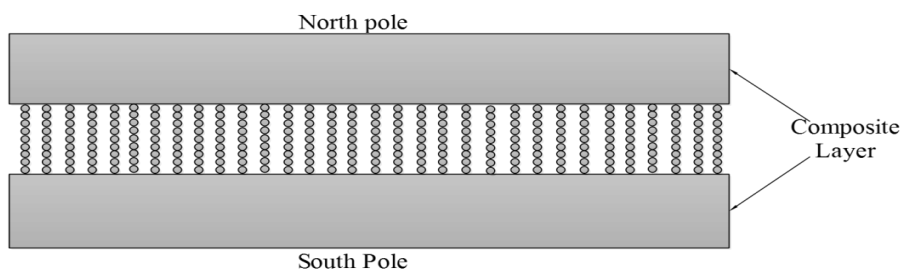
Figure 1.5 MRF core sandwich composite with magnetic field

Many research investigations were carried out in the semi-active vibration control structures made of MRF core aluminum sandwich beams (Yalcintas et al. (2003), Sapiński et al. (2009), Lara et al. (2009) and Rajamohan et al. (2010)). They observed that an increase in the applied magnetic field will increase the stiffness and damping properties of the MRF core aluminum sandwich beams. Whereas, the semi-active vibration control of MRF core composite (PMC and aluminum alloy based MMC) sandwich beams were yet to be investigated. Hence in this research work, an attempt has been done to determine the dynamic properties of MRF core bonded with PMC and MMC sandwich beams with the influence of externally applied magnetic fields.

1.4.1 Advantages of MRF core composite sandwich structures

In conventional structures, the global stiffness and damping properties are fixed and not possible to change. The MRF core composite sandwich structure is capable of changing the stiffness and damping properties by varying the externally applied magnetic field. As a result, MRF core composite sandwich structures are used to control structural frequency and damping behavior. Also, it can mitigate the resonance effect caused due to external excitation forces. Hence these MRF core composite

sandwich structures can control the sudden shock and it helps to improve human comfort and enhance the structural durability in automobiles, aerospace, marine, military, buildings and bridges. These MRF core composite sandwich structures are also used in vibration test units, acoustic devices and noise absorbing systems such as walls and panels in aerospace and automotive structures.

1.5 STRUCTURE OF THE THESIS

This thesis presents a detailed study of the dynamic analysis of MRF core composite sandwich beams. The dynamic properties of the MRF core composite sandwich beams are determined through the experimental free and forced vibration analysis under various magnetic flux densities. Initially, the PMC and MMC were prepared by the hand-layup method and stir casting method. The physical, mechanical and dynamic properties of the fabricated PMC and MMC are determined. Optimal PMC and MMC specimens are selected by considering their physical, mechanical and dynamic properties using MADM techniques. The MRF core sandwich beams of PMC top and bottom layers and MMC top and bottom layers were prepared and experimental investigations were carried out. The various parametric studies are also performed to investigate the effect of magnetic flux density, the thickness of MRF core, the thickness of the top and bottom layers on the variations of natural frequencies, damping ratio and frequency amplitude responses. This thesis contains nine chapters. The summary of each chapter is as follows:

Chapter 1 gives a brief introduction about PMC, MMC, MRF, MRF core sandwich beams and advantages of MRF core composite sandwich beams in controlling vibration excitations.

Chapter 2 describes a detailed discussion of the literature review conducted as part of this study and highlights the work carried out by other researchers. This chapter also brings out the research gap which forms the basis for the present study.

Chapter 3 provides the methodology of the research work. The details of the preparation of MRF and the characterization of MRF are discussed. The characterization test details of carbonyl iron powders (CI_p) and rheological characterization procedure of MRF

under various magnetic flux densities are discussed. The fabrication of PMC and MMC are detailed. The tests for physical, mechanical and dynamic characterization of the prepared composites are discussed in this chapter. The steps involved in the optimal selection of best composites using MADM techniques are discussed. Finally, the dynamic characterization procedure for MRF core composite sandwich beams using free and forced vibration characterization are discussed.

Chapter 4 discusses the results of CI_p microstructure, particle size, and magnetic properties. MRF sedimentation study and rheological analysis results are also discussed in this chapter.

Chapter 5 discusses the tensile, bending, Charpy impact, density, fracture toughness, interlaminar shear strength (ILSS) and free vibration characterization results of CGRP-PMC. Also, the selection of optimal CGRP-PMC samples considering the physical, mechanical and dynamic properties of CGRP-PMC materials using MADM techniques is discussed.

Chapter 6 presents the dynamic characterization results of CGRP-PMC-MRF core sandwich beams subjected to the influence of magnetic flux densities. The effect of various parameters such as magnetic flux density, the thickness of CGRP-PMC layers and MRF core layer on the natural frequencies, damping ratio and vibration amplitude suppression behavior of the CGRP-PMC-MRF core sandwich beams are investigated.

Chapter 7 discusses the results of microstructure, density, hardness, tensile, Charpy impact and free vibration characterizations of MMCs. Also, the selection of optimal MMCs samples considering the physical, mechanical and dynamic properties using MADM techniques is discussed.

Chapter 8 presents the dynamic characterization results of MRF core bonded with MMC top and bottom layers sandwich beams. The effect of various parameters such as magnetic flux densities and varying weight percentage (wt%) of SiC_p reinforced Al6082 MMCs top and bottom layers which changes the dynamic properties of the MMC-MRF core sandwich beams is analyzed using free and forced vibration analysis.

Chapter 9 Finally, conclusions are drawn from the present study mentioning the scope of future work is presented in this chapter.

CHAPTER 2

LITERATURE SURVEY

2.1 INTRODUCTION

In general, there is a need to reduce the excessive vibrations occurring in aerospace, buildings and automobiles structures that are induced due to external continuous harmonic excitation force and sudden impacts. The conventional materials are unable to vary their mechanical and dynamic properties and hence the structure failure occurs due to excessive vibration excitations. The drawback of conventional material can be overcome by using the magnetorheological fluid (MRF) core composite sandwich materials. The most promising smart material that offers possible actuation is the MRF. Many researches (Yalcintas et al. (2003), Sapiński et al. (2009), Rajamohan et al. (2010)) have discussed the vibration suppression analysis of the MRF core aluminum sandwich beams. They experimentally determined the changes in natural frequencies, damping ratios properties of MRF core aluminum sandwich beams for varying the magnetic field. Much of the research has been carried out on the MRF core aluminum sandwich beam. While research on MRF core composite sandwich beam structure is picking up in recent years. This chapter presents the state of the art of literature review on studies related to polymer matrix composite (PMC), metal matrix composite (MMC), MRF, and MRF core sandwich beams and their advantages in controlling vibration.

2.2 POLYMER MATRIX COMPOSITE

The PMCs have high strength to weight ratio than conventional materials and have a major role in automobiles, buildings and construction, aerospace, satellite, railways, marine, military, etc. The development of lightweight components helps to reduce fuel consumption in automobiles and aerospace applications. The chopped strand mat (CSM) glass fiber reinforcements are cost-effective and possess excellent physical and mechanical properties. The unsaturated polyester thermoset resins have

excellent bonding characteristics with CSM glass fiber reinforcements (Franz et al. (2002)).

Franz et al. (2002) investigated the blast load response of CSM glass fiber reinforced unsaturated polyester resin polymer matrix composite (CGRP-PMC) material under air pressure blasts. They determined that the damage effects increase with increasing blast impulse on the surface of CGRP-PMC material.

El-Tayeb et al. (2006), and El-Tayeb and Yousif (2007) fabricated 13-layered CGRP-PMC using a hand-layup method and performed friction and wear tests. They used scanning electron microscope (SEM) observation to determine the fiber debonding, fracture and fragmentation. Based on the experimental results, it was determined that the wear rate of CGRP-PMC increases with increasing the abrasive grits size and rotational speed.

Kafi et al. (2006) prepared hybrid PMC with jute fiber and E-glass CSM fiber reinforcement reinforced with polyester resin matrix using the hand-layup method. Based on the experimental results, it was determined that the hybrid PMC having 1:3 jute to E-glass fiber ratio had higher tensile and bending properties.

Chandradass et al. (2007) fabricated 0, 1, 3 and 5 wt% montmorillonite clay and CSM glass fiber reinforced vinyl ester matrix hybrid nanocomposites using hand lay-up process. They carried out an experimental and theoretical study of free vibration analysis and found that the composite specimen having 5 wt% montmorillonite clay had a better damping ratio of 0.0508.

Ramesh et al. (2013) prepared five-layered hybrid PMC of sisal-glass, jute-glass and sisal-jute-glass fiber reinforced polyester resin and determined the tensile, flexural, and impact properties. They used glass fiber layers in the top, middle and bottom of the composites and sisal and jute fiber layers in the second and fourth layers. It was found that the hybrid PMC possessed better mechanical properties than the single-reinforcement natural fiber PMC.

Arifin et al. (2014) investigated the impact characteristics of CSM and woven roving fabric (WR) reinforcement, reinforced with polyester or epoxy resin composites.

It was found that the three layers of CSM and six layers of WR reinforcement reinforced polyester resin hybrid composite had high impact strength.

Shokrieh et al. (2014) investigated the influence of adding different (0, 0.05, 0.1, 0.3, 0.5) wt% of multi-walled carbon nanotubes (MWCNT) to CGRP-PMC materials. It was found that the addition of MWCNT to CGRP-PMC materials is not significant in improving tensile strength. However, the flexural strength of the CGRP-PMC materials increased by 45% with the addition of 0.05 wt% MWCNT.

Moreno et al. (2015) prepared CGRP-PMC with 30.5 wt% CSM glass fiber reinforcement reinforced polyester resin and performed an experimental and numerical traction-compression biaxial test. It was observed that the failure of the CGRP-PMC specimen depends on the arm thickness and the central region thickness. They observed homogeneous shear fields in the central region of the specimen.

Modrea et al. (2015) fabricated four layers of CSM 600 (g m^{-2}) glass fiber reinforced with polyester resin using the hand-layup process and observed the delamination failure in CGRP-PMC specimens subjected to the tensile test. It was determined that the delamination failure occurred at 0.012 strain value.

Pingulkar et al. (2016) studied numerical free vibration characteristics of glass and carbon fibers reinforcement reinforced in the epoxy and vinyl ester matrix PMC using finite-element analysis software ANSYS. It was determined that the natural frequencies of the carbon fiber reinforced with the epoxy PMC are higher than the glass-fiber-reinforced epoxy PMC. Also, the natural frequencies of the carbon fiber reinforced with vinyl ester PMC are higher than the carbon fiber reinforced epoxy PMC.

Feiz and Khosravi (2019) studied the wear behavior effect of adding amino silanized montmorillonite (AS-Mt) nanoclay in CSM glass fiber reinforcement reinforced epoxy matrix hybrid PMCs. It was determined that the wear resistance of the CSM glass fiber reinforcement reinforced epoxy composite was improved by the incorporation of 5 wt% AS-Mt nanoclay.

Many researchers investigated the mechanical characteristics of glass fiber reinforced polyester resin composites. Based on the literature, it is concluded that CGRP-PMC has excellent mechanical properties. However, experimental investigation on multilayer viz. two-layer, four-layer and six-layered CGRP-PMC have not received much attention. Hence in this study two-layer, four-layer and six-layered CGRP-PMC specimens are fabricated using a hand-layup method and the physical, mechanical and dynamic characteristics of the prepared CGRP-PMC specimens are determined. The optimum CGRP-PMC specimens are determined using MADM techniques. Further, the fabricated CGRP-PMC materials are used as top and bottom layers of MRF core sandwich beams and dynamic characterization is performed.

2.3 METAL MATRIX COMPOSITE

Metal matrix composites (MMCs) are mainly used for its high strength to weight ratio in several domains like aerospace, aircraft, automobiles, landing gear cylinders, marine, military, fittings, and transportation equipment (Ezatpour et al. (2016)). MMCs are fabricated by a wide variety of processes, such as solid-state method (powder metallurgy and diffusion bonding), liquid-state method (stir casting and squeeze casting) and in-situ process (Lee et al. 1997). MMC processed through the stir casting method has the advantage of being one of the economical fabrication methods when compared to other techniques (Hashim et al. (1999)).

Solid-state processing involves bonding the particles or foil reinforcement into close contact with the matrix by applying suitable temperature and pressure. In the diffusion bonding method, foils are processed and in the powder metallurgy method, particles are processed (Matthews et al. 1999). Powder metallurgy is a manufacturing process for producing solid MMC from metal powders. The process has three steps i.e., mixing of powder, compacting and sintering. Mixing is generally carried out in planetary ball milling so as to get uniform mixing between matrix and reinforcement. The mixed powder is compacted in a die under the application of high pressure. The density of the compacted specimen is directly proportional to the amount of pressure applied. The compacted samples are sintered at temperature below the melting point of the metal powder in a furnace under controlled conditions. Vacuum and inert furnace

help to reduce the oxidation while sintering. The heating and cooling rate are important aspects that should be monitored while sintering. Sintering helps to remove porosity and improves the strength of the sample by bonding the molecules together (Angelo et al.2008) and Tsutsui (2012).

The stir casting is a liquid route method, the fabrication of MMC by stir casting technique includes a dispersion of particulate reinforcement into a molten matrix, followed by matrix solidification. The technical difficulties during the preparation of silicon carbide particles (SiC$_p$) reinforced aluminum alloy MMC is obtaining the uniform dispersion of reinforcement, good wettability amongst substances and low porosity of the material. By controlling the process variables of the stir casting process and also the amount of the reinforcement material added, it is possible to a large extent to get a composite with an expansive scope of mechanical properties (Inegbenebor et al. (2016)).

Aigbodion and Hassan (2007) studied the effects of SiC$_p$ reinforcement on Al/Si/Fe alloy MMCs produced by the double stir casting method. They added 0, 5, 10, 15, 20, 25 wt% SiC$_p$ reinforcement and analyzed, the physical and mechanical properties of MMCs. It was found that the addition of 20% SiC$_p$ increased the hardness values and impact energy by 1.08 and 15% respectively. Also, they found that the yield strength and ultimate tensile strength (UTS) increased by 26.25 and 25% for 20% SiC$_p$ reinforcement addition.

Ozden et al. (2007) studied the impact behavior of SiC$_p$ reinforced aluminum alloy MMCs under different (-176, 21, 100, 200, and 300 °C) temperature conditions. They manufactured composite specimens of Al2124, Al5083 and Al6063 alloys reinforced with 10 wt% SiC$_p$ reinforcement and performed Charpy impact test on extruded and heat-treated samples. It was determined that the impact energy of MMCs was influenced by the clustering of reinforcement and weak matrix-reinforcement bonding.

Umashankar et al. (2009) examined damping attributes of the cast and sintered aluminum beam. They manufactured aluminum beam by conventional casting and powder metallurgy methods. They evaluated the damping ratio of aluminum produced

through the powder metallurgy method and compared it with the monetarily accessible cast aluminum. The half-power bandwidth method was used to determine the damping ratio of the cast and sintered aluminum beam. It was determined that the presence of porosity and voids in cast aluminum beam have reduced damping ratio compared to the sintered aluminum beam.

Kumar et al. (2010) investigated the microstructure, density, hardness, mechanical and tribological characteristics of SiC_p and Al_2O_3 reinforcements reinforced aluminum alloy MMCs. They used a stir casting method for the preparation of Al6061-SiC_p and Al7075-Al_2O_3 composites with 0, 2, 4, 6 wt% of reinforcements. It was determined that in MMCs, the addition of SiC_p reinforcements improves wear-resistant than Al_2O_3 reinforcements.

Thimmarayan and Thanigaiyarasu (2010) studied the effect of three different particle size reinforcement on forged Al6082/SiC_p MMCs. They used a stir casting method for the preparation of 10 wt% SiC_p reinforced Al6082 MMCs with varying SiC_p size of 22, 12 and 3-μm. It was found that SiC_p reinforcement addition enhanced UTS, yield strength and reduced ductility of MMCs.

Kumar and Chauhan (2015) investigated machining studies considering the effect of cutting parameters of Al7075/SiC_p and Al7075/SiC_p/Gr_p (Graphite particles) hybrid MMCs. They investigated parameters like cutting speed, feed rate and surface roughness in turning operation. They found that Al7075/SiC_p/Gr_p hybrid MMC is simpler to machining and gave a good surface finish than Al7075/SiC_p MMCs.

Inegbenebor et al. (2018) dispersed SiC_p of two different grit sizes (320 and 1200) for four different wt% (2.5, 5, 7.5 and 10) in the aluminum matrix using the stir casting method. It was found that the SiC_p reinforced aluminum MMC had an increase in young's modulus and hardness. Also, 1200 grit size 7.5 wt% SiC_p reinforced aluminum MMC had greater mechanical properties.

Based on the literature review, it is concluded that SiC_p reinforced aluminum alloy MMCs has excellent mechanical properties. However, experimental investigation on different wt% SiC_p reinforced Al6082 and Al7075 MMCs have not received much attention. Hence in this research work, different wt% SiC_p reinforced Al6082 and

Al7075 MMCs are fabricated using a stir casting method and the physical, mechanical and dynamic characteristics of the fabricated MMCs specimens are determined. The optimum MMCs specimen is determined using MADM techniques. Further, the fabricated MMC samples are used as top and bottom layers of MRF core sandwich beams and dynamic characterization is performed.

2.4 MULTI ATTRIBUTE DECISION MAKING

The multi attribute decision making (MADM) techniques have been used to solve conflicting decision problems and to select the optimal alternatives. Rao (2006) proposed a methodology based on the combined analytic hierarchy process (AHP) and technique for order preference by similarity to ideal solution (TOPSIS) technique. They used AHP and TOPSIS methods for the selection of best-cutting tools made of different titanium alloys and the best workpiece of ferrous and non-ferrous alloys for turning, drilling and facing operations. It was concluded that the AHP and TOPSIS method can be applied to all tasks and suitable for all selection problems.

Shanian and Savadogo (2006) applied the TOPSIS technique for selecting the optimal material for metallic bipolar plates for fuel cell used in electric vehicles. Rao (2008) applied VIšekriterijumsko KOmpromisno Rangiranje (VIKOR) technique and solved Shanian and Savadogo (2006) material selection of metallic bipolar plates for fuel cell used in electric vehicles and compared both TOPSIS and VIKOR method results. It was found that the VIKOR technique is moderately straightforward and simple to apply when compared with the TOPSIS technique.

Dağdeviren (2008) proposed a methodology based on the AHP and preference ranking organization method for enrichment evaluation (PROMETHEE) method for the selection of milling machines in a manufacturing company. It was concluded that AHP and PROMETHEE methods are precise methods and are suitable for material selection problems.

Rao and Patel (2010) applied the PROMETHEE method to overcome the challenge of evaluating the overall candidate choices for decision making. They applied the PROMETHEE method for the selection of cutting fluid used for grinding operations in manufacturing companies. It was suggested that the application of PROMETHEE

can solve material selection issues, including any number of choice criteria, in manufacturing environments.

Rao and Patel (2010) proposed an integrated weighted method for material selection. They solved three different examples and compared the results with VIKOR, elimination and choice translating reality (ELECTRE) and TOPSIS methods. It was suggested that the procedure involving an integrated weighted method is intelligent, basic, and advantageous to execute when compared to the other MADM techniques.

Khorshidi et al. (2012) used fuzzy AHP and TOPSIS techniques for the selection of the best aluminum silicon magnesium MMCs. Khorshidi and Hassani (2013) carried out a comparison between TOPSIS and preference selection index (PSI) methods for deciding the quality and workability of Al/SiC$_p$ MMCs. They used powder metallurgy route for preparing MMC. They concluded that aluminum reinforced 5 wt% SiC$_p$ and 16 µm size reinforcement have better quality and workability compared to other composites.

Çalışkan et al. (2013) applied the AHP, extended PROMETHEE II (EXPROM2), TOPSIS and VIKOR decision models for the selection of the best tool holder material in milling machines. It was suggested that the AHP, EXPROM2, TOPSIS, and VIKOR methods can be used for selecting the best tool holder and to solve all material selection issues.

Zafarani et al. (2014) applied the AHP technique for selecting the most preferable Al/SiC$_p$ composite depending on their strength and workability. They manufactured Al/SiC$_p$ composite through the powder metallurgy method, with different particle sizes of SiC$_p$ reinforcement. Based on AHP method, it was found that aluminum reinforced with 10 wt% SiC$_p$ and 16 µm size reinforcement gives better strength compared to other composites.

Kluczek and Gladysz (2015) used AHP and TOPSIS method to distinguish chances and reduce the ecological effects of the painting procedure while painting central heating boilers in a polish company. Their study outlined the advantages of a clean, non-contaminating innovation that successfully removes the utilization of unsafe chemicals and avoids harmful solid waste.

Prakash and Barua (2015) applied fuzzy AHP and TOPSIS methods for ranking the reverse logistics to select the alternatives in an electronics company. Wang et al. (2016) investigated a study of the hybrid MADM method combining simple additive weighting (SAW) and TOPSIS methods. It was observed that the results obtained were highly similar to the MADM results derived from previous studies.

Ezatpour et al. (2016) manufactured Al7075/Al$_2$O$_3$ metal matrix nanocomposites by the traditional stir casting method. They found that the composite microstructure showed uniform dispersion of nanoparticles in the matrix. They also found that the increase in addition of Al$_2$O$_3$ reinforcement in Al7075 alloy increased UTS, compression strength and hardness. They utilized the PSI method to choose the best sample considering the strength and workability of Al7075/Al$_2$O$_3$ metal matrix nanocomposites. They found that Al7075 alloy reinforced with 0.4 and 0.8 wt% Al$_2$O$_3$ composite have the best combination of strength and workability.

Kaliszewski and Podkopaev (2016) provided a simple framework for interpretations of rankings. Their framework was based on the classical MADM, in particular on the simple additive weighting (SAW) method. They presented how to derive weights for the SAW method and usage of the derived weights in the ranking process.

Azdast et al. (2018) used twin screw extruder for fabricating 16 samples of MWCNT reinforced with melt polyamide 6 PMC. The PMC samples were characterized to determine the tensile, hardness, and impact properties. They used the AHP method to determine the weights for the criteria. Further, TOPSIS and multi-objective optimization on the basis of ratio analysis (MOORA) techniques were applied for the selection of the best PMC.

Mangera et al. (2018) used the ELECTRE III method for paediatric prosthetic knee material selection and found that Al7175 is the best material. Therefore, based on literature reviews it is observed that MADM techniques can be applied for the selection of materials in the decision-making process.

In this research, the optimum CGRP-PMC sample considering their different criterion such as density, ultimate tensile strength (UTS), bending strength, impact

strength, absorbed energy, damping ratio, fracture toughness, and interlaminar shear strength (ILSS) properties were used for MADM techniques. However, the selection of optimal composite for multi-application is difficult to determine manually based on the aforementioned properties of the two-layer, four-layer, and six-layered CGRP-PMC. The optimum MMCs of different wt% SiC_p reinforced Al6082 and Al7075 alloy MMCs were selected using MADM techniques. The attributes such as density, UTS, hardness, impact energy and damping ratio are considered in MADM techniques. Hence, in this research work, MADM techniques such as AHP, TOPSIS and PROMETHEE methods are applied for the selection of the optimal PMC and MMC.

2.5 MAGNETORHEOLOGICAL FLUID

Rabinow (1948) introduced MRF for clutch applications. It was observed that the MRF clutch have better performance than the electrorheological fluid (ERF) clutch. The MRF is a smart fluid and the rheological properties of MRF depend on the concentration and density of carbonyl iron particle (CI_p), particle size, shape, distribution, properties of the carrier fluid, additional additives, applied magnetic field, temperature and other factors (jolly et al. 1999). The MRF is often mentioned as a Bingham plastic and behaves with linear viscoelastic properties within the pre-yield regions (Li et al. 1999). MRF behaves like a liquid without a magnetic field but becomes quasi-solid with the application of the magnetic field. The rheological properties of MRF are measured and characterized using a rheometer (Laun et al. 2012).

Carlson et al. (1996, 2000) examined the fundamental design principles for devices utilizing controllable fluid and compared the ability of ERF and MRF. ERF was found to possess lower yield strength, high-voltage requirement, and contaminant sensitivity compared to MRF. Because of these hurdles, MRFs are poised to enable controllable fluid technology to grow out of its infancy into a viable commercially successful domain.

Seval and Pradeep (2002) prepared MRF based on 33 and 40 vol% of CI_p with different average particle sizes, 7–9 µm and 2 µm and considered silicone oil as base fluid. They observed that the saturation magnetization values of 2.03 and 1.89 T using vibrating sample magnetometer (VSM) measurements for 7–9 µm and 2 µm size CI_p.

It was observed that the yield stress of 7–9 µm CI_p MRF is higher than 2 µm CI_p MRF i.e., the yield stress of finer particle-based MRF decreased relatively due to smaller magnetization. Kumbhar et al. (2015) have recommended that 45% of CI_p filled silicone oil base fluid for the brake application. The physical and rheological properties of MRF is shown in Table 2.1.

Table 2.1 Properties of MRF (Carlson and Jolly. 2000)

Properties	Typical value
The maximum yield strength in the absence of magnetic field	2-3 kPa
The maximum yield strength in the presence of magnetic field	50- 100 kPa
Magnetic field	150-250 kA/m
Plastic viscosity	0.1-1.0 Pa·s (at 25°C)
Operable temperature range	-40 to 150 °C
Contaminants	unaffected by most impurities
Response time	few milliseconds
Density	3-4 g/cm^3
Maximum energy density	0.1 J/cm^3
Power supply (typical)	25 V, 1-2 A
Device actuation	Electromagnet or permanent magnet

Ashtiani et al. (2015) presented a review on the MRF preparation and stabilization. It was observed that the MRF stability was mainly affected due to the higher density of the magnetizable particles and lower viscosity of carrier fluid. Hence, it was suggested that the density of magnetizable particles can be reduced by coating them. Also, the viscosity of carrier fluid can be increased by adding a stabilizer surfactant. Based on their review, it was concluded that CI_p and silicone oil materials are the first choices for MRF preparation.

Cheng et al. (2016) prepared 11 MRF samples with different volume % CI_p varying from 10 to 50% dispersed in silicone oil and analysed the sedimentation

stability of MRF. It was determined that MRF with lower volume % CI_p will settle faster than those in higher volume % CI_p.

Gurubasavaraju et al. (2017) prepared 25, 30 and 35 volume percentage CI_p mixed in the silicone oil carrier fluid along with 1% lithium grease additives. Using response surface methodology (RSM) it was determined that MRF having 30% volume CI_p with silicone oil carrier fluid is the optimal MRF for damper applications.

Acharya et al. (2019) prepared six MRF having 60, 70 and 80 wt% CI_p with two different particle sizes of 2.9 microns and 8.27 microns mixed in the polyalphaolefin oil carrier fluid. Using a multi-objective genetic algorithm it was determined that MRF having 2.9 microns size and 74.48 wt% CI_p with polyalphaolefin oil carrier fluid have the maximum damping force and minimum viscosity.

The rheological properties of MRF can endure immediate and reversible changes when subjected to the magnetic field. Applications of MRF are seen in dampers, clutches, brakes, semi-active controlled suspension seats, aircraft wings, ships, polishing device, hydraulic valves, robot, composite structures with MRF core enclosed between beams, plates, panels, and bars (Wang and Meng (2001), Spaggiari et al. (2019)).

Based on the literature review, it is observed that MRF having 30 volume percentage CI_p mixed in the silicone oil have excellent rheological properties. Hence in this research work, MRF is prepared with 30% volume CI_p, 70% volume silicone oil and 2-gram grease as additives for 100 ml MRF.

2.6 MRF CORE SANDWICH BEAMS

Sandwich structures are widely used in aerospace, automobiles and building structures in order to take advantage of their lesser weight with improved dynamic properties of the system. Worldwide there is a need for new smart materials having exceptional strength and stiffness for the above mentioned industrial and commercial purposes (Birman and Kardomateas (2018)).

Initially, researchers investigated experimental vibration amplitude suppression of aluminum sandwich beam with ERF core (Yalcintas and Coulter (1995)). It was observed that the amplitude suppression was possible by controlling the applied electric field to the ERF core in the sandwich beam. Also, it was observed that the complex shear modulus of ERF changes with the applied electrical field and this effect, in turn, changes the dynamic characteristics of the sandwich beam.

Yalcintas and Dai (2003) investigated the dynamic characteristics of adaptive sandwich beams made out of MR materials. It was observed that the natural frequencies, vibration amplitude responses, mode shapes and damping ratio of the MR materials sandwich beam can be changed by varying the applied magnetic field. At 700 gauss magnetic flux density, the MRF adaptive sandwich beams have a 30% increase in natural frequency and vibration amplitudes decreased up to 20 dB.

Sun et al. (2003) analyzed the vibration minimization capabilities of MRF core with aluminum top and bottom layers sandwich beam subjected to different magnetic fields. It was observed that the natural frequencies shift to higher frequencies with increase in the external applied magnetic field.

Yeh and Shih (2006) considered the dynamic stability of the MRF core sandwich beam under axial harmonic load conditions. They determined that the sandwich beam natural frequencies in each mode and loss factor at higher mode increased with the applied magnetic flux density.

Lara-Prieto et al. (2009) experimentally studied the vibration suppression characteristics of MRF core with aluminum top and bottom layer sandwich beams. It was observed that the sandwich beam vibration responses can be controlled in the form of variations in vibration amplitude response and shifts in natural frequency. At 0.24 T magnetic flux density, the MRF core aluminum sandwich beams have a 17.5% increase in natural frequency and vibration amplitudes decreased up to 15.7 dB.

Rajamohan et al. (2009) investigated the dynamic characteristics of the MRF core between two aluminum layers. It was observed that the natural frequencies and the damping ratio of the MRF core aluminum sandwich beams were increased by increasing the external applied magnetic field.

Recently, researchers are focusing on determining the dynamic characteristics of composite sandwich structures having MRF core enclosed between beams and plates. Manoharan et al. (2014) studied the dynamic characteristics of the PMC sandwich plate with the MRF core. It was observed that the stiffness of the sandwich plate increased with an increase in the applied magnetic field. Also, the effectiveness of the sandwich plate increased with the reduction in vibration peak amplitude for increasing the applied magnetic flux density.

Talebitooti and Fadaee (2019) analyzed the vibration response of carbon nanotubes reinforced functionally graded materials with MRF core by numerical methods. They found that the natural frequency of the MRF core functionally graded sandwich beam decreased with an increase in the thickness of the MRF core.

2.7 MOTIVATION FROM LITERATURE SURVEY

Many researches have carried on the experimental vibration analysis of MRF core sandwich beams having aluminum top and bottom layers. Also, few researchers started to investigate the dynamic characteristics of the sandwich structure having MRF core enclosed between composite plates. However, the experimental research on sandwich structures having MRF core enclosed between different wt% of SiC_p reinforced Al6082 MMC beams and different layers of CGRP-PMC beams are yet to be explored. Hence, the present work is attempted to analyze the controllability of MRF core enclosed with various wt% of SiC_p reinforced Al6082 MMC sandwich beams subjected to different magnetic flux density. Also, to analyze the vibration controllability of CGRP-PMC-MRF core sandwich beams of varying the thickness of the top, bottom and middle layers subjected to different magnetic flux density. The rheological characteristics of the inhouse prepared MRF under the effect of the magnetic flux densities and without the magnetic flux density are determined. Free and forced vibration analysis of MMC-MRF core sandwich beams and CGRP-PMC-MRF core sandwich beams subjected to 0, 200, 400 and 600 gauss magnetic flux densities which influence the variation of natural frequency, damping ratio, and frequency amplitude responses are studied.

2.8 OBJECTIVES OF RESEARCH WORK

The aim of this research work is to study has under the influence of magnetic fields. The specific objectives of the research work are listed as follows:

1. To develop and investigate the improvement in vibration damping of a sandwich beam comprising of PMC or MMC as face layer and MRF core.
2. To optimize core thickness for vibration damping of the sandwich beam under varying magnetic fields.
3. To investigate and find an optimum combination of face layer and core using dynamic analysis of the sandwich beams.

2.9 SCOPE OF RESEARCH WORK

1. Fabrication of different layers such as two-layer, four-layer and six-layered chopped strand mat glass fiber reinforced unsaturated polyester resin polymer matrix composite (CGRP-PMC).
2. Fabrication of different wt% of SiC_p reinforced Al6082 and Al7075 MMC.
3. Finding material properties of the prepared PMC and MMC by material characterization analysis.
4. Preparation of MRF and determining the properties of MRF by rheological characterization.
5. Dynamic analysis of the MRF core sandwich composite beam to find the natural frequency, damping ratio, and frequency amplitude response at varying magnetic fields.

2.10 SUMMARY

In the literature review, it was observed that the vibration suppression capabilities of MRF core sandwich beams are presented. Most of the research work is carried out in MRF core aluminum sandwich beams. The reversible rheological properties of MRF was used to change the dynamic properties of the composite sandwich structures. Free vibration analysis was used to determine the natural frequency and damping ratio of the MRF core sandwich beams. Forced vibration

analysis was used to determine the frequency amplitude response of the MRF core sandwich beams. Based on the literature, research investigations carried on dynamic characterization of MRF core enclosed aluminum sandwich beams results have shown increased natural frequencies, improved damping ratios and increased vibration amplitude suppression capabilities with influences of the external applied magnetic field.

The research gap found from the literature review is that a study on the dynamic characteristics of MRF core composite sandwich beams should be carried out. Hence, in this research work, dynamic analysis of PMC and MMC sandwich beam with MRF core are experimentally analyzed.

CHAPTER 3

METHODOLOGY

3.1 INTRODUCTION

In this chapter, the methodology followed for experimental investigation on the dynamic characteristics of MRF core composite sandwich beams is presented. This study consists of three stages:

(i)   Preparation and rheological characterization of MRF.

(ii)   Fabrication and physical, mechanical and dynamic characterization of CGRP-PMC and MMCs and selection of optimal composites.

(iii)   Fabrication of CGRP-PMC-MRF core and MMC-MRF core sandwich beams and determining the dynamic properties.

3.2 METHODOLOGY
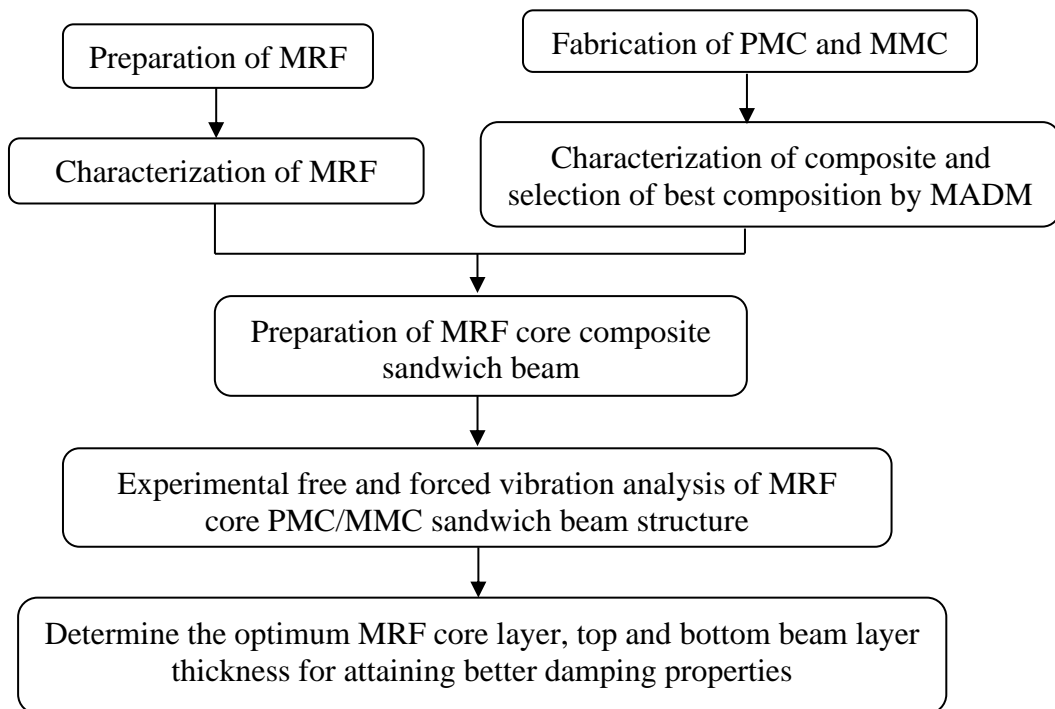
Figure 3.1 Methodology

Figure 3.1 shows the methodology of the research work. The MRF was prepared inhouse and the rheological properties of MRF were measured using a rheometer. The PMC and MMC were fabricated by hand layup and stir casting methods respectively.

3.3 PREPARATION AND CHARACTERIZATION OF MRF

The MRF having a 30% volume of carbonyl iron powder (CI_p), 70% volume of silicone oil and two-gram lithium grease as additives for 100 ml MRF are prepared. The shape, size and magnetization properties of CI_p were measured using a scanning electron microscope (SEM), particle size distribution (PSD) and vibrating sample magnetometer (VSM) instruments. The sedimentation study of MRF was carried out to determine the CI_p settling time period in silicone oil. The rheological characterization of MRF was carried out to determine the rheological properties of MRF respectively. Figure 3.2 shows the flowchart followed for the preparation and characterization of MRF.
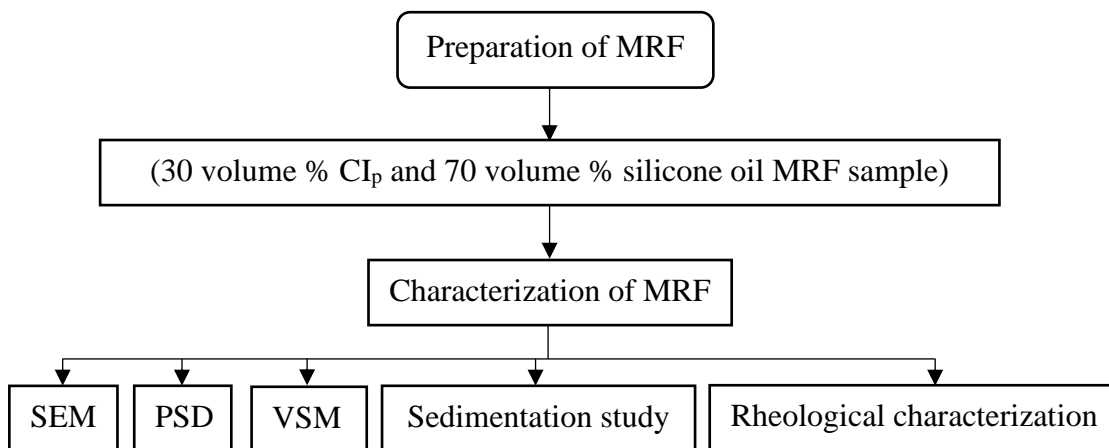
Figure 3.2 Preparation and characterization of MRF

3.3.1 Materials

The carbonyl iron powder (CI_p), silicone oil and lithium grease are the materials used for preparing MRF. The CI_p (Make: Chengdu Nuclear 857 New Materials Co., Ltd., China) is used as the magnetizable particles in the MRF. While silicone oil SS SF 350 (Make: Supreme silicones, Maharashtra, India) is used as the carrier fluid. Lithium grease (Make: SKF, India) performs as an antifriction agent and stabilizer. The

properties of CI_p specified by the supplier are provided in Table 3.1 and that of silicone oil in Table 3.2.

Table 3.1 Properties of CI_p (Chengdu Nuclear 857 New Materials Co., Ltd., China)

Physical properties	Carbonyl iron powder
Purity (%)	99.7
Bulk density (g cm^{-3})	2.79

Table 3.2 Properties of silicone oil SS SF 350, (Supreme silicones, Maharashtra, India)

Physical properties	Silicone oil SS SF 350
Viscosity (Pa-s)	0.340
Density (g cm^{-3})	0.965

3.3.2 Preparation of magnetorheological fluid

The MRF is prepared in-house at room temperature. The MRF composed of 30% volume CI_p and 70% volume silicone oil (carrier fluid) and two grams of lithium grease were used for preparing 100 ml MRF. The main purpose of adding lithium grease is to reduce the sedimentation of CI_p in the carrier fluid. Initially, two grams of grease was added to the silicone oil and continuously stirred at 500 rpm using a mechanical stirrer (Make: REMI lab stirrer RQ-5 Plus instrument) for 12 hours. After grease gets homogeneously mixed with silicone oil, CI_p is added to the silicone oil-grease solution. Then the CI_p-silicone oil-grease solution is stirred at 500 rpm in room temperature for 48 hours and MRF is prepared (Premalatha et al. (2012), Ashtiani et al. (2015) and Gurubasavaraju et al. (2017)). Figure 3.3 (a), (b) and (c) show the required materials used for MRF preparation, mixing of silicone oil-grease solution and CI_p-silicone oil-grease solution.

27
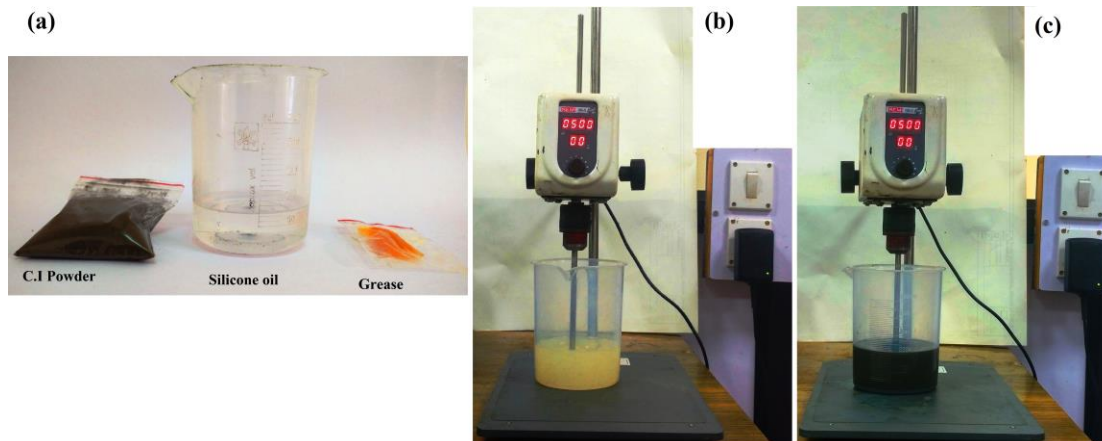
Figure 3.3 MRF preparation (a) Materials used, (b) Silicone oil-grease solution, and (c) CI_p-silicone oil-grease solution

3.3.3 Microstructure, size and magnetic properties of CI_p

The microstructure of CI_p is observed by using the FESEM instrument (Make: ZEISS Sigma, Germany). Particle size distribution (PSD) analysis is carried out to measure the average particle size of the CI_p. The particle size histogram and cumulative values of CI_p were measured (Make: CILAS 1064 particle size analyzer). The magnetic properties of CI_p are measured using a vibrating sample magnetometer (VSM) instrument (Make: Lakeshore VSM 7410S).

3.3.4 Sedimentation study

The sedimentation ratio is one of the important technical parameters that reveal the amount of settling of CI_p in the carrier fluid. The sedimentation in the MRF is mainly influenced by the density of CI_p and viscosity of silicone oil. The sedimentation ratio of CI_p can be controlled by the addition of lithium grease in the MRF (Cheng et al. (2016 and 2018)). Settling of CI_p in carrier fluid is a serious problem that affects the performance of MRF. Since the CI_p has a high density than silicone oil, the CI_p will start to settle in the MRF after a certain period. Hence, sedimentation investigation is performed to determine the sedimentation ratio of the MRF.

3.3.5 Rheological characterization

The rheological properties of MRF can be quickly and reversibly controlled with the application of the external applied magnetic field. At off-state condition (without magnetic field) the CI_P are randomly oriented in the carrier fluid and during the on-state condition (with the magnetic field), the CI_P align and form a chain-like structure. Hence, the MRF provides a reversible rheological effect by introducing a magnetic field. This reversible rheological effect of MRF subject to the external applied magnetic field makes it as a smart fluid (Jolly et al. (1999), and Li et al. (1999)).
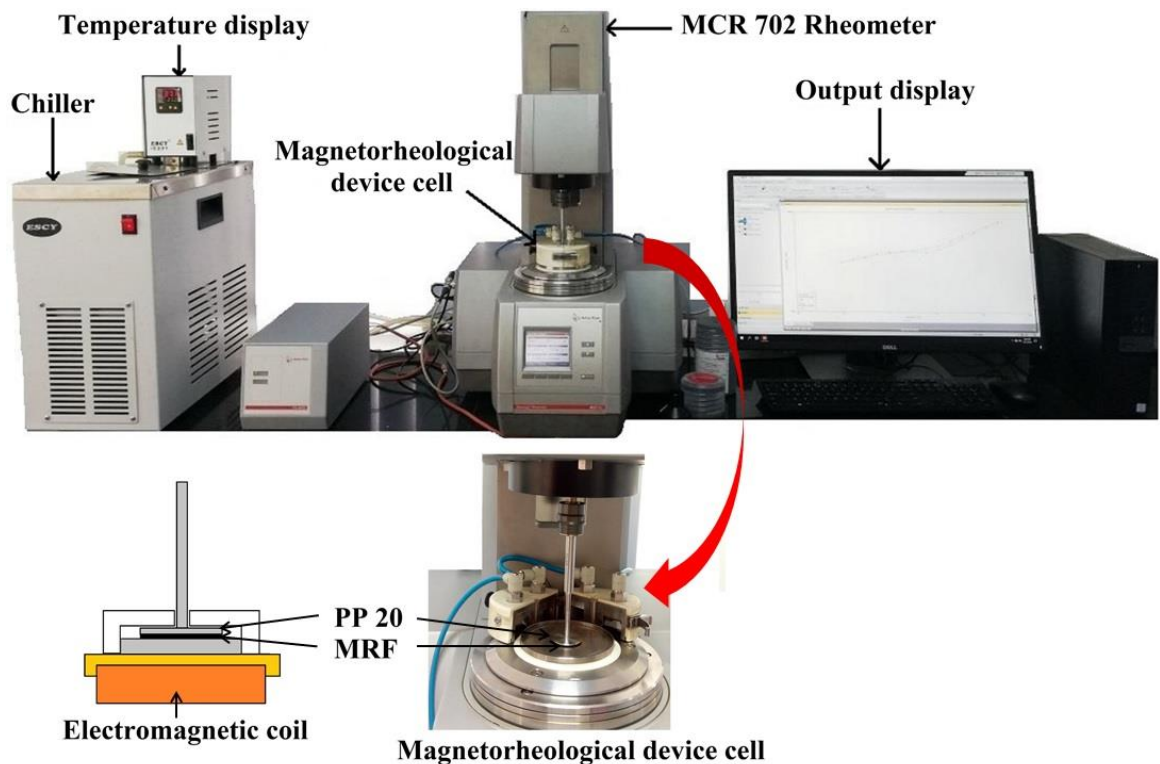
Figure 3.4 MCR 702 Anton Paar Rheometer

The rheological properties of MRF are measured using a rheometer (Make: MCR 702 Anton Paar) shown in figure 3.4. The rheometer with magnetorheological device cell, chiller, temperature display device and computer connected to the rheometer for measuring the data are the modules of the rheometer. The MRF is placed between 20 mm diameter parallel plates with a 1 mm gap between them and rheological analysis was performed. The rheological properties of MRFs are examined with and without the magnetic field at an operating temperature of 25 °C. The oscillatory

frequency sweep test is carried out at a frequency range of 0.1–100 Hz with a constant shear strain amplitude of 0.1%.

3.4 FABRICATION AND CHARACTERIZATION OF PMC

The methodology followed for the fabrication and characterization of two-layer, four-layer and six-layered CGRP-PMC are shown in figure 3.5.

```
                    ┌──────────────────────┐
                    │  Fabrication of PMC   │
                    └──────────┬───────────┘
                               ▼
        ┌──────────────────────────────────────────────┐
        │  (CGRP-PMC specimens – Hand-layup method)      │
        │  ┌────────────┐ ┌────────────┐ ┌────────────┐ │
        │  │Two-layered │ │Four-layered│ │Six-layered │ │
        │  └────────────┘ └────────────┘ └────────────┘ │
        └──────────────────────┬─────────────────────────┘
                               ▼
                  ┌──────────────────────────┐
                  │ Characterization of PMC   │
                  └──────────────────────────┘
```

| Density | Tensile | Flexural | Impact | Fracture | ILSS | Free vibration analysis |
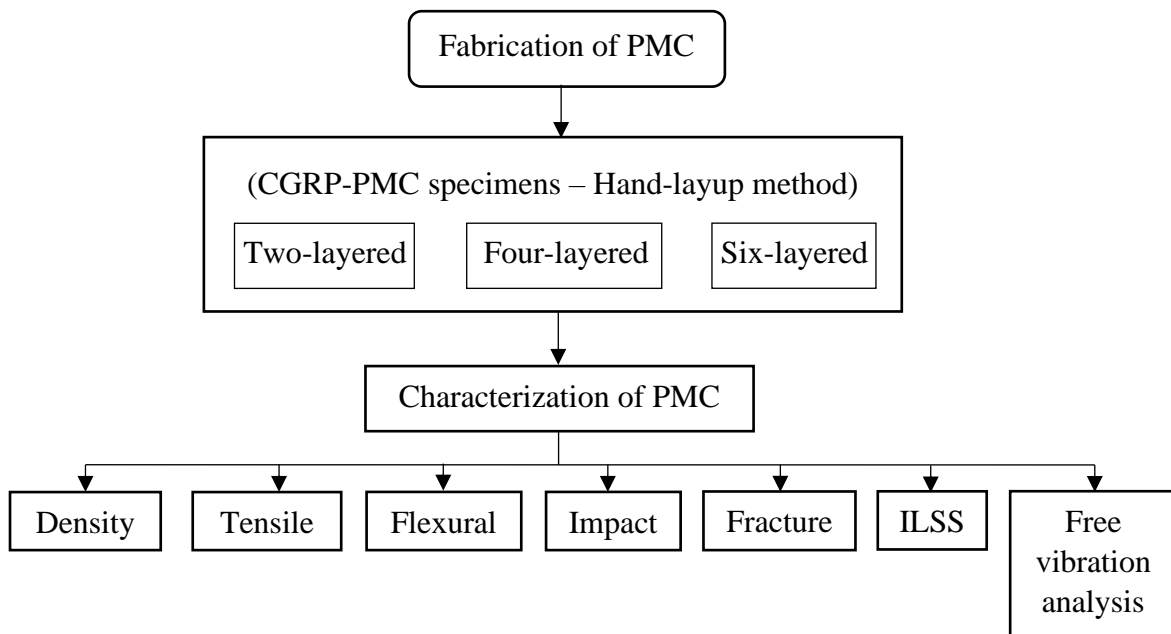
Figure 3.5 Fabrication and characterization of PMC

3.4.1 Fabrication of PMC

The CSM glass fiber of 450 g m-2 is reinforced with unsaturated polyester resin and specimens of two-layer, four-layer and six-layered CGRP-PMC were prepared using the hand-layup method. Figures 3.6–3.8 shows the schematic view of two-layer, four-layer, and six-layered CGRP-PMC fabrication. A mould of cross-section 250 mm x 250 mm was used for CGRP-PMC sample preparation. Images of two-layer, four-layer and six-layered CGRP-PMC are shown in figure 3.9. Initially, a 2 wt % cobalt accelerator and methyl ethyl ketone peroxide (MEKP) catalyst were pre-mixed with the polyester resin. A release agent is applied over the mould and then the prepared polyester resin is spread over the release agent. Before the polyester resin gets dried

CSM glass fiber is placed over polyester resin and again polyester resin is spread over this CSM glass fiber. Then second layer CSM glass fiber is kept over the polyester resin and above this CSM glass fiber polyester resin is applied again. By using a roller, polyester resin is equally distributed to the surface of CSM. Voids between the layers are properly squeezed out. After this, the CGRP-PMC material is allowed to cure at room temperature. Similarly, four-layer and six-layered CGRP-PMC specimens were prepared.
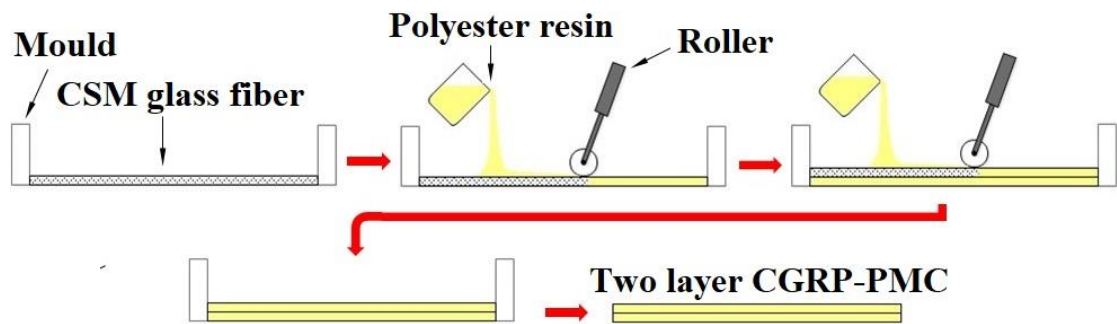
Figure 3.6 Schematic view of Two-layer CGRP-PMC fabrication
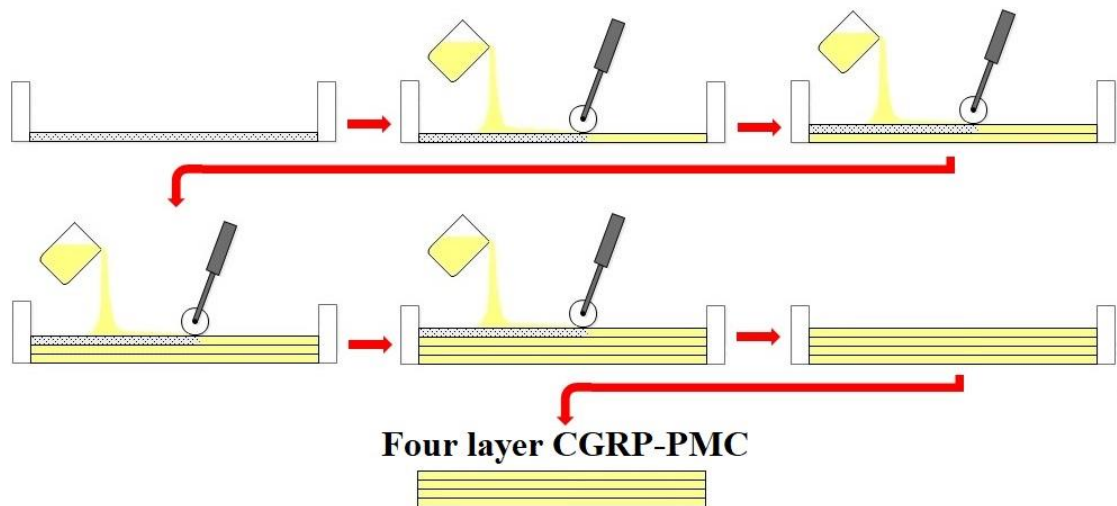
Figure 3.7 Schematic view of Four-layer CGRP-PMC fabrication
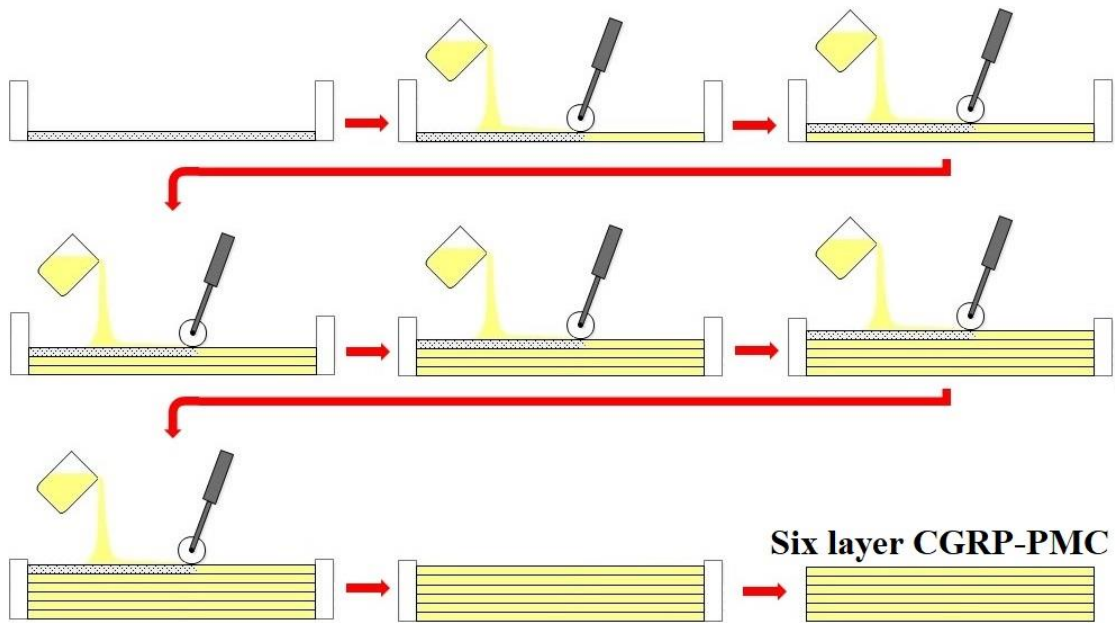
Figure 3.8 Schematic view of Six-layer CGRP-PMC fabrication
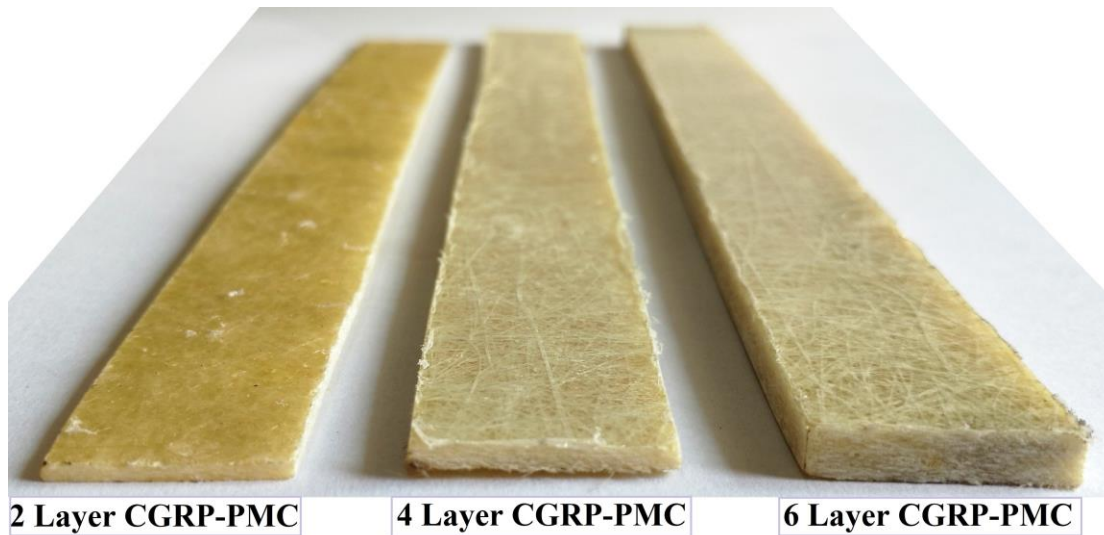
Figure 3.9 Images of two-layer, four-layer and six-layered CGRP-PMC

3.4.2 Mechanical properties of reinforcement and matrix

The mechanical properties of CSM and polyester resin are shown in Table 3.3 and the composition of CGRP-PMC is shown in Table 3.4.

Table 3.3 Mechanical properties of reinforcement and matrix (Arifin et al. (2014)).

Material	Young's modulus (GPa)	Poisson's ratio	Density (g/cm^3)
CSM	75	0.2	2.54
Polyester resin	3.5	0.25	1.161

The volume percentage of reinforcement and matrix was calculated by using the rule of mixture equation (3.1).

$$V_C = V_f + V_m \tag{3.1}$$

where,

V_C is the volume of CGRP-PMC material.

V_f is the volume of CSM.

V_m is the volume of resin.

Table 3.4 Composition of CGRP-PMC (Heckadka et al. (2015))

CGRP-PMC	Specimen thickness (mm)	CSM fiber vol.%	Polyester resin vol. %
Two-layers	2	22	78
Four-layers	3.5	24	76
Six-layers	5	26	74

3.4.3 Density

The density of CSM glass fiber reinforcement and unsaturated polyester resin matrix are 2.54 and 1.161 g cm^{-3}. The actual density of the CGRP-PMC material was determined by using the density measurement kit apparatus based on the Archimedes principle. The theoretical density of CGRP-PMC specimens (ρ_c) was calculated by using the Rule of Mixtures as shown in equation (3.2).

$$\rho_C = \rho_f V_f + \rho_m V_m \tag{3.2}$$

where, ρ_C is the density of CGRP-PMC.

ρ_f is the density of CSM fiber.

ρ_m is the density of polyester resin.

3.4.4 Tensile test

The tensile test CGRP-PMC specimens are prepared based on the ASTM D3039 standard and tested in the universal testing machine (UTM) (Make: Tinus Olsen H75KS), operated at room temperature. The specimens are cut at 250 mm length and 25 mm width. The gage length is taken as 150 mm and the speed of testing is set as 2 mm/min in the UTM.

3.4.5 Flexural test

The flexural test CGRP-PMC specimens are prepared based on the ASTM D790 standard and tested in UTM (Make: Tinus Olsen H75KS), operated at room temperature. The span length of 16 times the thickness of samples is prepared. The speed of testing (crosshead motion) in UTM is determined using equation (3.3).

$$R = \frac{ZL^2}{6d} \tag{3.3}$$

where,

R = rate of crosshead motion (mm/min).

L = support span (mm).

d = depth of beam (mm).

Z = rate of straining of the outer fiber (mm/mm/min), $Z = 0.01$.

The flexural experimental result helps to determine the maximum bending load and maximum bending stress that CGRP-PMC material can withstand when an external bending load is applied.

3.4.6 Charpy impact test

The Charpy impact test is conducted based on ISO 179-1/1eU CHARPY standard in the impact testing machine (Make: ZWICK ROELL HIT50P), operated at room temperature. Charpy impact test has been carried out to find the impact strength and absorbed energy of CGRP-PMC specimens.

3.4.7 Fracture toughness

Fracture toughness test has been carried out to determine the ability of CGRP-PMC specimens containing a crack to resist fracture. Fracture toughness specimens are prepared based on the ASTM D5045 standard and a three-point bend test is conducted in UTM, operated at room temperature. The fracture load P_Q, obtained from the analysis is used to determine K_Q values (MPa.m$^{1/2}$) as a measure of fracture toughness by using equation (3.4).

$$K_Q = \left(\frac{P_Q}{BW^{1/2}} \right) f(x) \tag{3.4}$$

where (0<x<1),

$$f(x) = 6x^{1/2} \frac{\left[1.99 - x(1-x)(2.15 - 3.93x + 2.7x^2) \right]}{(1+2x)(1-x)^{3/2}} \tag{3.5}$$

where, B = specimen thickness (cm), W = specimen width (cm), a = crack length (cm), x = a/W.

3.4.8 Interlaminar shear strength

Interlaminar shear strength (ILSS) helps to determine the de-lamination in the laminated specimens. ILSS test specimens are prepared based on the ASTM D2344 standard and tested in UTM, operated at room temperature. ILSS calculated by using short beam strength equation (3.6).

$$F = 0.75 \frac{P}{bh} \tag{3.6}$$

where,

      F = short-beam strength (MPa),

      P = maximum load observed during the test (N),

      b = measured specimen width (mm),

      h = measured specimen thickness (mm).

3.4.9 Free vibration analysis

The natural frequency and damping ratio of CGRP-PMC materials are determined using experimental free vibration analysis. The effective dimension of two-layer, four-layer, and six-layered CGRP-PMC beams are 200 mm length and 25 mm width.
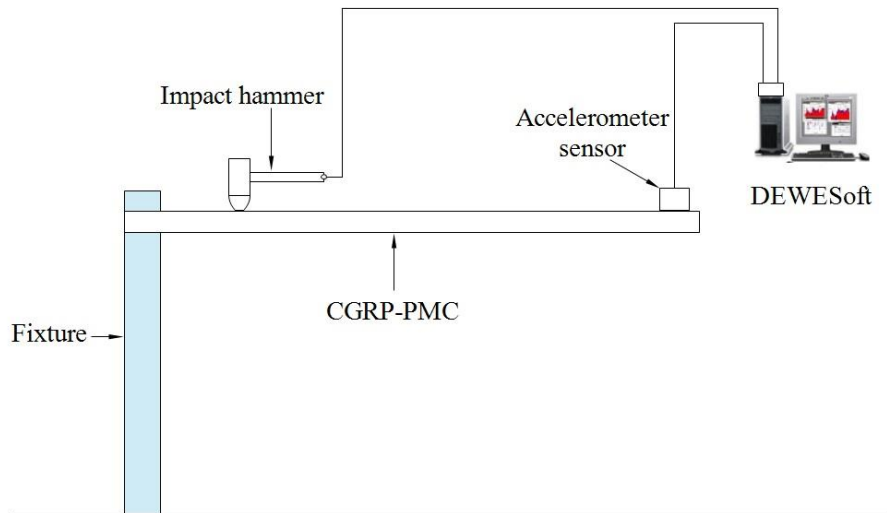
Figure 3.10 Schematic view of the experimental setup for free vibration analysis

The schematic view of the experimental free vibration analysis setup is shown in figure 3.10. The accelerometer sensor is placed at 25 mm away from the free end of the beam. Modal analysis using impulse hammer excitation is carried out based on the ASTM E756-05 standard. The experimental setup consists of a modal analysis data acquisition software (DEWESoft) with the data acquisition system (Make: DEWETRON), accelerometer sensor (Make: Kistler) and a fixture for holding the CGRP-PMC beams. The modal analysis impulse hammer is used to excite the CGRP-PMC beams. The time-domain signals are converted into frequency domain signals using fast Fourier transform (FFT). The natural frequency of the beam is determined from the periodic peaks of the FFT curve. The first four modes of natural frequencies and damping ratios of CGRP-PMC cantilever beams are measured.

3.5 FABRICATION AND CHARACTERIZATION OF MMCs

The flowchart in figure 3.11 shows the methodology followed for the fabrication and characterization of MMC. The different wt% (0, 1, 2, 3, 4, 5, 7.5, 10, 15 and 20 wt%) SiC_p reinforced Al6082 and Al7075 MMC was fabricated by the stir casting method.

```
                    ┌─────────────────────┐
                    │  Fabrication of MMC │
                    └──────────┬──────────┘
                               │
┌──────────────────────────────▼──────────────────────────────┐
│           (MMC specimens – Stir casting method)              │
│ 20 Specimens of different wt% (0, 1, 2, 3, 4, 5, 7.5, 10, 15 │
│      and 20 wt%) SiCp reinforced Al6082 and Al7075 MMCs      │
└──────┬────────────────────────────┬───────────────────┬──────┘
       │                            │                   │
       │              ┌─────────────▼────────────┐      │
       │              │  Characterization of MMC │      │
       │              └─────────────┬────────────┘      │
  ┌────▼───┐ ┌────────┐ ┌───────────▼──┐ ┌──────────┐ ┌─▼──────┐
  │Density │ │Hardness│ │Tensile       │ │Impact    │ │Wire EDM│
  │        │ │        │ │strength      │ │energy    │ │        │
  └────────┘ └────────┘ └──────────────┘ └──────────┘ └────────┘
```
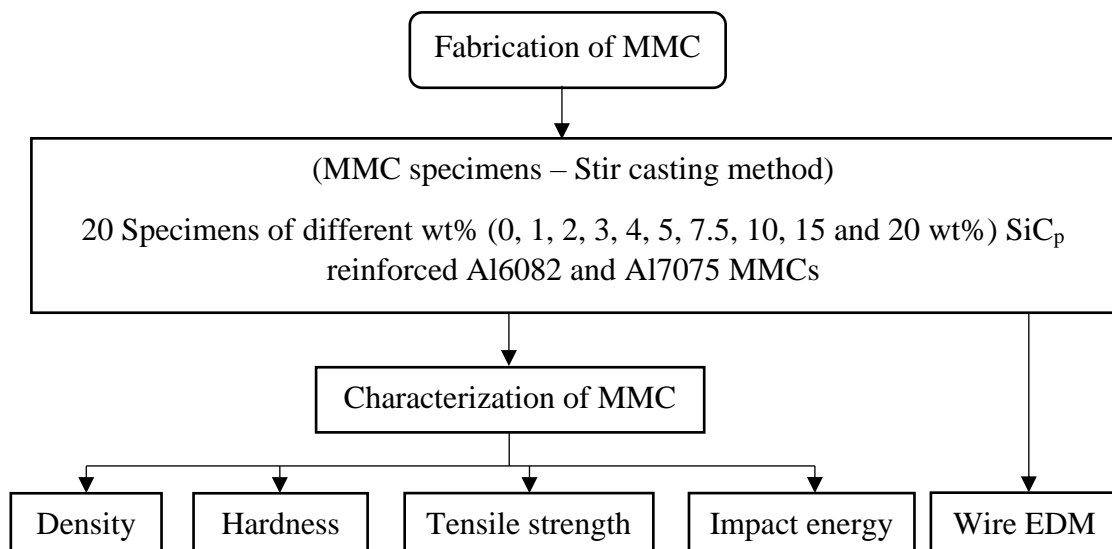
Figure 3.11 Fabrication and characterization of MMC

3.5.1 Materials of MMC

The materials used for preparing MMC are Al6082 and Al7075 aluminum alloys supplied by PMC corporation, Bangalore, India, and silicon carbide particles (SiC_p) of 99.9 % purity and particle size of 400 mesh supplied by Central drug house private limited, New Delhi, India. Degassing tablets were taken as a reference to remove the oxides and impurities present in the MMCs. The oil hardened non-shrinking steel (OHNS) procured from Hi-Tech sales corporation, Mangalore, India was used for making the mold. The MMCs were fabricated using a stir casting method (Hashim et al. (1999)). The chemical composition of the Al6082 and Al7075 aluminum alloy matrix used in this study are shown in Table 3.5.

Table 3.5 Chemical composition of aluminum alloys (wt%) (PMC corporation, Bangalore, India) (El-Sabbagh et al. (2012) and Mobasherpour et al. (2013))

	Mg	Zn	Cr	Cu	Mn	Si	Ti	Fe	Al
Al6082	0.6 - 1.2	0.2	0.25	0.1	0.4 - 1	0.7 - 1.3	0.1	0.5	Bal.
Al7075	2.1 - 2.9	5.1 - 6.1	0.18 - 0.28	1.2 - 2	0.3	0.4	0.2	0.5	Bal.

3.5.2 Fabrication of MMC

Figure 3.12 shows the schematic view of the stir casting furnace setup. The MMCs were fabricated using the stir casting process as per the following procedure. The aluminum alloy ingot was heated up to 700 °C in a graphite crucible in a heating furnace. The aluminum alloy starts to melt at 650 °C and the temperature in the heating furnace was raised up to 720 °C. The SiC_p was preheated to 300 °C to enhance the interface reaction with aluminum alloy. The required quantity of preheated SiC_p was added to the molten aluminum alloy and stirred continuously for uniform distribution. The mechanical stirrer was rotated at 500 rpm and the temperature in the heating furnace was raised up to 780 °C and stirred for 5 minutes. The OHNS mold was preheated to 300 °C which improves the flowability of molten metal. Degassing agents were added to remove the impurities and oxygen interface reaction oxides. The oxides and impurities were then removed and molten metal was poured immediately after stirring into the preheated mold and cooled at room temperature (Sajjadi et al. (2012) and Kumar et al. (2014)). After complete solidification, the samples were removed from the mold. Figure 3.13 shows the stir casting experimental setup.
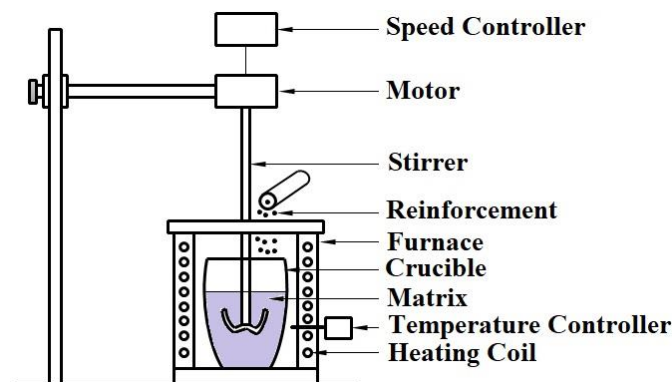
Figure 3.12 Schematic view of stir casting furnace setup

Figure 3.13 MMCs stir casting experimental setup

Table 3.6 Matrix and reinforcement for MMCs preparation

Sample No.	MMCs	Al6082 alloy (g)	Al7075 alloy (g)	SiC$_p$ (g)
S1	Al6082	1000	-	-
S2	1% SiC$_p$/Al6082	990	-	10
S3	2% SiC$_p$/Al6082	980	-	20
S4	3% SiC$_p$/Al6082	970	-	30
S5	4% SiC$_p$/Al6082	960	-	40
S6	5% SiC$_p$/Al6082	950	-	50
S7	7.5% SiC$_p$/Al6082	925	-	75
S8	10% SiC$_p$/Al6082	900	-	100
S9	15% SiC$_p$/Al6082	850	-	150
S10	20% SiC$_p$/Al6082	800	-	200
S11	Al7075	-	1000	-
S12	1% SiC$_p$/Al7075	-	990	10
S13	2% SiC$_p$/Al7075	-	980	20
S14	3% SiC$_p$/Al7075	-	970	30
S15	4% SiC$_p$/Al7075	-	960	40
S16	5% SiC$_p$/Al7075	-	950	50
S17	7.5% SiC$_p$/Al7075	-	925	75
S18	10% SiC$_p$/Al7075	-	900	100
S19	15% SiC$_p$/Al7075	-	850	150
S20	20% SiC$_p$/Al7075	-	800	200
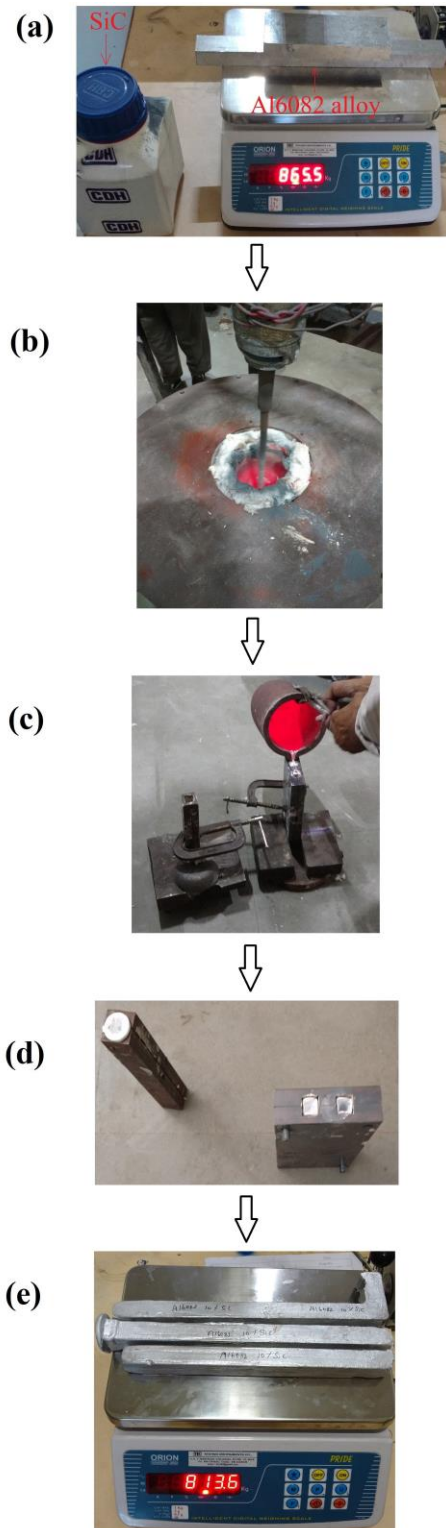
Figure 3.14 MMCs fabrication process (a) aluminum alloy matrix and SiC$_p$
reinforcement measurement, (b) Stirring operation of matrix and reinforcement in a
heating furnace, (c) Pouring molten metal to OHNS mold, (d) Solidification, and
(e) Fabricated MMCs.

The steps in the processing of MMCs through stir casting method is shown in figure 3.14. The prepared MMCs have a dimension of 250 mm x 20 mm x 20 mm. Table 3.6 shows the aluminum alloy matrix and SiC$_p$ reinforcement proportions used for 20 MMCs sample preparation.

MMC characterization such as density test, tensile test, impact test and hardness tests are carried out. The MMC samples were machined using wire electro-discharge machining (WEDM) to get the required beam dimensions.

3.5.2 Density

The actual density of the composite materials is measured by using the Archimedes principle, while the theoretical density was calculated using the rule of mixture. Considering w_m, w_r, w_c as the mass of matrix, reinforcement and composites.

$$w_m + w_r = w_c \tag{3.7}$$

$$\frac{w_m}{w_c} + \frac{w_r}{w_c} = 1 \tag{3.8}$$

$$W_m + W_r = 1 \tag{3.9}$$

where W_m is the matrix mass fraction and W_r is the reinforcement mass fraction. The theoretical density of the composite (ρ_c) in terms of the mass fraction is shown in equation (3.10).

$$\frac{W_m}{\rho_m} + \frac{W_r}{\rho_f} = \frac{1}{\rho_c} \tag{3.10}$$

where ρ_m is the density of the matrix and ρ_f is the density of fiber. The density of SiC reinforcement is 3.21 g/cm^3. The density of the as-received Al6082 matrix is 2.71 g/cm^3 and the density of the Al7075 matrix is 2.81 g/cm^3.

3.5.3 Hardness test

The Vickers microhardness test is carried out in microhardness tester machine at 100 N load for 10 seconds. Hardness is the characteristic of a material, which conveys the protection from perpetual disfigurement. Vickers hardness test is conducted based on ASTM E92-82 standards.

3.5.4 Impact test

The Charpy (simple beam) impact test is performed based on ASTM E23-16b. Figure 3.15 shows the schematic view of the Charpy test sample. The dimensions of the Charpy impact specimens are given in Table 3.7.
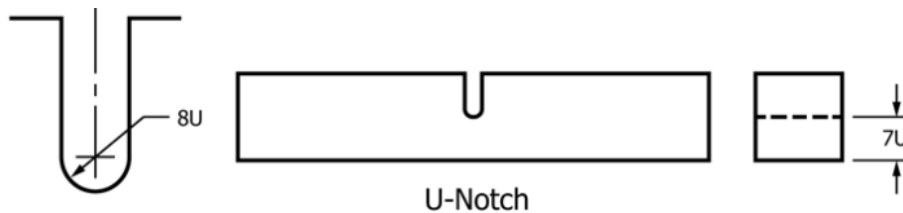
Figure 3.15 Schematic view of the Charpy impact test sample.

Table 3.7 Charpy impact test sample dimensions and allowable tolerance

Standard Specimen	Dimensions (mm)	Tolerance (mm)
Length of specimen	55	+0/-2.5
Centering of notch		±1
Width	10	±0.075
Thickness	10	±0.075
7U-Ligament length	5	±0.075
8U-Radius of notch	1	±0.025

3.5.5 Tensile test

The Tensile specimens are prepared based on ASTM E8/E8M-16a. The dimensions of tensile samples are shown in figure 3.16 and Table 3.8. The ability of the MMCs to resist breaking under tensile load is measured in the tensile test. The tensile test of the prepared MMCs is conducted by using a SHIMADZU AG-XPlus 100 kN

Tensile tester instrument operated at a constant crosshead speed of 1 mm min^{-1} at room temperature.
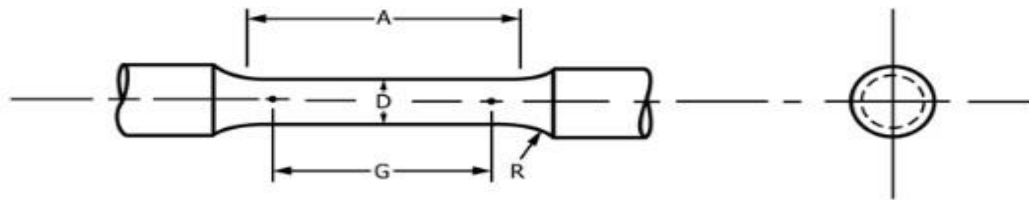
Figure 3.16 Schematic view of the tensile test sample

Table 3.8 Tensile test sample with gauge length four times diameter

Standard Specimen	Dimensions (mm)
G- Gauge length	16.0±0.1
D- Diameter	4.0±0.1
R- Radius of fillet	4
A- Length of the reduced parallel section	20

3.5.6 Free vibration analysis

The free vibration analysis is performed to determine the natural frequency and damping ratio of the fabricated MMCs beams. Experimental free vibration analyses were performed based on the ASTM E756-05 standard using impact hammer excitation. The effective dimensions of the MMCs samples are 200 mm × 20 mm × 2 mm. The required dimensions of MMCs were machined using the wire electro-discharge machining (WEDM) method.
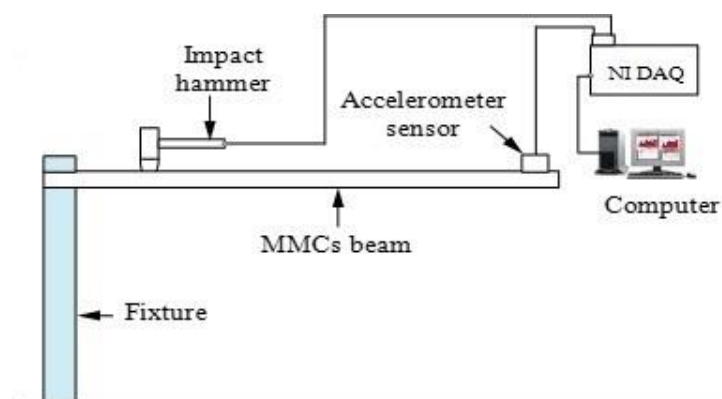
Figure 3.17 Schematic view of free vibration analysis experimental setup

The schematic diagram of the experimental free vibration analysis setup is shown in figure 3.17. The impact hammer was used to excite the MMCs cantilever beam. The accelerometer sensor was used to measure the vibration data and through NI9234 DAQ (data acquisition) the signals are transferred to the LabVIEW 2017 software for further analysis. By using a Fast Fourier Transform (FFT) technique, the time domain signals were converted to frequency domain signals. The natural frequencies of the beams are identified from peaks in the Frequency Response Function (FRF). The first three natural frequencies are measured and the corresponding damping ratios for the MMCs beam are obtained using the half-power bandwidth technique (Rajini et al. (2012) and Rajesh et al. (2016)). The damping ratio (ζ) of the MMCs beam is determined by relating to the loss factor (η) as shown in equations (3.11) and (3.12). The loss factor is defined as the amount of energy dissipated per cycle to the stored energy during vibration (Carfagni et al. (1998)).

$$\eta = 2\zeta \tag{3.11}$$

$$\eta = \frac{\omega_+ - \omega_-}{\omega_n} \tag{3.12}$$

where, ω_+ and ω_- are the positive and negative frequency reduction, ω_n is the natural frequency.

3.5.7 Response surface methodology

The response surface methodology (RSM) is a statistical technique used for the modeling and analysis of the relationships between the response and the independent parameters (Vishwakarma et al. (2017)). The examination of the response curve and optimum solutions are analyzed with the help of DESIGN-EXPERT software. The objective of RSM is to optimize the independent parameters to achieve better response parameters. The response parameters are the dependent parameters (density, impact energy, UTS, hardness, and natural frequency), while the factor parameters are the independent parameters (aluminum alloy matrix and SiC reinforcement). RSM consists of three steps. The first step is the determination of the independent parameters and their levels. The second step is the determination of the model design and verification

of the model. The data required for the response models are commonly selected from the experimental results. The analysis of variance (ANOVA) is used for evaluating the relation between the independent and dependent parameters. The significant and insignificant parameters of the model are determined. The third step is to obtain the response surface plots and determination of optimum solution (Gurubasavaraju et al. (2017)).

3.6 MULTI-ATTRIBUTE DECISION MAKING

Multi-attribute decision making (MADM) is an approach utilized to tackle issues including determination from a limited quantity of choices. The MADM strategy specifies how attribute (criteria) data is to be handled with a specific goal. In this research, MADM techniques are applied to select the optimum CGRP-PMC and MMCs. The attributes considered for CGRP-PMC materials selection are the density, UTS, bending strength, impact strength, absorbed energy, fracture toughness, ILSS and damping ratio. In MMCs material selection the attributes considered are the density, UTS, hardness, impact energy, and damping ratio. The specific goal of using MADM techniques is to determine the best composite sample considering the physical, mechanical and dynamic properties of the composite materials.

3.6.1 Analytic hierarchy process

The analytic hierarchy process (AHP) method is one of the decision-making techniques, was developed by Saaty (1980). AHP method disintegrates decision-making problems into an arrangement of hierarchies of objectives, attributes, and alternatives (Rao (2007)). Steps involved in solving the AHP method problems are as follows.

Step 1: Hierarchical structure, number of alternatives and attributes

The first step is to determine the objectives, alternatives, and attributes to be represented in a hierarchical structure. Then the alternatives and corresponding attributes are arranged as shown in equation (3.13).

$$A = [x_{ij}]_{n \times m} = \begin{bmatrix} x_{1,1} & x_{1,2} & \cdots & x_{1,j} & \cdots & x_{1,m} \\ x_{2,1} & x_{2,2} & \cdots & x_{2,j} & \cdots & x_{2,m} \\ \vdots & \vdots & \ddots & \vdots & \ddots & \vdots \\ x_{i,1} & x_{i,2} & \cdots & x_{i,j} & \cdots & x_{i,m} \\ \vdots & \vdots & \ddots & \vdots & \ddots & \vdots \\ x_{n,1} & x_{n,2} & \cdots & x_{n,j} & \cdots & x_{n,m} \end{bmatrix} \tag{3.13}$$

where, x_{ij} are the values of the ith alternatives and j[th] attributes.

i belong to 1, 2,...., n; and j belong to 1, 2,...., m;

Step 2: Normalization matrix

In step 2, the Normalized values of step 1 attributes are determined.

Step 3: Determining the relative importance matrix (Decision maker)

A square matrix is constructed with criteria compared to itself is given a value 1. The diagonal values in the square matrix are always 1 i.e., in comparison with the same criteria $b_{ii} = b_{jj} = 1$ and $b_{ji} = 1/ b_{ij}$. The relative importance value 1 specifies equal importance, 3 specifies moderate importance, 5 specifies strong importance, 7 specifies very strong importance and 9 specifies absolute importance. Whereas remaining numbers 2, 4, 6 and 8 specifies the intermediate values (Zafarani et al. (2014)).

Step 4: Geometric mean

The geometric mean strategy for AHP is widely used to decide the relative standardized weights of the criteria, in view of its effortlessness, simple assurance of the greatest eigenvalue and decrease in the irregularity of decisions. The geometric mean is calculated by using equation (3.7).

$$GM_j = \left[\prod_{j=1}^{m} x_{ij} \right]^{1/m} \tag{3.14}$$

where m denotes the number of attributes (criteria).

Step 5: Determining normalized weights w_j.

The normalized weights for each attribute are calculated using equation (3.8).

$$w_j = \frac{GM_j}{\sum_{j=1}^{m} GM_j} \qquad (3.15)$$

Step 6: Consistency check

Table 3.9 Relative Index value

Attributes	3	4	5	6	7	8	9	10
RI	0.52	0.89	1.11	1.25	1.35	1.4	1.45	1.49

Table 3.9 shows the relative index (RI) value of the attributes. For the weights to be allowable, the consistency ratio (CR) should be less than 0.1. By substituting equation (3.17) in equation (3.16) CR value is determined.

$$CR = CI / RI \qquad (3.16)$$

$$CI = (\lambda_{max} - m) / m - 1 \qquad (3.17)$$

where, λ_{max} is the maximum eigenvalue and m is the number of attributes. A smaller consistency index (CI) value leads to consistency. For the weights to be allowable, the consistency ratio $CR = CI/RI$ should be less than 0.1.

Hence, the weights for each attribute are determined by using the AHP method and these weights are substituted in SAW, WPM, TOPSIS and PROMETHEE methods to determine the rank of the composites.

Step 7: Determination of score and rank

Method 1. Simple Additive Weighting approach (SAW)

In this method, each attribute is given weights and the addition of all attribute weights should be 1 (Kaliszewski and Podkopaev (2016)). Individually alternative is evaluated with respect to all attributes. The SAW method score is determined by using equation (3.18).

$$P_i = \sum_{j=1}^{M} w_j x_{ij} \qquad (3.18)$$

where,

w_j is the weights of the attributes and x_{ij} is the corresponding values of alternative and attribute in normalization matrix step 2.

Method 2. Weighted Product Model (WPM)

WPM technique is similar to the SAW method, the primary difference is the replacement of addition in the method there with multiplication. The WPM method score is determined by applying equation (3.19).

$$P_i = \prod_{j=1}^{M} [(x_{ij})_{normal}]^{wj} \tag{3.19}$$

3.6.2 TOPSIS method

TOPSIS method was developed by Hwang and Yoon (1981). Many researchers used the TOPSIS method for ranking the samples (Shanian and Savadogo (2006), Jahan et al. (2010), Çalişkan et al. (2013), Bhuyan et al. (2015), Yazdani and Payam (2015), Bhowmik et al. (2018)). Steps involved in solving the TOPSIS method are as follows.

Step 1. The normalization of the decision matrix.

The normalization of decision matrix is carried out using equation (3.20).

$$n_{ij} = \frac{x_{ij}}{\sqrt{\sum_{i=1}^{n} x^2_{ij}}} \tag{3.20}$$

Step 2. Normalized weighted decision matrix, V_{ij}

The normalized weighted decision matrix is determined by substituting equations (3.20) in (3.21).

$$V_{ij} = n_{ij} \, w_j \tag{3.21}$$

where, w_j = associated weights of the attributes substituted from the AHP method.

Step 3. Ideal (best) and ideal (worst) solutions

Ideal (best) and ideal (worst) solutions can be expressed as equation (3.22).

$$\left\{V_1^+, V_2^+, ..., V_n^+\right\} = \left\{(\max V_{ij} \left| j \in J\right.), (\min V_{ij} \left| j \in J'\right.)\left|\right. \right\}$$
$$\left\{V_1^-, V_2^-, ..., V_n^-\right\} = \left\{(\min V_{ij} \left| j \in J\right.), (\max V_{ij} \left| j \in J'\right.)\left|\right. \right\}$$

(3.22)

where J belongs to the beneficial attributes and J' belongs to the non-beneficial attributes.

Step 4. Obtain the separation measures

This step involves determining the separation measures of each alternative. The Euclidian distance between ideal and nadir ideal solution can be expressed as equation (3.23).

$$S_i^+ = \left\{\sum_{j=1}^{n}(V_{ij} - V_j^+)^2\right\}^{0.5}$$
$$S_i^- = \left\{\sum_{j=1}^{n}(V_{ij} - V_j^-)^2\right\}^{0.5}$$

(3.23)

Step 5. Relative closeness coefficient

The relative closeness coefficient of an individual alternative to the ideal solution is determined using equation (3.24).

$$C_i = \frac{S_i^-}{S_i^- + S_i^+}$$

(3.24)

where relative closeness coefficient (C_i) should be obtained in a range between $0 \leq C_i \leq 1$. The alternatives having high values of C_i implies that the rank is better.

3.6.3 PROMETHEE method

PROMETHEE method was developed by Brans and Vincke (1985), Brans et al. (1986). Dağdeviren (2008), Rao and Patel (2010) applied the PROMETHEE method for the selection of suitable samples and this method is widely used for its simplicity. Considering the number of alternatives and selection criteria,

$$\max\{c_1(a), c_2(a), ..., c_j(a), ..., c_n(a) \left| a \in C\right.\}$$

(3.25)

where

C is the finite set of possible alternatives,

c_n denotes n criteria to be maximised,

For each alternative $c_j(a)$, an estimation of the alternative's contribution is compared for each separate criterion. While comparing two alternatives $a1, a2 \in C$, the results of this comparison were expressed as preference P. The index for preference is 0 or 1.

$$P_{j(a1,a2)} = F_j[c_j(a1) - c_j(a2)] \qquad (3.26)$$

$$0 \le P_{j(a1,a2)} \le 1 \qquad (3.27)$$

F_j is a non-decreasing function of the difference (d) between two alternatives a1 and a2 over the criteria c_j. The selection of a specific preference function for a criterion is derived by the simple difference between the values of the criterion c_j for alternatives a1 and a2. The multicriteria preference index $\prod$ is defined as the sum of the average weights of the preference function P_j.

$$\prod(a1, a2) = \frac{\sum_{j=1}^{n} w_j P_j(a1, a2)}{\sum_{j=1}^{n} w_j} \qquad (3.28)$$

The leaving flow $\phi^+(a)$ depends on how an alternative dominates remaining alternatives in set C and it is determined by equation (3.29)

$$\phi^+(a) = \sum_{x \in C} \pi(a, x) \qquad (3.29)$$

The entering flow $\phi^-(a)$ depends on how an alternative dominated by remaining alternatives in set C is determined by equation (3.30)

$$\phi^-(a) = \sum_{x \in C} \pi(x, a) \qquad (3.30)$$

50

The net flow $\phi(a)$ is the difference between leaving flow and the entering flow and can be determined by equation (3.31)

$$\phi(a) = \phi^+(a) - \phi^-(a) \qquad (3.31)$$

Higher net flow value is preferred and based on that ranking is done.

3.7 FABRICATION AND DYNAMIC CHARACTERIZATION OF CGRP-PMC-MRF CORE SANDWICH BEAMS
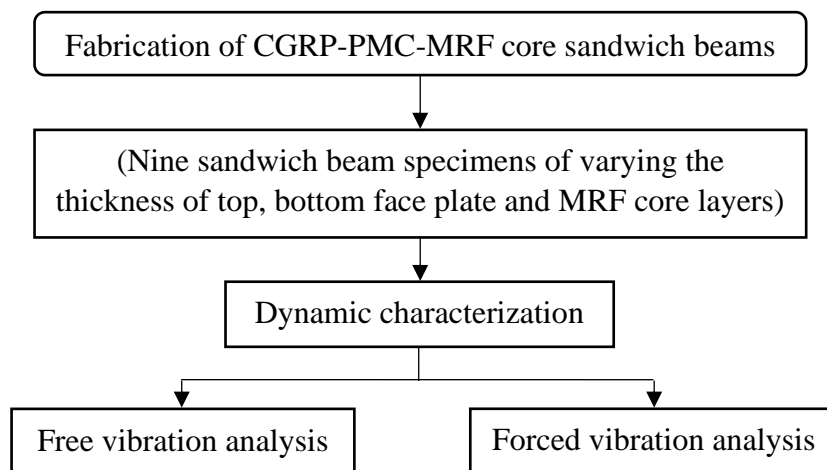
Figure 3.18 Fabrication and dynamic characterization of CGRP-PMC-MRF core sandwich beams

The methodology followed for the fabrication and dynamic characterization of CGRP-PMC-MRF core sandwich beams is shown in figure 3.18. Free vibration analysis is performed to determine the natural frequencies and damping ratio of CGRP-PMC-MRF core sandwich beams. Forced vibration analysis is performed to determine the frequency amplitude response of CGRP-PMC-MRF core sandwich beams.

3.7.1 Fabrication of CGRP-PMC-MRF core sandwich beams

The two-layer, four-layer, and six-layered CGRP-PMC materials of 2 mm, 3.5 mm and 5 mm thickness are used as top and bottom layers of sandwich beams. The inhouse prepared MRF is used as the core of the sandwich beams. Figure 3.19 shows the description of the CGRP-PMC-MRF core sandwich beam.
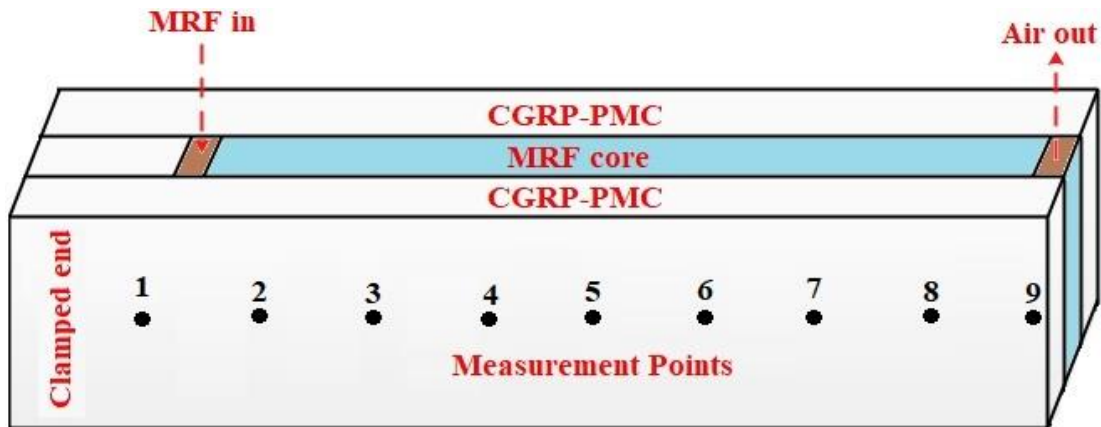
Figure 3.19 Description of CGRP-PMC-MRF core sandwich beam

The top and bottom layers of CGRP-PMC beam layers were fixed using Araldite adhesive, having 2 mm, 3.5 mm and 5 mm gap middle core. The typical thickness of araldite adhesive is 0.1 mm which is just sufficient to transfer the load. The effective thickness of araldite adhesive is 0.125 – 0.25 mm. (Okafor et al. (2005) and Ramji et al. (2013)). The ends of the middle core were covered using silicone sealant and a small gap is kept for filling MRF. The MRF is filled inside the middle core using a syringe. Then, the gap for filling MRF is also sealed using a silicone sealant. The prepared samples are kept for 12 hours curing at room temperature. Nine CGRP-PMC-MRF core sandwich beams are prepared and experimental free and forced vibration analysis is performed.

3.7.2 Free vibration analysis of CGRP-PMC-MRF core sandwich beams

MRF core sandwich beam has the ability to change its dynamic properties with the help of an external applied magnetic field. Figure 3.20 shows the schematic view of the experimental free vibration setup used for determining the natural frequency and damping ratios of CGRP-PMC-MRF core sandwich beams subjected to the influence of the external non-homogeneous magnetic field. The experimental setup consists of a modal analysis data acquisition software (DEWESoft) with the data acquisition system (Make: DEWETRON), gaussmeter, accelerometer sensor (Make: Kistler), four permanent magnets (ferrite iron magnets) and a fixture for holding the sandwich beams. Considering the permanent magnets placing, the two magnets are arranged in top plates in such a way that equal poles repel each other and the remaining two magnets are

52

arranged in bottom plates in such a way that top and bottom plate magnets magnetic poles attract each other (Lara-Prieto et al. (2010)).
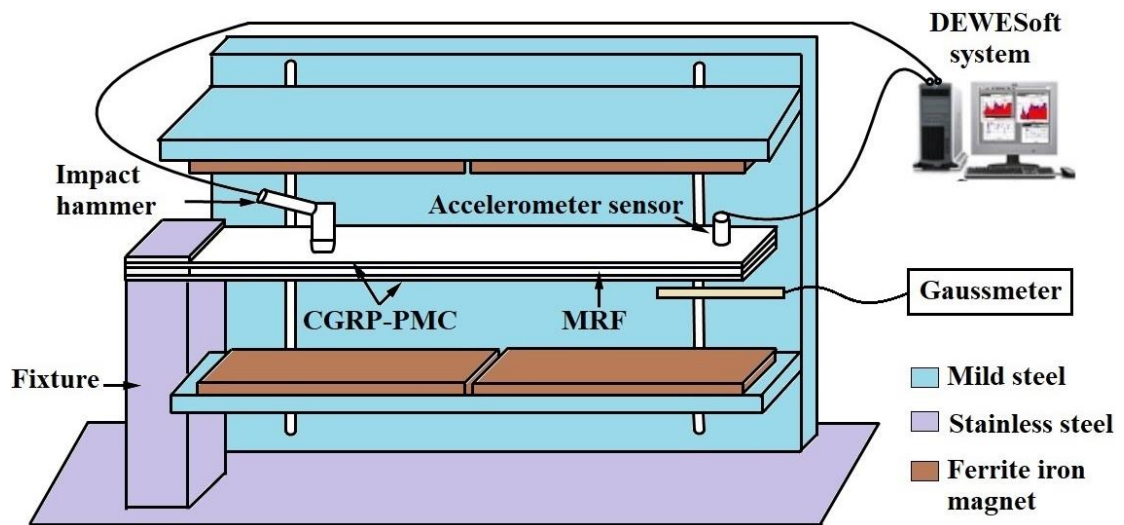
Figure 3.20 Schematic view of free vibration analysis experimental setup

The fixture and base of the experimental setup are made of stainless steel material. The top and bottom plates of the experimental setup are made of mild steel material. Hence, the ferrite iron permanent magnets are attached to the mild steel top and bottom plates.
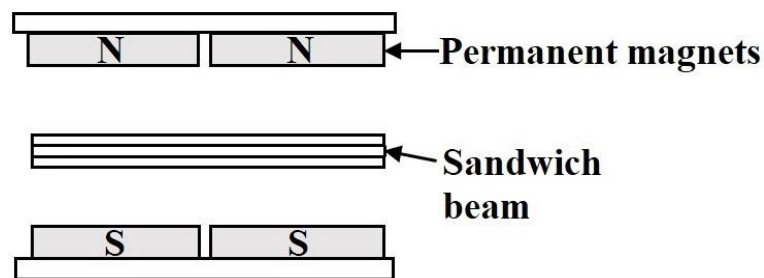
Figure 3.21 Schematic view of permanent magnets arrangement

Figure 3.21 shows the schematic view of permanent magnets arrangement. The distance between the top and bottom permanent magnets position is varied vertically for 0, 200, 400 and 600 gauss magnetic flux density. The magnetic flux density applied to the beam surface is measured using gaussmeter, horizontally at a 2 mm gap from the beam surface. The first three modes, natural frequency and damping ratios of sandwich

beams were determined through free vibration analysis. The dynamic behavior of sandwich structures determined at zero gauss magnetic flux density is considered as passive vibration excitations. Also, the dynamic behavior of sandwich structures analyzed at 200 G, 400 G and 600 G magnetic flux density conditions are considered as semi-active vibration control.

The frequency response function (FRF) curves generated while impacting with impulse hammer helps to determine the resonant frequency of the sandwich beams. The damping ratio was determined based on the circle fit method from the Nyquist circle plot. Figure 3.22 shows the Nyquist circle plot with resonant natural frequency and angular frequencies points. The angular frequency points one below and one above the resonant natural frequency point are noted in the Nyquist circle plot. The equation for calculating the damping ratio using the Nyquist circle plot is determined by equation (3.32).

$$\zeta = \frac{\omega_1^2 - \omega_2^2}{2\omega_n^2 \left[\tan \dfrac{\theta_1}{2} + \tan \dfrac{\theta_2}{2} \right]} \tag{3.32}$$

where ω_n refers to the resonant natural frequency, ω_1 and ω_2 are angular frequencies, θ_1 and θ_2 are the angles between angular frequencies.
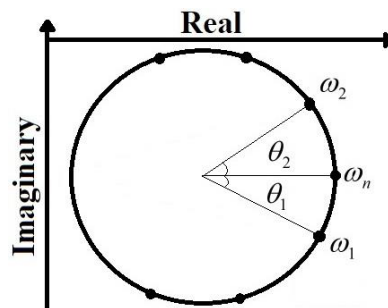
Figure 3.22 Nyquist circle plot

The schematic view of the flexibility of the CGRP-PMC-MRF core sandwich beam subjected to without magnetic field and with the magnetic field is shown in figure 3.23. The CGRP-PMC-MRF core sandwich beams have a smart behavior of controlling its displacement x to reduced displacement x-Δx by applying the external magnetic

54

field. Hence, the flexibility of the CGRP-PMC-MRF core sandwich beam can be controlled by applying the magnetic field. The stiffness of the CGRP-PMC-MRF core sandwich beam can be increased subjected to the external applied magnetic field. Equation (3.33) relates the natural frequency, stiffness, mass, acceleration due to gravity and the static deflection for a single degree of freedom system.

$$\omega_n = \sqrt{\frac{k}{m}} = \sqrt{\frac{g}{\delta}} \qquad (3.33)$$

where,

ω_n, k, m, g and δ are the natural frequency, stiffness, mass, acceleration due to gravity and the static deflection of the sandwich beam respectively.
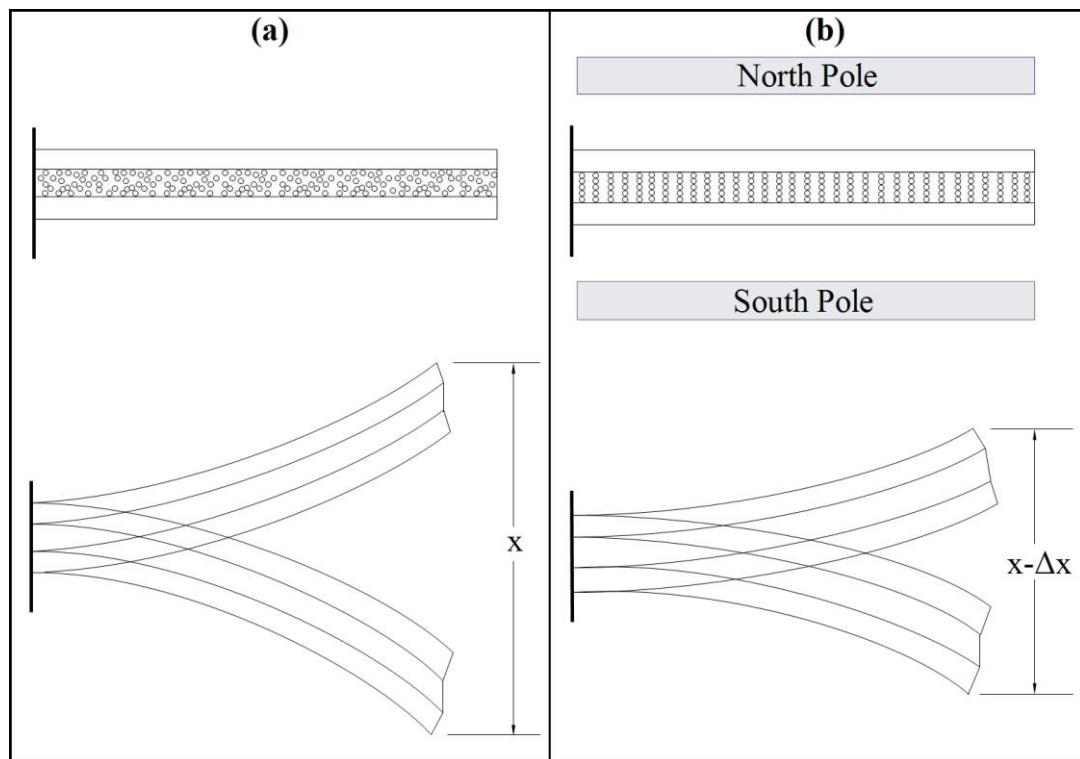
Figure 3.23 Schematic view of the flexibility of the CGRP-PMC-MRF core sandwich beam (a) without magnetic field, (b) with the magnetic field.

Free vibration modal analysis using impulse hammer excitation is carried out based on the ASTM E756-05 standard. The sandwich beam is marked with eight divisions of 25 mm distance for acquiring response data. The accelerometer sensor is

55

placed at 175 mm from the fixed end. The natural frequency and damping ratios of the fabricated CGRP-PMC-MRF core sandwich beams subjected to the influence of the external magnetic field are analyzed. (Ganapathi et al. (1999), Civalek (2004), Howson and Zare (2005), Han and Elliott (2007), Baltacıoglu et al. (2010), Romaszko (2013), Węgrzynowski (2014), Li et al. (2015), Mirzaei and Kiani (2016), Chuaqui et al. (2018), Vo-Duy et al. (2018)).

3.7.3 Forced vibration analysis of CGRP-PMC-MRF core sandwich beams

The schematic view of the experimental forced vibration analysis setup used to determine the excitation frequency amplitude response of the sandwich beams with and without the influence of the magnetic field is shown in figure 3.24.
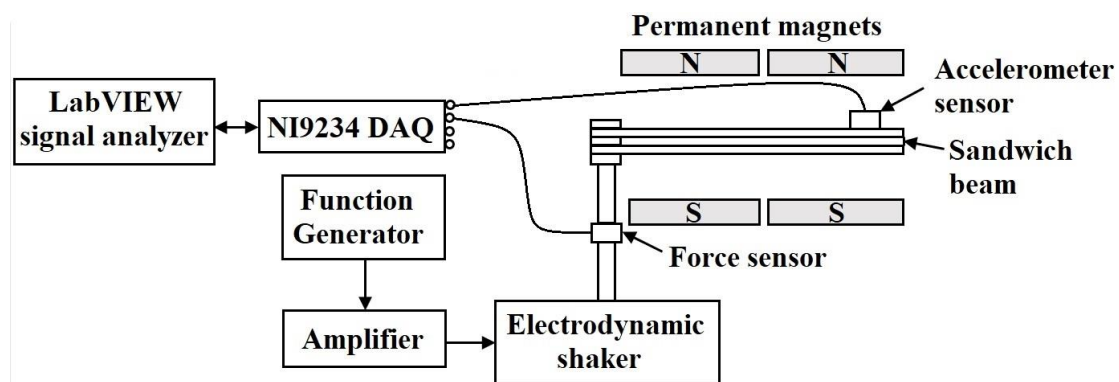
Figure 3.24 Schematic view of forced vibration analysis experimental setup

The experimental setup consists of 50 kgf electrodynamic shaker, digital switching power amplifier, function generator, accelerometer sensor, force transducer, NI 9234 DAQ and LabVIEW 2017 software. The CGRP-PMC-MRF core sandwich beams are analysed for harmonic sinusoidal base excitation varying from 10 to 1000 Hz. Using the function generator, the required electrodynamic shaker excitation information is sent to the amplifier. The input gain to the electrodynamic shaker is controlled using the amplifier. The accelerometer sensor measures the transverse vibration frequency response signals measured from CGRP-PMC-MRF core sandwich beams. The NI-9234 data acquisition (DAQ) collects the frequency response signals from the accelerometer sensor and analyzed using LabVIEW (Lara-Prieto (2009), Rajamohan (2010), Hu et al. (2011) and Kumar et al. (2015)).

3.8 DYNAMIC CHARACTERIZATION OF MMC-MRF CORE SANDWICH BEAMS

The same methodology followed for the dynamic characterization of CGRP-PMC-MRF core sandwich beams is followed for MMC-MRF core sandwich beams. Five sandwich beams of MRF core with 0, 5, 10, 15 and 20 wt% SiC_p reinforced Al6082 MMC top and bottom layers sandwich beams were prepared. The dynamic properties of the MMC-MRF core sandwich beam subjected to 0, 200, 400 and 600 Gauss magnetic flux density are analyzed through free and forced vibration analysis. The procedure for the fabrication of the MMC-MRF core sandwich beam is the same as mentioned in section 3.7.1. Free and forced vibration analysis of MMC-MRF core sandwich beams are experimentally investigated, the procedure is similar to the experimental investigation mentioned in section 3.7.2 and 3.7.3.

3.9 SUMMARY

This chapter describes the methodology and experimental details of the research work. The procedure for the preparation and characterization of MRF is described. The PMC and MMC fabrication using the hand-layup method and stir casting method was described. The physical, mechanical and dynamic characterization of the prepared composites were described. The procedure for the selection of optimal composites considering the physical, mechanical and dynamic properties using MADM techniques were described. The fabrication procedure for CGRP-PMC-MRF core sandwich beams and MMC-MRF core sandwich beams were described. The experimental procedure for the dynamic characterization of CGRP-PMC-MRF core sandwich beams and MMC-MRF core sandwich beams subjected to the influence of non-homogeneous magnetic fields were described.

CHAPTER 4

CHARACTERIZATION OF MAGNETORHEOLOGICAL FLUID

4.1 INTRODUCTION

Magnetorheological fluid (MRF) consists of micron-sized magnetizable particles suspended in a non-magnetic fluid medium and have the characteristics of large variations in their viscosity on the application of a magnetic field. This varying property of MRF makes them suitable for many applications. MRF applications are categorized into two classes: controllable devices (dampers, brake and clutches) and adaptive structures (beams, plates, bars, rods, aircraft wings and engine mounts).

4.2 MRF CHARACTERIZATION

The physical, mechanical and rheological characterization procedure for MRF is already been explained in chapter 3 methodology section 3.3.

4.2.1 Microstructure of CI_p

The primary characteristics of CI_p such as microstructure, particle size, and magnetic properties are determined. The microstructure of CI_p is observed by using the FESEM instrument (Make: ZEISS Sigma, Germany). Fig. 4.2 shows the microstructure of CI_p at 4000X magnification and figure 4.3 shows the microstructure of CI_p at 25000X magnification. Based on figures 4.1 and 4.2, the CI_p microstructure reveals near spherical shape with varying particle size. It is expected that the spherical shape CI_p provides a better rheological response to MRF than other shapes CI_p (Japka et al. 1988).
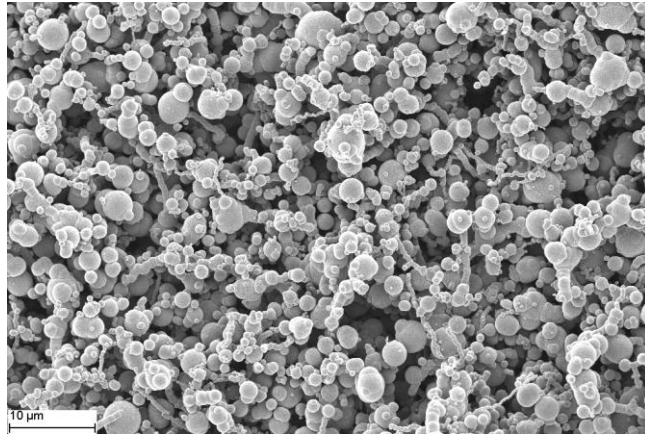
Figure 4.1 Microstructure of CI_p at 4000X magnification
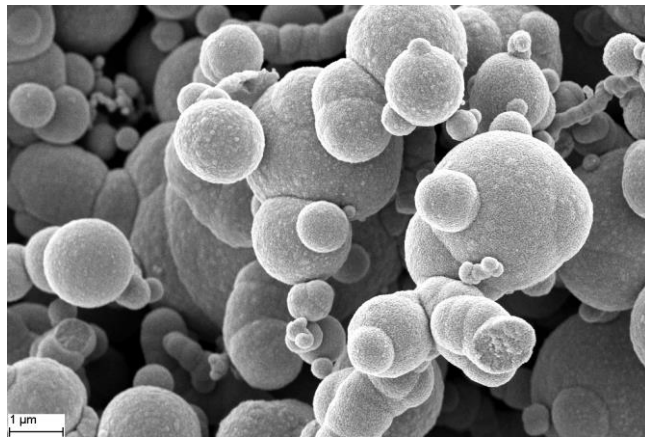
Figure 4.2 Microstructure of CI_p at 25000X magnification

4.2.2 CI_p size measurement

The particle size distribution (PSD) analysis is carried out to measure the average size of the CI_p. Fig. 4.3 shows the particle size histogram and cumulative values of CI_p measured using the particle size analyzer (Make: CILAS 1064).
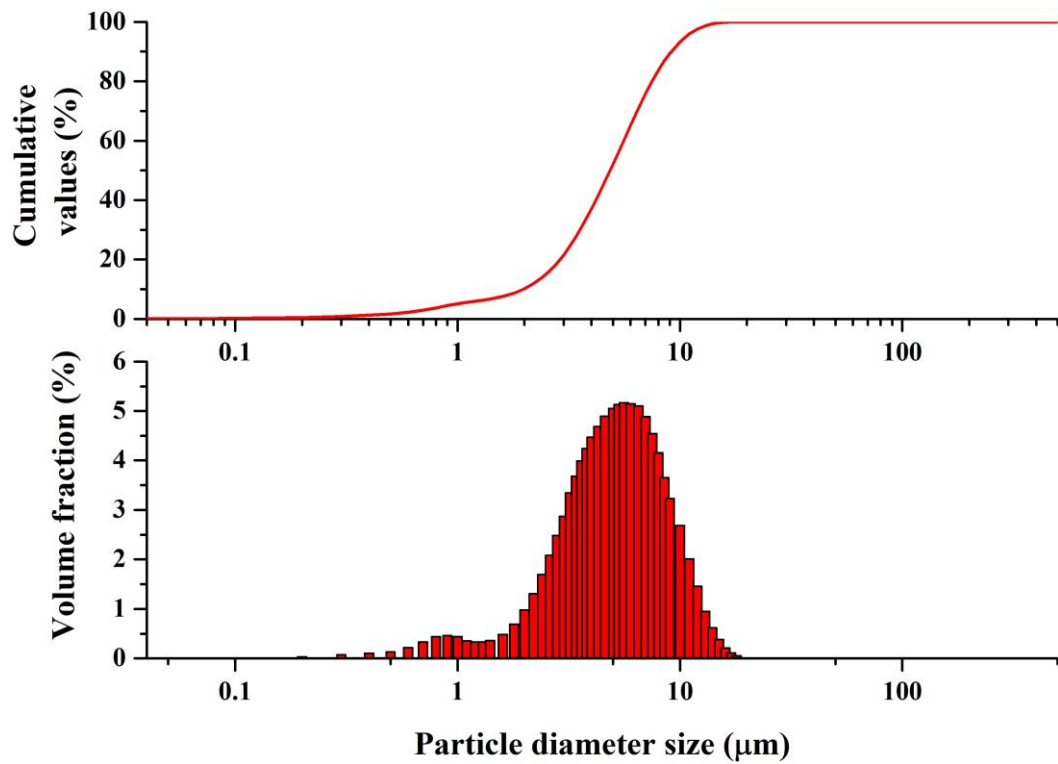
Figure 4.3 PSD of CI_p

The minimum and maximum diameter sizes of CI_p are observed as 0.04 µm and 17 µm. The average mean diameter of CI_p was measured as 5.27 µm. The average mean diameter of CI_p ranging between 1 µm to 10 µm provides better rheological properties in MRF (Japka et al. 1988). Hence the procured CI_p is suitable for the MRF preparation.

4.2.3 Magnetization of CI_p

The magnetic properties of CI_p are measured using a vibrating sample magnetometer (VSM) instrument. Figure 4.4 shows the magnetization properties of hysteresis loops of CI_p. The magnetic properties were measured in the powder state of CI_p by using a VSM. The magnetic properties of CI_p measured are shown in Table 4.1.

Table 4.1 Magnetic properties of CI_p

Coercivity	14.116 gauss
Saturation	2.1497 emu
Retentivity	8.5011×10^{-3} emu
Sensitivity	6 emu
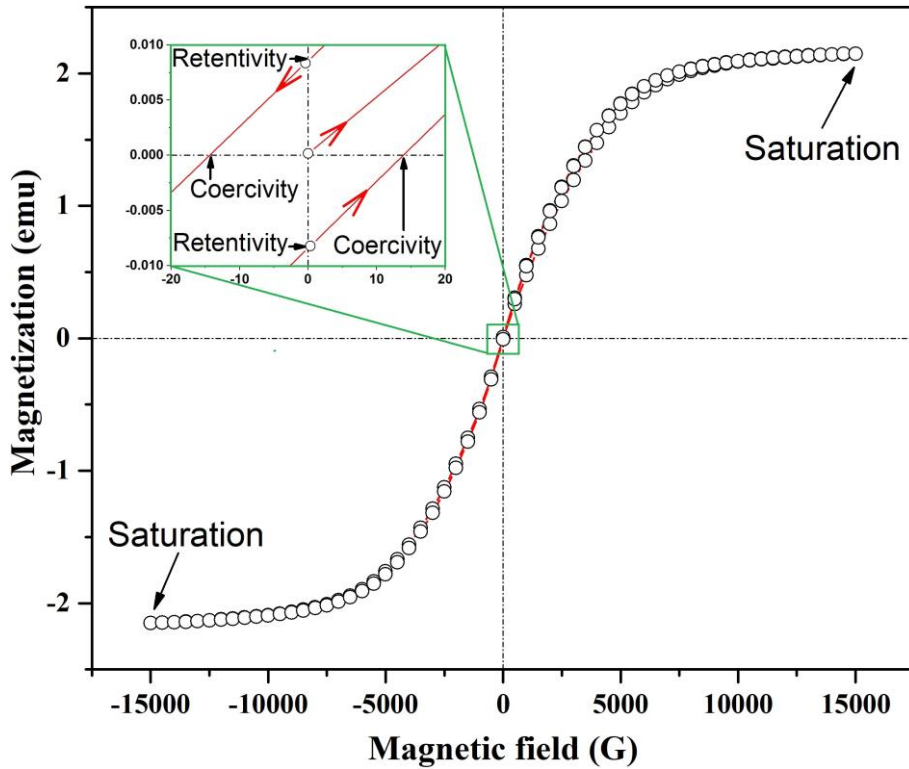
Figure 4.4 VSM data of magnetic CI_p

The MRF yield stress depends on the saturation magnetization of CI_p, higher the value of saturation magnetization indicates higher yield stress of MRF (Genc and Phule (2002)).

4.2.4 Sedimentation study

The sedimentation ratio is one of the important parameters that reveal the settling of CI_p in the carrier fluid. The density, size of CI_p mainly influences the sedimentation in the MRF. The sedimentation ratio of CI_p can be controlled by the addition of lithium grease in the MRF (Cheng et al. (2016 and 2018)). Settling of CI_p in carrier fluid is a serious problem that affects the performance of MRF. Since CI_p has a higher density than silicone oil, the CI_p will start to settle in the MRF after a certain period. Hence, sedimentation investigation is performed to determine the sedimentation ratio of the MRF. The inhouse prepared MRF was poured in a 50 ml glass beaker and the settling of CI_p was visually observed. Initially, the sedimentation readings were measured at an interval of 2 hours for the first couple of days. However, the

sedimentation of CI_P was found to be very minimum in the carrier fluid, the MRF sedimentation measurement was carried out for 24 hours interval.
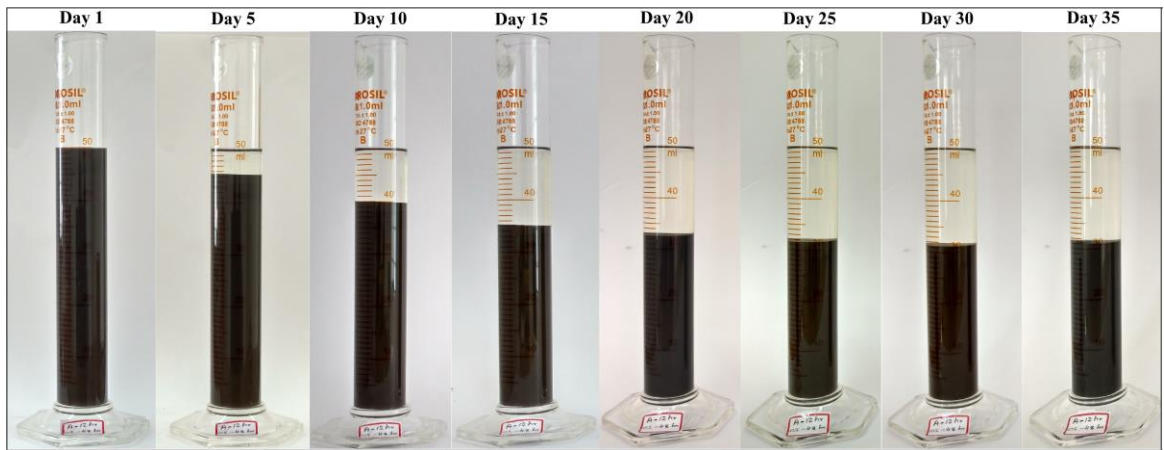
Figure 4.5 MRF sedimentation visual observation images

The visual observation of MRF sedimentation in the beaker was observed and sedimentation images of day 1st day, 5th day, 10th day, 15th day, 20th day, 25th day, 30th day and 35th day are shown in figure 4.5.
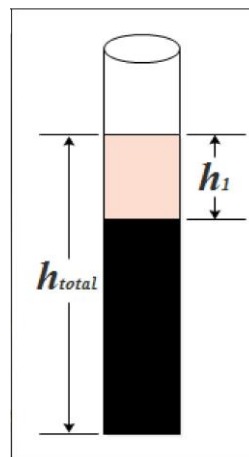
Figure 4.6 Sedimentation ratio measurement

The schematic view of measuring the sedimentation ratio of MRF by visual observation is shown in figure 4.6. The sedimentation ratio (SR) is the ratio of the height of CI_P settled (h_1) to the total height of the MRF column (h_{total}) measured during the time (t) (Cheng et al. (2016 and 2018)). The equation for calculating the sedimentation ratio SR(t) is given by equation (4.1).

$$SR(t) = \frac{h_1}{h_{total}} \tag{4.1}$$
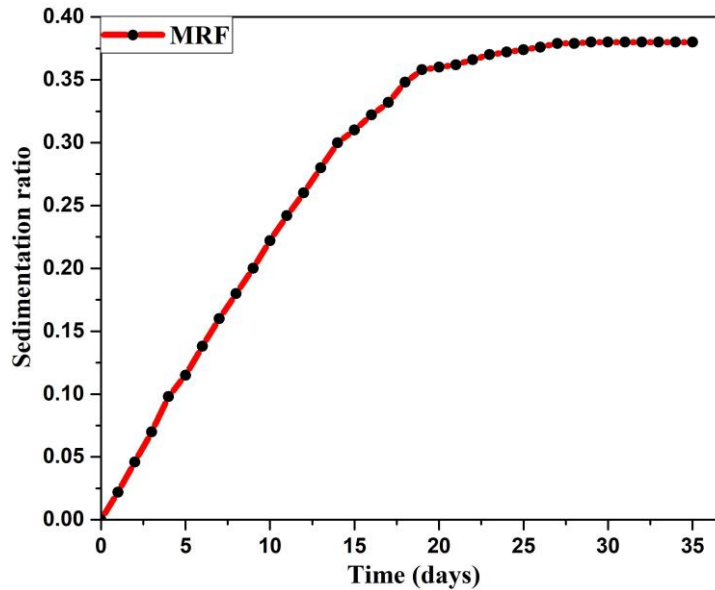
Figure 4.7 Sedimentation ratio of MRF

The sedimentation ratio of MRF measured in a 50 ml glass beaker with respect to time is shown in figure 4.7. The sedimentation ratio result reveals that CI_p got completely settled after 28 days. Therefore, the in-house prepared MRF has very good sedimentation stability. Also, based on the sedimentation study, all the experimental work has been performed immediately after preparing MRF. Hence, the rheological characterization of MRF and vibration analysis of sandwich beams was performed immediately after the preparation of MRF.

4.2.5 Rheological Characterization

The rheological properties of MRF are measured using a rheometer (Make: MCR 702 Anton Paar) as shown in figure 3.4. The inhouse prepared MRF is placed between 20 mm diameter parallel plates with a 1 mm gap between them and rheological analysis was performed. The rheological properties of MRFs are examined with and without the magnetic field at a temperature of 25 °C. The oscillatory frequency sweep test is carried out for 0.1–100 Hz frequency with a constant shear strain amplitude of 0.1%. Since the MRF is used as the core for composite sandwich beams, the frequency

sweep test was analyzed. Figure 4.8 shows the viscosity versus magnetic flux density of MRF at a constant shear rate of 1 s^{-1}. It is observed that the viscosity of MRF increased with an increase in magnetic flux density and saturated at 0.63 T.
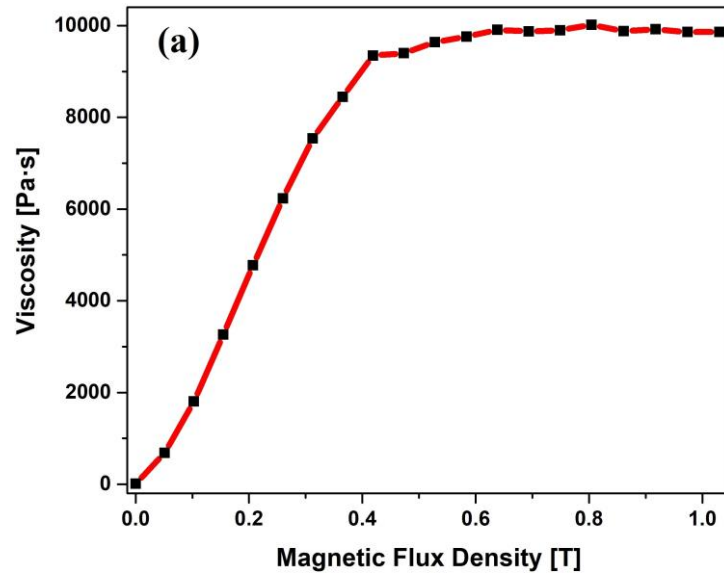
Figure 4.8 Viscosity versus magnetic flux density

Figure 4.9 shows the viscosity and shear stress versus the shear rate at zero magnetic flux density. The results showed that without the magnetic field, the MRF behaves as the shear-thinning fluid i.e. increase in shear rate results in the reduction of viscosity of MRF. It is observed that at 0.1 s^{-1} shear rate, the viscosity of MRF is 73.83 Pa-s and at 100 s^{-1} shear rate, the viscosity of MRF is reduced to 1.18 Pa-s. It is also observed that the shear stress of MRF increased with an increase in the shear rate at zero magnetic flux density.
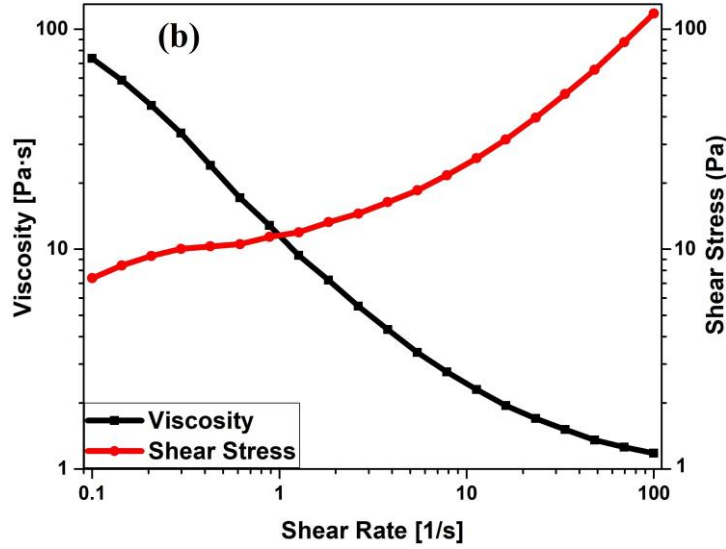
Figure 4.9 Viscosity and shear stress versus shear rate

The rheological properties of MRF measured at 0.1% shear strain for four different magnetic flux densities are shown in figures 4.10-4.15. Complex shear modulus (G^*) expressed as a function of frequency (ω) is related to the storage modulus (G') and loss modulus (G'') of MRF and it is given by Eq. (4.2). Also, the storage modulus and loss modulus support to determine the loss factor (η) of the MRF and it is given by Eq. (4.3).

$$\mathbf{G^*(\omega) = G'(\omega) + iG''(\omega)} \tag{4.2}$$

$$\mathbf{\eta(\omega) = \frac{G''(\omega)}{G'(\omega)}} \tag{4.3}$$

The variation in complex shear modulus versus frequency corresponding to different magnetic flux densities is shown in figure 4.10. The result reveals that the complex shear modulus of MRF increased by increasing the applied magnetic flux density. Also, the complex shear modulus of MRF increased with an increase in the oscillating frequency.
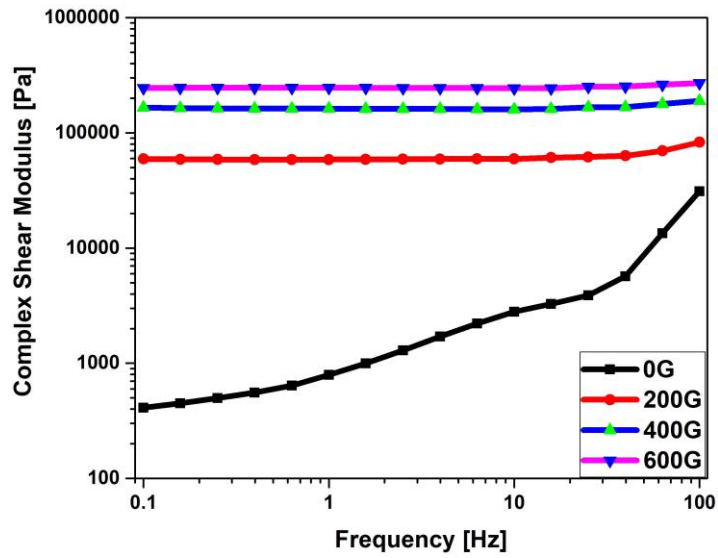
Figure 4.10 Complex shear modulus versus frequency

The variation of storage modulus versus frequency for different magnetic flux densities is shown in figure 4.11. At zero gauss magnetic flux density, it is observed that the MRF storage modulus increased with increase in frequency from 0.1 Hz to 25 Hz frequency and with further increase in frequency the storage modulus shows a decreasing trend. However, at 200 G, 400 G, and 600 G gauss magnetic flux densities the storage modulus of MRF increased with an increase in frequency. It is also observed that the storage modulus increased with the increase in the applied magnetic flux densities.
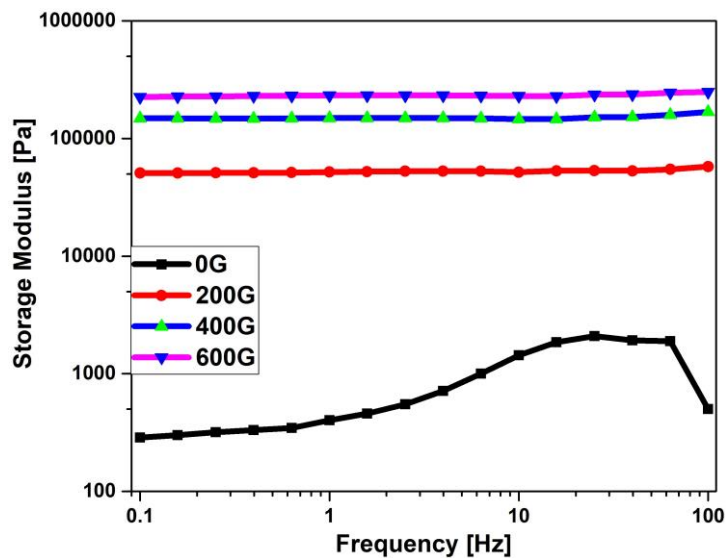
Figure 4.11 Storage modulus versus frequency
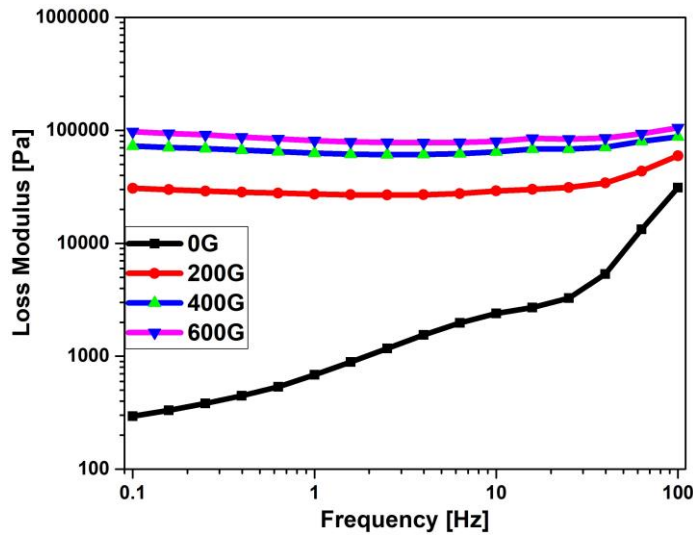
Figure 4.12 Loss modulus versus frequency

The loss modulus versus frequency of MRF for different magnetic flux densities is shown in figure 4.12. The result reveals that the loss modulus of MRF enhanced with increase in the magnetic flux density. Based on figures 4.11 and 4.12, it is observed that at the absence of magnetic field, the magnitude of loss modulus obtained is higher than the magnitude of the storage modulus. However, at 200 G, 400 G, and 600 G magnetic flux densities the magnitude of storage modulus is higher than the magnitude of the loss modulus.
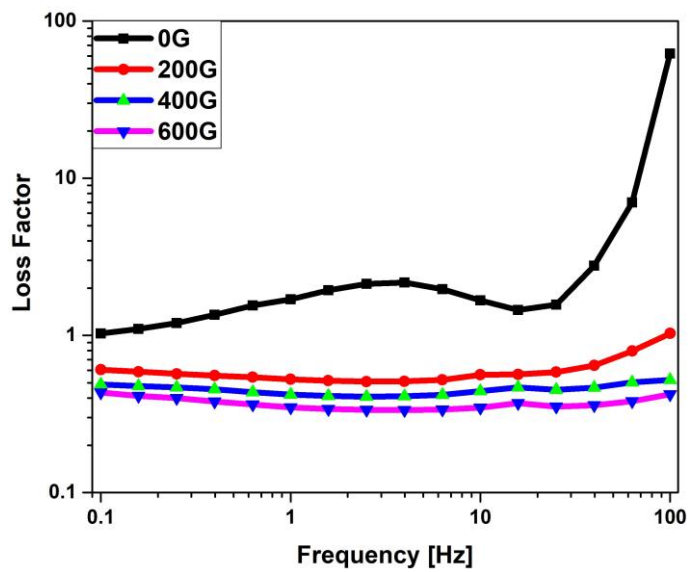
Figure 4.13 Loss factor versus frequency

The loss factor versus frequency corresponding to different magnetic flux densities is shown in figure 4.13. The result indicates that the loss factor of MRF decreased with an increase in the magnetic flux density.
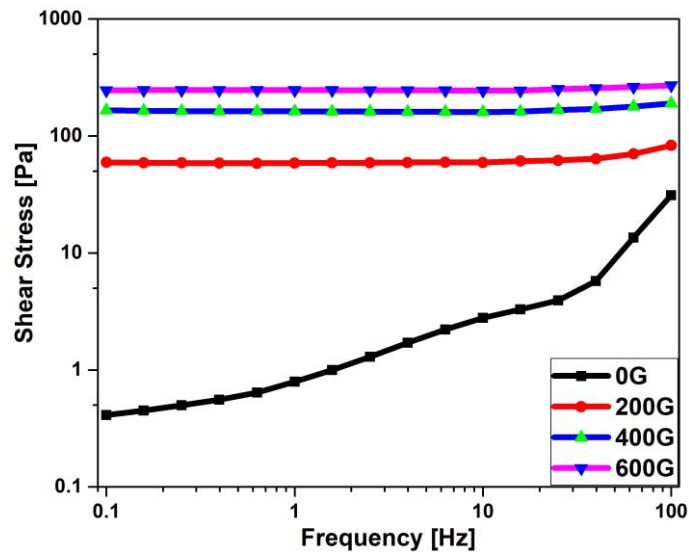
Figure 4.14 Shear stress versus frequency

The shear stress versus frequency corresponding to different magnetic flux density is shown in figure 4.14. Since the analysis was carried for 0.1% shear strain, linear shear stress was observed from 0.1 Hz to 10 Hz frequency. However, the shear stress of MRF increased with an increase in the external applied magnetic flux density and at higher than 10 Hz frequencies.
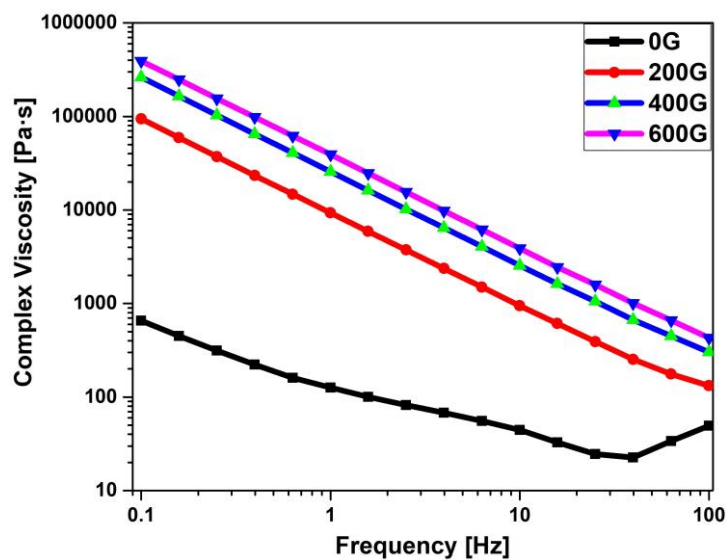
Figure 4.15 Complex viscosity versus frequency

Table 4.2 MRF rheological properties equations at different magnetic flux density as a function of frequency

MRF	Magnetic flux density (gauss)	As a function of frequency, ω (Hz)
Complex shear modulus (G^*) (Pa)	0	$G^* = -0.001518\omega^4 + 0.2985\omega^3 - 15.17\omega^2 + 356.4\omega + 436.6$
	200	$G^* = -0.000634\omega^4 + 0.1212\omega^3 - 5.082\omega^2 + 173.8\omega + 5.87\text{e}+04$
	400	$G^* = 0.001718\omega^4 - 0.3801\omega^3 + 28.1\omega^2 - 459\omega + 1.631\text{e}+05$
	600	$G^* = 0.001807\omega^4 - 0.4014\omega^3 + 28.7\omega^2 - 420.8\omega + 2.463\text{e}+05$
Storage modulus (G') (Pa)	0	$G' = -0.0003292\omega^4 + 0.06939\omega^3 - 5.269\omega^2 + 164.9\omega + 234.5$
	200	$G' = -0.0008801\omega^4 + 0.1776\omega^3 - 10.8\omega^2 + 249.4\omega + 5.134\text{e}+04$
	400	$G' = 0.0006379\omega^4 - 0.1552\omega^3 + 13.29\omega^2 - 219\omega + 1.488\text{e}+05$
	600	$G' = -0.0005559\omega^4 + 0.06432\omega^3 - 0.4654\omega^2 + 150.9\omega + 2.301\text{e}+05$
Loss modulus (G'') (Pa)	0	$G'' = -0.001468\omega^4 + 0.2834\omega^3 - 13.67\omega^2 + 308.8\omega + 370.1$
	200	$G'' = 0.0004345\omega^4 - 0.1034\omega^3 + 10.12\omega^2 - 99.9\omega + 2.842\text{e}+04$
	400	$G'' = 0.002898\omega^4 - 0.603\omega^3 + 39.84\omega^2 - 638.3\omega + 6.656\text{e}+04$
	600	$G'' = 0.006644\omega^4 - 1.319\omega^3 + 83.13\omega^2 - 1593\omega + 8.771\text{e}+04$
Loss factor (η)	0	$\eta = 1.367\text{e}-06\omega^4 + -9.5\text{e}-05\omega^3 + 0.00175\omega^2 + 0.01358\omega + 1.524$
	200	$\eta = 1.855\text{e}-08\omega^4 - 4.097\text{e}-06\omega^3 + 0.0003192\omega^2 - 0.004733\omega + 0.5542$
	400	$\eta = 1.824\text{e}-08\omega^4 - 3.703\text{e}-06\omega^3 + 0.000232\omega^2 - 0.003673\omega + 0.4473$
	600	$\eta = 3.028\text{e}-08\omega^4 - 5.941\text{e}-06\omega^3 + 0.000368\omega^2 - 0.007268\omega + 0.3817$
Shear Stress (τ) (Pa)	0	$\tau = -1.504\text{e}-06\omega^4 + 0.0002956\omega^3 - 0.01501\omega^2 + 0.3552\omega + 0.4373$
	200	$\tau = -3.777\text{e}-07\omega^4 + 7.08\text{e}-05\omega^3 - 0.002203\omega^2 + 0.1335\omega + 58.73$
	400	$\tau = 2.879\text{e}-06\omega^4 - 0.0005985\omega^3 + 0.03982\omega^2 - 0.6109\omega + 163.2$
	600	$\tau = 2.936\text{e}-06\omega^4 - 0.0006155\omega^3 + 0.04031\omega^2 - 0.5741\omega + 246.4$
Complex viscosity (ν) (Pa s)	0	$\nu = 0.0001759\omega^4 - 0.03523\omega^3 + 2.234\omega^2 - 49.5\omega + 305.2$
	200	$\nu = 0.02677\omega^4 - 5.32\omega^3 + 331.7\omega^2 - 7109\omega + 3.698\text{e}+04$
	400	$\nu = 0.07455\omega^4 - 14.81\omega^3 + 923.6\omega^2 - 1.979\text{e}+04\omega + 1.028\text{e}+05$
	600	$\nu = 0.1115\omega^4 - 22.16\omega^3 + 1382\omega^2 - 2.962\text{e}+04\omega + 1.541\text{e}+05$

The variation in complex viscosity for MRF was determined with respect to the frequency at different magnetic flux densities and the same is shown in figure 4.15. The complex viscosity of MRF decreases with an increase in frequency at a constant magnetic flux density. This reduction in complex viscosity indicates the shear-thinning effect of MRF. However, the complex viscosity increases with increase in the external applied magnetic flux density. Non-newtonian complex viscosity of MRF plays an important role in the behavior of the MRF. Complex viscosity is the combination of steady shear viscosity and viscous viscosity measured under the linear viscoelastic region of MRF (Jolly et al. 1999). However, the complex viscosity of MRF decreased with an increase in oscillatory frequency. It also increased with increase in the applied magnetic flux density. The fourth-order polynomial equations are obtained for the MRF rheological properties with respect to the frequency using curve fitting through MATLAB software and are shown in Table 4.2.

4.3 CONCLUSIONS

The MRF is prepared with 30% volume CI_p and 70% volume silicone oil. The microstructure, particle size distribution, magnetization, and sedimentation ratio of CI_p were determined. The CI_p has a high saturation magnetization of 2.1497 emu and the MRF showed good sedimentation stability where particles settled completely after 28 days. The oscillatory frequency sweep rheological characterization of the MRF with and without the magnetic field was analyzed. The results showed that without the magnetic field, the MRF behaves as a shear-thinning fluid. It was found that the complex shear modulus, storage modulus, loss modulus, complex viscosity and shear stress rheological properties of MRF increases with the increase in applied magnetic flux density. Whereas, the loss factor of MRF decreased with the increase in the applied magnetic flux density. Also, the complex viscosity of MRF decreased with increasing oscillating frequency.

4.4 SUMMARY

This chapter includes the preparation, physical and rheological characterization of MRF. The oscillatory frequency sweep rheological characterization of the MRF with

and without the magnetic field was analyzed. The rheological properties of MRF subjected to 0 G, 200 G, 400 G and 600 G magnetic flux densities are determined.

CHAPTER 5

CHARACTERIZATION OF POLYMER MATRIX COMPOSITE

5.1 INTRODUCTION

Composites play a vital role in engineering applications. Chopped strand mat (CSM) glass fiber reinforced unsaturated polyester resin polymer matrix composites (CGRP-PMC) are being exposed for use in many structural applications because of their high strength and stiffness to weight ratio. Due to their excellent structural performance, the CGRP-PMC are applied in automobile, aerospace, buildings, marine and military applications. In this chapter, physical, mechanical and dynamic characterization of two-layer, four-layer and six-layered CGRP-PMC are analysed and optimal PMC is selected using MADM techniques.

5.3 CHARACTERIZATION OF PMC

The physical, mechanical and dynamic characterization procedure for CGRP-PMC material is already been explained in chapter 3 methodology section 3.4.

5.3.1 Density

The density is the physical property of a material. The procedure for measuring the actual and theoretical density of the CGRP-PMC material is mentioned in chapter 3 methodology section 3.4.3. Based on the analysis it was found that the density of six-layered CGRP-PMC specimen is lower than two-layer and four-layered CGRP-PMC specimens. The reason for the reduction in density is due to increase in porosity (or voids/micro voids/air gaps). The porosity in the CGRP-PMC increases with increase in the number of layers of CSM glass fiber (Butt et al. (2019)). Figure 5.1 shows the density measurement apparatus used to measure the density of the materials. Table 5.1 shows the actual and theoretical densities of the CGRP-PMC materials.

Figure 5.1 Density measurement kit

Table 5.1 Density of CGRP-PMC

CGRP-PMC	Density	
	Actual (g/cm^3)	Theoretical (g/cm^3)
Two-layers	1.456	1.464
Four-layers	1.463	1.491
Six-layers	1.445	1.519

5.3.2 Tensile characterization

The tensile characteristics of CGRP-PMC specimen are obtained to analyze the effectiveness and behavior of composites against the tensile load. The procedure for conducting tensile characterization is mentioned in chapter 3 methodology section 3.4.4. Figure 5.2 shows the experimental setup for the CGRP-PMC specimen.

Figure 5.2 Experimental tensile setup

The experimental tensile test results of two-layer, four-layer, six-layered CGRP-PMC specimens are shown in figure 5.3 and Table 5.2. The results reveal that for CGRP-PMC the nature of material failure has occurred by means of linear plastic strain. Six-layered CGRP-PMC material has achieved maximum tensile stress of 144 MPa, two-layer and four-layered CGRP-PMC material has tensile stress of 81.6 and 118 MPa respectively. From the results obtained, it is identified that the tensile strength of CGRP-PMC improved with increase in the number of layers of CSM glass fiber reinforcement.
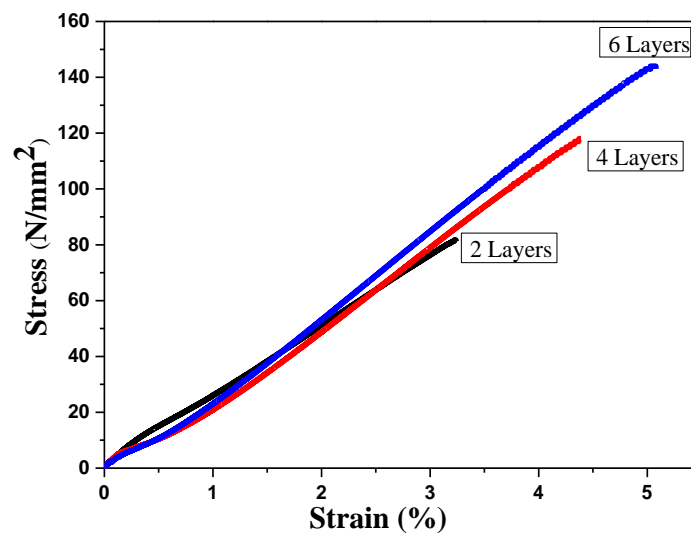
Figure 5.3 Tensile stress versus strain curve of CGRP-PMC specimens

Table 5.2 Tensile properties of CGRP-PMC

Composite samples	Tensile load (N)	Tensile stress (MPa)	Tensile Modulus (MPa)	Elongation (%)
Two-layers	4070	81.6	3280	3.25
Four-layers	10900	118	3390	4.41
Six-layers	18500	144	3800	5.08

5.3.3 Bending (Flexural) Test

The flexural experimental result helps to determine the maximum bending load and maximum bending stress that CGRP-PMC material can withstand when external bending load is applied. The procedure for conducting flexural characterization is mentioned in chapter 3 methodology section 3.4.5. The experimental flexural results are shown in figure 5.4 and Table 5.3.

Based on the results obtained, it is observed that the two-layered CGRP-PMC material has more strain percentage with respect to stress than four-layer and six-layered CGRP-PMC material. Hence, it is identified that the two-layered CGRP-PMC material has less stiffness compared to four-layer and six-layered CGRP-PMC material. Also, it is determined that the six-layered CGRP-PMC specimen has the maximum ability to withstand the bending load when compared to two-layer and four-layered CGRP-PMC material. It is inferred that the strength and flexural modulus of CGRP-PMC increases with increase in the number of layers of CSM glass fiber reinforcement.
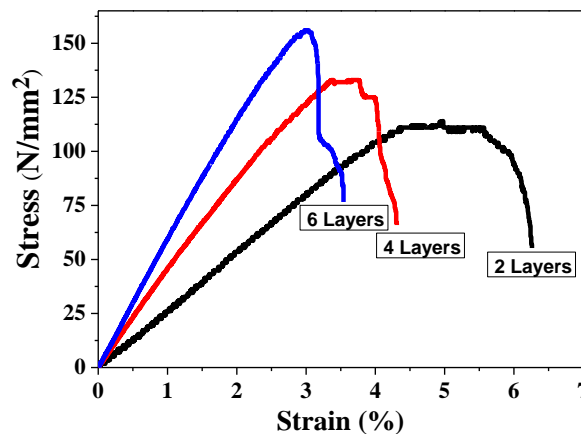
Figure 5.4 Flexural stress versus strain curve of CGRP-PMC specimens

Table 5.3 Flexural properties of CGRP-PMC

CGRP-PMC samples	Maximum flexural load (N)	Flexural Stress (MPa)	Flexural Modulus (MPa)
Two-layers	110	114	2700
Four-layers	280	133	4490
Six-layers	398	156	5910

5.3.4 Charpy Impact Test

The Charpy impact test has been carried out to find the impact strength and absorbed energy of CGRP-PMC specimens. The procedure for conducting Charpy impact test characterization is mentioned in chapter 3 methodology section 3.4.6. Figures 5.5 and 5.6 show the impact strength and absorbed energy of two-layer, four-layer and six-layered CGRP-PMC specimens.
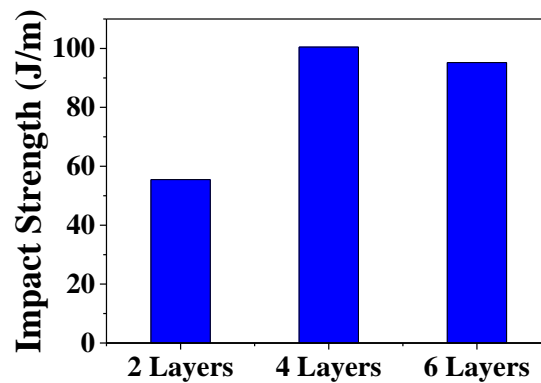
Figure 5.5 Impact strength of CGRP-PMC specimens

It is observed that the four-layered CGRP-PMC have higher impact strength than two-layer and six-layered CGRP-PMC specimens. The six-layered CGRP-PMC specimens have higher absorbed energy than two-layer and four-layered CGRP-PMC specimens.
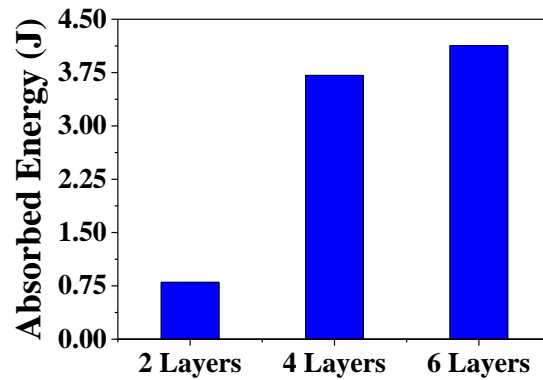
Figure 5.6 Absorbed energy of CGRP-PMC specimens.

The cross-sectional SEM images of two-layer, four-layer and six-layered CGRP-PMC specimens subjected to the Charpy impact test are shown in figures 5.7-5.9. These SEM images help to identify the interface between the matrix and reinforcement of CGRP-PMC materials. Figure 5.9 shows the fractured matrix and separated CSM glass fiber reinforcement of the two-layered CGRP-PMC specimen. Figures 5.10 and 5.11 reveal that the behavior of failure of CGRP-PMC materials due to the impact test arises through polyester matrix breakage and CSM glass fiber reinforcement pull out.
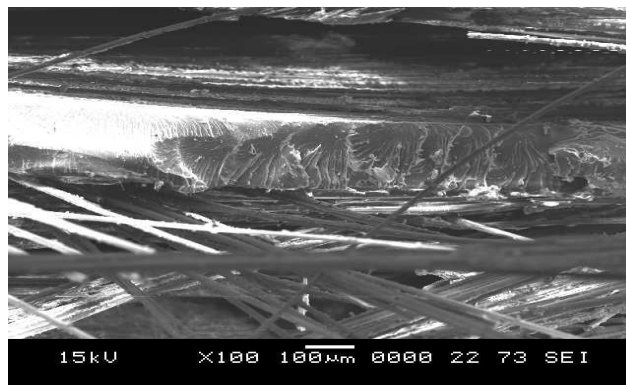
Figure 5.7 Cross-sectional SEM image of two-layer CGRP-PMC specimens
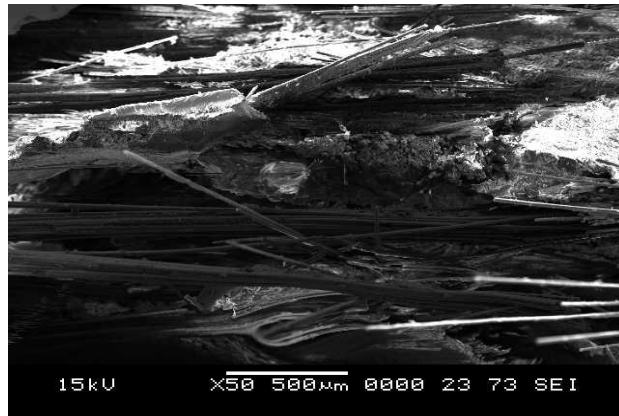
Figure 5.8 Cross-sectional SEM image of four-layer CGRP-PMC specimens
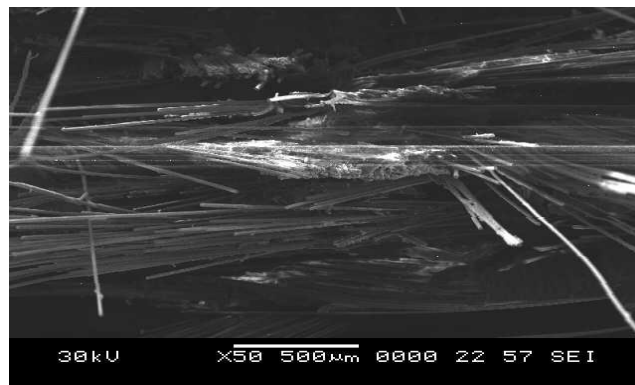
Figure 5.9 Cross-sectional SEM image of six-layer CGRP-PMC specimens

5.3.5 Fracture toughness

The fracture toughness test has been carried out to determine the ability of CGRP-PMC specimens containing a crack to resist fracture. Figure 5.10 shows the two-layered CGRP-PMC specimen fracture toughness testing in UTM.

Figure 5.10 Fracture toughness testing in UTM

The fracture toughness results of two-layer, four-layer, and six-layered CGRP-PMC specimens are shown in figure 5.11. The fracture toughness result reveals that the ultimate force required for fracturing the specimen increase with the increase in layers, whereas ultimate stress and modulus of elasticity of four-layered CGRP-PMC specimen is higher than two-layer and six-layered CGRP-PMC specimens.
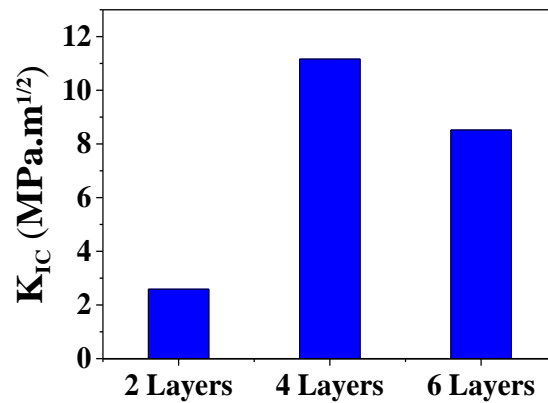
Figure 5.11 Fracture toughness of CGRP-PMC specimens

5.3.6 Interlaminar Shear Strength

The interlaminar shear strength (ILSS) result of CGRP-PMC specimens is shown in figure 5.12. The maximum ILSS occurred at the mid thickness of the beam. Based on the experimental result obtained, the four-layered CGRP-PMC material has more ILSS than two-layer and six-layered CGRP-PMC specimens.
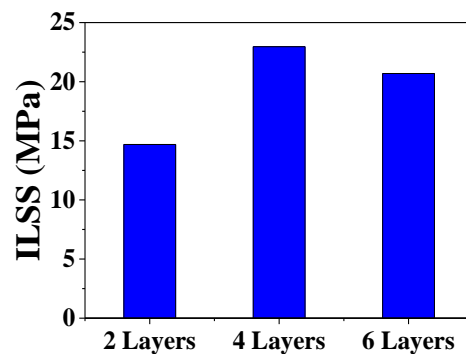
Figure 5.12 Interlaminar shear strength of CGRP-PMC specimens.

5.3.7 Experimental free vibration analysis

The transverse vibrations of two-layer, four-layer, and six-layered CGRP-PMC cantilever beams were determined using free vibration analysis. The modal analysis impulse hammer was used to excite the CGRP-PMC beams. The time-domain signals are converted into frequency domain signals using fast Fourier transform (FFT). The natural frequency of the beam is determined from the periodic peaks of the FFT curve.
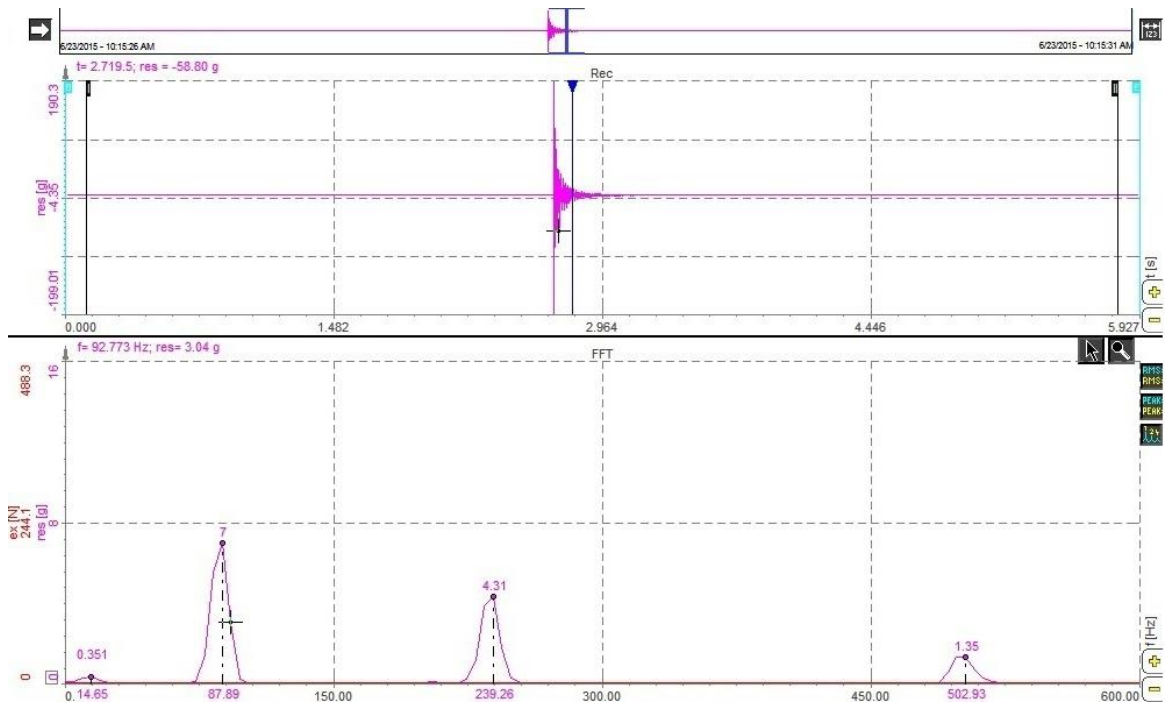
Figure 5.13 Experimental free vibration analysis of two-layer CGRP-PMC beam

Figure 5.13 shows the experimental free vibration results of two-layered CGRP-PMC composite beam measured using DEWESOFT software. The first four modes of natural frequencies and damping ratios of CGRP-PMC cantilever beams are measured and shown in Table 5.4. The natural frequency of CGRP-PMC has increased with respect to an increase in the number of layers of CSM in CGRP-PMC materials. Hence, from the experimental result, it was found that natural frequencies of CGRP-PMC material will increase with increase in the number of layers of CSM.

Table 5.4 Experimental free vibration analysis results

CGRP-PMC	1st mode		2nd mode		3rd mode		4th mode	
	Natural freq. (Hz)	Damping ratio	Natural freq. (Hz)	Damping ratio	Natural freq. (Hz)	Damping ratio	Natural freq. (Hz)	Damping ratio
Two-layers	14.65	0.027732	87.89	0.025274	239.26	0.028854	502.93	0.024113
Four-layers	29.30	0.021949	165.5	0.021077	512.70	0.023292	1044	0.025174
Six-layers	48.83	0.026901	292.97	0.022815	786.13	0.025145	1513.87	0.02421

5.4 MADM

The optimal CGRP-PMC specimen depending on the physical, mechanical and dynamic properties were determined by using MADM techniques such as AHP, TOPSIS and PROMETHEE. The steps involved in solving MADM techniques are discussed in detail in section 3.6. After the determination of the weights of various attributes utilizing the AHP method, the MADM techniques were connected to the CGRP-PMC selection problem.

5.4.1 Analytical hierarchy process (AHP)

Step 1: Determining the number of Alternatives and Attributes

This study has three alternatives and eight attributes. Figure 5.14 shows the objectives (selection of best composite), attributes (density, UTS, bending strength, impact strength, absorbed energy, damping ratio, fracture toughness, ILSS) and alternatives (two-layer, four-layer, and six-layered CGRP-PMC) represented in a hierarchical structure.
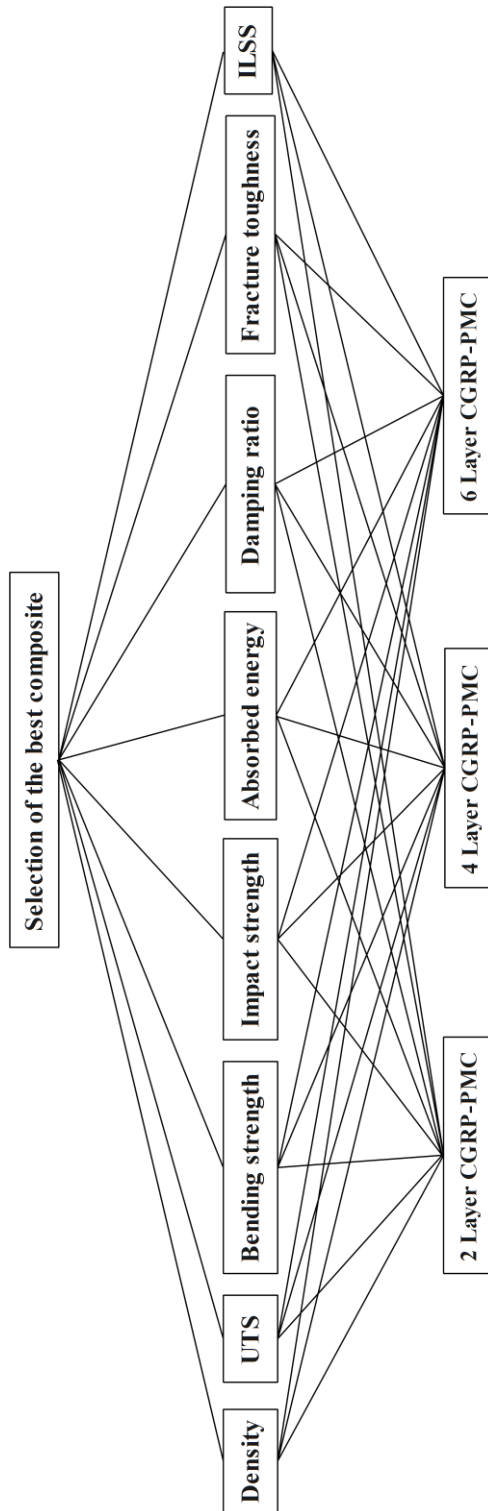
Figure 5.14 Decision hierarchy structure

Table 5.5 Data of CGRP-PMC

Sl. No	CGRP-PMC	Density g/cm^3	UTS (MPa)	Bending strength (MPa)	Impact strength (KJ/m^2)	Absorbed Energy (J)	Damping ratio	Fracture Toughness (MPa.m$^{1/2}$)	ILSS (MPa)
1	Two-layers	1.456	81.6	114	57.39	0.81	0.0277	2.59	14.69
2	Four-layers	1.463	118	133	104.76	3.74	0.0219	11.165	22.96
3	Six-layers	1.445	144	156	96.19	4.42	0.0269	8.52	20.69

The experimental data for three CGRP-PMC alternative specimens are shown in Table 5.5. The main objective is to select the best CGRP-PMC considering the physical, mechanical and dynamic properties. In the given attributes, considering the density low value is preferred whereas mechanical and dynamic properties such as

UTS, bending strength, impact strength, absorbed energy, damping ratio, fracture toughness and ILSS, high values are preferred.

Step 2: Normalization matrix

The CGRP-PMC data present in table 5.5 is normalized as,

Density	UTS	Bending strength	Impact strength	Absorbed energy	Damping ratio	Fracture toughness	ILSS
0.99244	0.56666	0.73076	0.54782	0.18325	1	0.23197	0.63980
0.98769	0.81944	0.85256	1	0.84615	0.79146	1	1
1	1	1	0.91819	1	0.97003	0.76309	0.90113

Step 3: Determining the relative importance matrix (Decision maker)

The relative importance matrix is decided depending on the wide application of PMC. The damping ratio is considered as the most important attribute when compared to other parameters, followed by UTS, bending strength, impact strength, absorbed energy, density, fracture toughness and interlaminar shear strength.

	Density	UTS	Bending strength	Impact strength	Absorbed energy	Damping ratio	Fracture toughness	ILSS
Density	1	1/3	1/3	1/2	1/2	1/4	2	2
UTS	3	1	1	2	2	1/2	4	4
Bending strength	3	1	1	2	2	1/2	4	4
Impact strength	2	1/2	1/2	1	1	1/3	3	3
Absorbed energy	2	1/2	1/2	1	1	1/3	3	3
Damping ratio	4	2	2	3	3	1	5	5
Fracture *toughness*	1/2	1/4	1/4	1/3	1/3	1/5	1	1
ILSS	1/2	1/4	1/4	1/3	1/3	1/5	1	1

Step 4: Geometric mean

The geometric mean is derived based on equation (3.14)

$$(1 \times 1/3 \times 1/3 \times 1/2 \times 1/2 \times 1/4 \times 2 \times 2)^{1/8} = 0.63894$$

$$(3 \times 1 \times 1 \times 2 \times 2 \times 1/2 \times 4 \times 4)^{1/8} = 1.76923$$

$$(3 \times 1 \times 1 \times 2 \times 2 \times 1/2 \times 4 \times 4)^{1/8} = 1.76923$$

$$(2 \times 1/2 \times 1/2 \times 1 \times 1 \times 1/3 \times 3 \times 3)^{1/8} = 1.05199$$

$$(2 \times 1/2 \times 1/2 \times 1 \times 1 \times 1/3 \times 3 \times 3)^{1/8} = 1.05199$$

$$(4 \text{ x } 2 \text{ x } 2 \text{ x } 3 \text{ x } 3 \text{ x } 1 \text{ x } 5 \text{ x } 5)^{1/8} = 2.78316$$

$$(1/2 \text{ x } 1/4 \text{ x } 1/4 \text{ x } 1/3 \text{ x } 1/3 \text{ x } 1/5 \text{ x } 1 \text{ x } 1)^{1/8} = 0.40291$$

$$(1/2 \text{ x } 1/4 \text{ x } 1/4 \text{ x } 1/3 \text{ x } 1/3 \text{ x } 1/5 \text{ x } 1 \text{ x } 1)^{1/8} = 0.40291$$

Step 5: Determining normalized weights w_j

The normalized weights of the attributes are determined based on equation (3.15). Hence, the obtained weights for the attributes are Density 0.06473, UTS 0.17925, Bending strength 0.17925, Charpy impact strength 0.10658, Absorbed energy 0.10658, Damping ratio 0.28197, Fracture toughness 0.04082 and interlaminar shear strength 0.04082 respectively.

The relative index, RI value corresponds to eight attributes is 1.4 (Rao 2007). After solving CI and RI values using equations (3.16) and (3.17), CR value was found to be 0.01013 which is less than 0.1 and hence the weights are determined.

Step 6: Determination of Score and Range

Simple Additive Weighting approach (SAW) and Weighted Product Model (WPM) are solved using equation (3.18) and (3.19), Obtained scores and rank were shown in Table 5.6.

Table 5.6 Scores and rank of SAW and WPM

Sl. No	CGRP-PMC	SAW		WPM	
		Score	Rank	Score	Rank
1	Two layers	0.692281	3	0.617924	3
2	Four layers	0.865215	2	0.861712	2
3	Six layers	0.969126	1	0.967577	1

Based on the above result, it is observed that six-layered CGRP-PMC gives better physical, mechanical and dynamic properties compared to two and four layers CGRP-PMC considering eight different criteria.

5.4.2 TOPSIS

Step 1: PMC data

The CGRP-PMC material properties shown in Table 5.7 are used for the AHP method and the same data is used for the TOPSIS method.

Step 2: Determination of Normalization decision matrix

The normalization of step 1 is determined based on equation (3.20),

Density	UTS	Bending strength	Impact strength	Absorbed energy	Damping ratio	Fracture toughness	ILSS
0.57787	0.40144	0.486	0.37421	0.13855	0.6241	0.18136	0.42928
0.58065	0.58051	0.56701	0.68308	0.63971	0.49396	0.78179	0.67095
0.57351	0.70842	0.66506	0.6272	0.75602	0.6054	0.59658	0.60461

Step 3: Determination of the weighted normalized matrix

The weights of each attribute, calculated from equation (3.15) obtained from the AHP method were used for this study. The weighted normalized matrix is obtained based on the equation (3.21).

Density	UTS	Bending strength	Impact strength	Absorbed energy	Damping ratio	Fracture toughness	ILSS
0.03740	0.07195	0.08711	0.03988	0.01476	0.17597	0.00740	0.01752
0.03758	0.10405	0.10163	0.07280	0.06818	0.13928	0.03191	0.02738
0.03712	0.12698	0.11921	0.06684	0.08057	0.17070	0.02435	0.02468

Step 4: Determination of ideal best and ideal worst solutions

The ideal best and ideal worst solutions were determined based on equation (3.15)

$$V_1^+ = 0.03712 \quad V_1^- = 0.03758$$

$$V_2^+ = 0.12698 \quad V_2^- = 0.07195$$

$$V_3^+ = 0.11921 \quad V_3^- = 0.08711$$

$$V_4^+ = 0.07280 \quad V_4^- = 0.03988$$

$$V_5^+ = 0.08057 \quad V_5^- = 0.01476$$

$$V_6^+ = 0.17597 \quad V_6^- = 0.13928$$

$$V_7^+ = 0.03191 \quad V_7^- = 0.00740$$

$$V_8^+ = 0.02738 \quad V_8^- = 0.01752$$

Step 5: Calculation of the distances to the positive and negative ideal reference points

The distance of positive and negative separation measures was determined based on equation (3.22) and results are shown in Table 5.9.

Step 6: Calculation of the relative closeness coefficient C_i of each sample and quality assessment

The relative closeness coefficient for each PMC sample was determined based on the equation (3.23) and results are shown in Table 5.7.

Table 5.7. Positive and negative ideal reference points, relative closeness coefficient and Rank of CGRP-PMC

Sl. No	CGRP-PMC	S_i^+	S_i^-	C_i	Rank
1	Two layers	0.100851	0.036697	0.266796	3
2	Four layers	0.048323	0.076655	0.613346	2
3	Six layers	0.011303	0.102188	0.900403	1

Based on the ranks obtained through the TOPSIS method, it is observed that the six-layered CGRP-PMC gives better physical, mechanical and dynamic properties compared to two-layer and four-layered CGRP-PMC.

5.4.3 PROMETHEE

The PROMETHEE method is used for the selection of suitable CGRP-PMC specimens. The steps involved in solving the PROMETHEE method are mentioned in section 3.6.3. The CGRP-PMC data is identified with respect to their weights and maximization. Table 5.8 shows the alternatives (two-layer, four-layer, six-layered CGRP-PMC specimens) and corresponding criteria (C1 (density), C2 (UTS), C3 (bending strength), C4 (impact strength), C5 (absorbed energy), C6 (damping ratio), C7 (fracture toughness) and C8 (ILSS)). Here, the criteria to be maximized were determined and weights for the criteria were selected from the AHP for the study.

Table 5.8. Alternatives with respect to criterion and corresponding weights

Alternatives (PMC)	Attributes (Criteria)							
	C1	C2	C3	C4	C5	C6	C7	C8
Two-layers	1.456	81.6	114	57.39	0.81	0.027732	2.59	14.69
Four-layers	1.463	118	133	104.76	3.74	0.021949	11.165	22.96
Six-layers	1.445	144	156	96.19	4.42	0.026901	8.52	20.69
Maximize	No	Yes	Yes	Yes	Yes	Yes	Yes	Yes
Weights	0.06473	0.17925	0.17925	0.10658	0.10658	0.28197	0.04082	0.04082

Table 5.9 shows the preference values P resulting from the pairwise comparisons of the three alternatives a1, a2 and a3 (two-layer, four-layer, six-layered CGRP-PMC specimens) with respect to the criterion C1, C2, C3, C4, C5, C6, C7, C8. Table 5.10 shows the weighted preference values P resulting from the pairwise comparisons of the three alternative PMC with respect to criterion C1, C2, C3, C4, C5, C6, C7, C8. Table 5.11 shows the final preference matrix with the leaving flow, entering flow, net flow, and rank of the CGRP-PMC samples. Based on the rank of PMC, the six-layered CGRP-PMC is determined as the best alternative.

Table 5.9 Preference values of alternatives with respect to criteria

C1	a1	a2	a3
a1	-	1	0
a2	0	-	0
a3	1	1	-

C2	a1	a2	a3
a1	-	0	0
a2	1	-	0
a3	1	1	-

C3	a1	a2	a3
a1	-	0	0
a2	1	-	0
a3	1	1	-

C4	a1	a2	a3
a1	-	0	0
a2	1	-	1
a3	1	0	-

C5	a1	a2	a3
a1	-	0	0
a2	1	-	0
a3	1	1	-

C6	a1	a2	a3
a1	-	1	1
a2	0	-	0
a3	0	1	-

C7	a1	a2	a3
a1	-	0	0
a2	1	-	1
a3	1	0	-

C8	a1	a2	a3
a1	-	0	0
a2	1	-	1
a3	1	0	-

Table 5.10 Weighted preference values of alternatives with respect to criteria

C1	a1	a2	a3
a1	-	0.06473	0
a2	0	-	0
a3	0.06473	0.06473	-

C2	a1	a2	a3
a1	-	0	0
a2	0.17925	-	0
a3	0.17925	0.17925	-

C3	a1	a2	a3
a1	-	0	0
a2	0.17925	-	0
a3	0.17925	0.17925	-

C4	a1	a2	a3
a1	-	0	0
a2	0.10658	-	0.10658
a3	0.10658	0	-

C5	a1	a2	a3
a1	-	0	0
a2	0.10658	-	0
a3	0.10658	0.10658	-

C6	a1	a2	a3
a1	-	0.28197	0.28197
a2	0	-	0
a3	0	0.28197	-

C7	a1	a2	a3
a1	-	0	0
a2	0.04082	-	0.04082
a3	0.04082	0	-

C8	a1	a2	a3
a1	-	0	0
a2	0.04082	-	0.04082
a3	0.04082	0	-

Table 5.11 Final preference matrix with leaving, entering, net flow and Rank

Sl. No.	CGRP-PMC	a1	a2	a3	$\phi^+(a)$	$\phi^-(a)$	$\phi(a)$	Rank
1	Two-layers	-	0.34670	0.28197	0.62867	1.37133	-0.74266	3
2	Four-layers	0.65330	-	0.18822	0.84152	1.15848	-0.31696	2
3	Six-layers	0.71803	0.81178	-	1.52981	0.47019	1.05962	1

Based on the ranks, it can be seen that six-layered CGRP-PMC gives better physical, mechanical and dynamic properties compared to two-layer and four-layered CGRP-PMC.

5.5 DISCUSSIONS

The density test shows that four-layered CGRP-PMC material has more density than two-layer and six-layered CGRP-PMC material. In two-layered CGRP-PMC material, the volume percentage of resin is more than the volume percentage of reinforcement and in six-layered CGRP-PMC material, the volume percentage of reinforcement is more than the volume percentage of resin. However, in four-layered CGRP-PMC the volume percentage of resin and reinforcement are almost equal. Hence, from the density analysis results, it was revealed that an equal volume percentage of the polyester resin matrix and CSM glass fiber reinforcement have higher densities composites.

The experimental tensile result indicates that increase in the number of layers in CGRP-PMC samples will increase the tensile strength in the CGRP-PMC material. The flexural experimental results show that increase in the number of layers of CSM glass fiber will increase the maximum bending load and decrease the strain percentage of CGRP-PMC specimens. The four-layered CGRP-PMC material has high impact strength, fracture toughness and ILSS than two-layer and six-layered CGRP-PMC material.

Free vibration analysis is used to determine the natural frequency and damping ratios of the CGRP-PMC. The natural frequency of CGRP-PMC had increased with respect to the increase in number of layers of CSM in CGRP-PMC specimens. Hence from the experimental analysis, it was found that stiffness of CGRP-PMC material will increase with increase in the number of layers of CSM glass fiber reinforcement.

The two-layer, four-layer and six-layered CGRP-PMC had unique best individual properties. Considering the first mode in free vibration analysis the two-layer CGRP-PMC had the highest damping ratio. But the four-layer CGRP-PMC had higher impact strength, fracture toughness and interlaminar shear strength. However, the six-layer CGRP-PMC had lower density and higher UTS, bending strength and absorbed energy. Considering above all properties of the two-layer, four-layer and six-layered CGRP-PMC, the selection of optimum composite for multi-application was difficult

manually. Hence, MADM techniques such as AHP, SAW, WPM, TOPSIS and PROMETHEE were applied for the selection of best CGRP-PMC.

Based on MADM techniques, it was found that six-layered CGRP-PMC material is better than two-layer and four-layered CGRP-PMC. Hence from the study, it was revealed that six-layered CGRP-PMC will be most suitable for real-time practical applications.

5.6 CONCLUSIONS

Four-layered CGRP-PMC material has high impact strength, fracture toughness, and ILSS when compared to two-layer and six-layered CGRP-PMC material. It is observed that for better mechanical characteristics of CGRP-PMC, proper interaction between matrix and reinforcement is required. Hence, it is identified that an equal volume percentage of CSM glass fiber reinforcement and polyester resin matrix CGRP-PMC achieves better mechanical properties. Six-layered CGRP-PMC material has the highest ultimate tensile strength and flexural strength than two-layer and four-layered CGRP-PMC.

The experimental free vibration results revealed that six-layered CGRP-PMC had high natural frequencies than two-layer and four-layered CGRP-PMC. Hence, from the experimental analysis, it is determined that the stiffness of composites increases with an increase in the number of layers of CSM glass fiber reinforcement.

Based on MADM techniques, the six-layered CGRP-PMC material is observed as optimum CGRP-PMC when compared to the two-layer and four-layered CGRP-PMC. The rank of samples obtained is similar in all MADM (SAW, WPM, TOPSIS and PROMETHEE) methods.

5.7 SUMMARY

The fabrication of two-layer, four-layer and six-layered CGRP-PMC have been carried out using the hand-layup technique. The density, tensile, flexural, impact, ILSS, fracture toughness properties have been evaluated through material characterization. Experimental free vibration analysis was carried out to determine the natural frequency

and damping ratio of the CGRP-PMC materials. MADM techniques such as AHP, SAW, WPM, TOPSIS and PROMETHEE methods were used to determine the optimal CGRP-PMC materials. By using MADM techniques, six-layered CGRP-PMC was selected as the optimal CGRP-PMC material.

CHAPTER 6

DYNAMIC ANALYSIS OF CGRP-PMC-MRF CORE SANDWICH BEAMS

6.1 INTRODUCTION

In this chapter, the semi-active vibration control of sandwich beams made of CGRP-PMC and MRF core were experimentally investigated. The two-layer, four-layer and six-layered CGRP-PMC prepared using the hand-layup technique are used as top and bottom layers of the sandwich beams. The in-house prepared MRF with 30% volume of CI_p and 70% volume silicone oil is used as the core of the sandwich beams. Nine cantilever sandwich beams of varying thickness of the top and bottom layers CGRP-PMC beams and middle MRF core are prepared. The MRF core is activated with a non-homogeneous magnetic field using permanent magnets. The first three modes, natural frequencies and damping ratios of the CGRP-PMC-MRF core sandwich beams are determined through free vibration analysis using DEWESoft modal analysis software. The frequency amplitude response of the CGRP-PMC-MRF core sandwich beams through forced vibration analysis is determined using LabVIEW. The effect of various parameters such as magnetic flux density, the thickness of CGRP-PMC layers and MRF core layer on the natural frequencies, damping ratio and vibration amplitude suppression behavior of the CGRP-PMC-MRF core sandwich beams are investigated.

6.2 FABRICATION OF CGRP-PMC-MRF CORE SANDWICH BEAMS

The two-layer, four-layer, and six-layered CGRP-PMC materials prepared using hand layup method are used as top and bottom layers of sandwich beams. The procedure for the fabrication of CGRP-PMC-MRF core sandwich beams is explained in detail in section 3.7.1. Figure 3.19 shows a detailed description of the CGRP-PMC-MRF core sandwich beam fabrication. Nine CGRP-PMC-MRF core sandwich beams of varying MRF core thickness, top and bottom CGRP-PMC face layers sandwich beams are fabricated. The prepared CGRP-PMC-MRF core sandwich beams were named as A1, A2, A3, A4, A5, A6, A7, A8, and A9.

Table 6.1 describes the top and bottom layer and core layer thickness variation in A1 to A9 specimens with other dimensional information. Figure 6.1 (a) and (b) show the schematic and photograph view of fabricated sandwich beams. The natural frequencies, damping ratio and vibration amplitude suppression behavior of fabricated CGRP-PMC-MRF core sandwich beams are analyzed using experimental free and forced vibration analysis.

Table 6.1 Dimension of CGRP-PMC-MRF core sandwich beams

Specimen	CGRP-PMC Top and Bottom layers Length (mm)	MRF core Length (mm)	Width (mm)	CGRP-PMC Top and Bottom layer Thickness (mm)	MRF core Thickness (mm)
A1	225	200	20	2	2
A2	225	200	20	2	3.5
A3	225	200	20	2	5
A4	225	200	20	3.5	2
A5	225	200	20	3.5	3.5
A6	225	200	20	3.5	5
A7	225	200	20	5	2
A8	225	200	20	5	3.5
A9	225	200	20	5	5
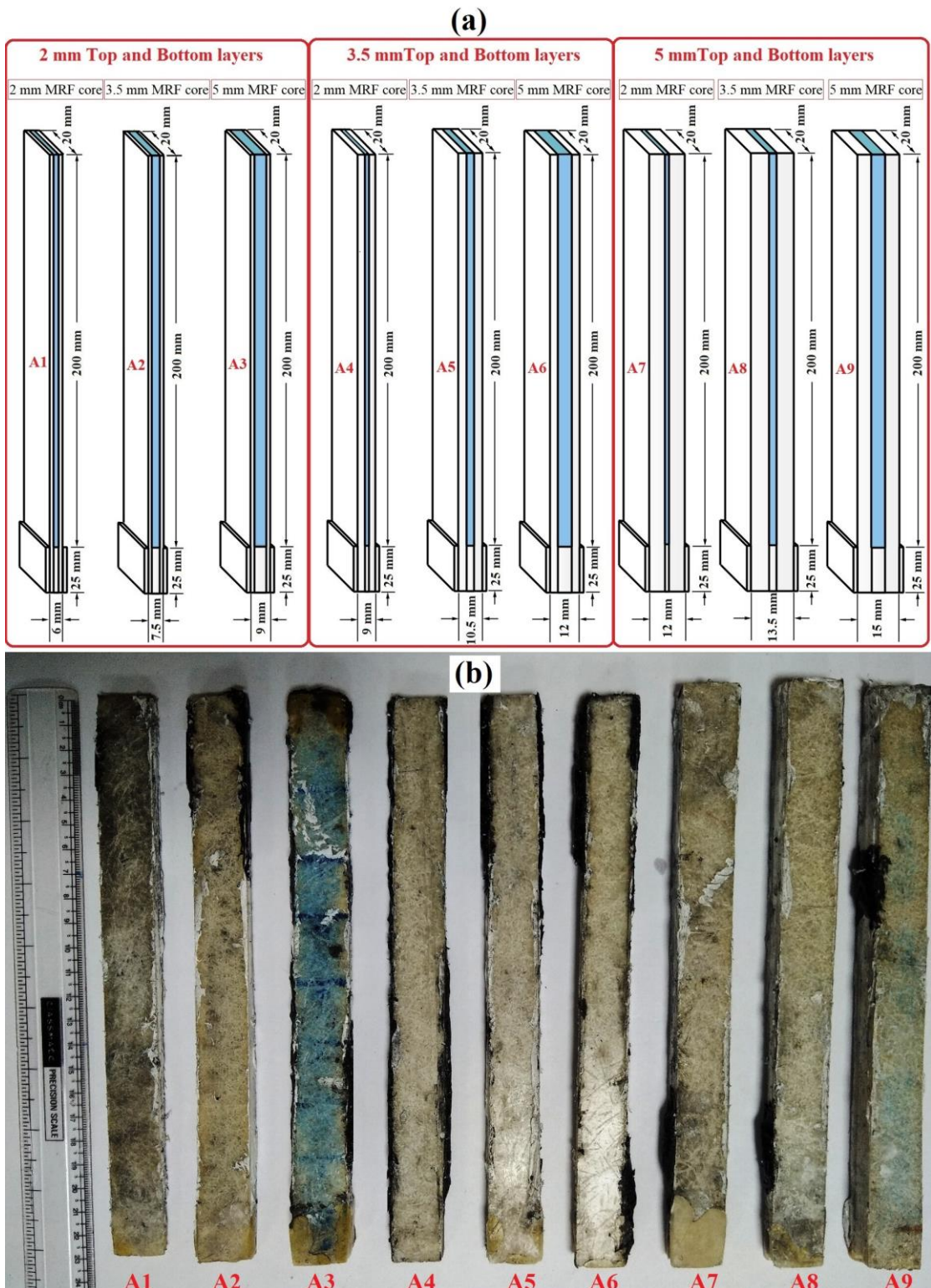
Figure 6.1 A1, A2, A3, A4, A5, A6, A7, A8 and A9 CGRP-PMC-MRF core sandwich beams (a) Schematic view and (b) Photograph view

6.3 FREE VIBRATION CHARACTERIZATION

Free vibration modal analysis using impulse hammer excitation is carried out based on the ASTM E756-05 standard. MRF core sandwich beam has the ability to change its dynamic properties with the help of an external applied magnetic field (Manoharan et al. (2014)). Fig. 6.2 shows the experimental free vibration setup used for determining the natural frequency and damping ratios of CGRP-PMC-MRF core sandwich beams subjected to the influence of the external applied non-homogeneous magnetic field. The distance between the top and bottom permanent magnets position is varied vertically to realize 0, 200, 400 and 600 gauss magnetic flux densities on the MRF core. The sandwich beam is marked with eight divisions of 25 mm distance and impact hammer was impacted on the marked places and average response data was measured. The accelerometer sensor is placed at 175 mm from the fixed end of the CGRP-PMC-MRF core sandwich beam. The first three modes, natural frequencies and damping ratios of the fabricated CGRP-PMC-MRF core sandwich beams subjected to the influence of the external magnetic field are analyzed.
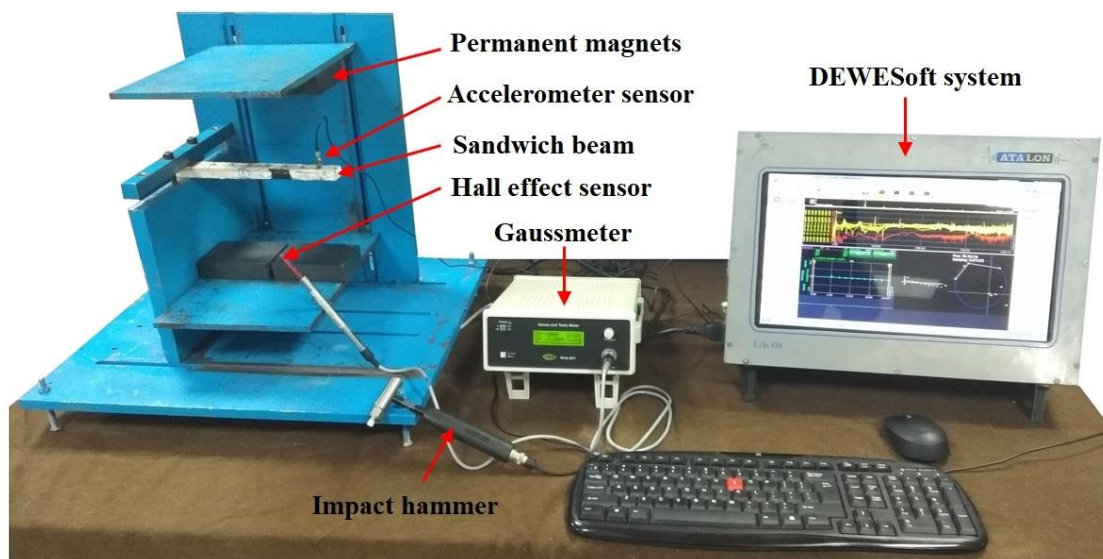
Figure 6.2 Free vibration analysis experimental setup

The natural frequencies and damping ratios of the CGRP-PMC-MRF core sandwich beams are strongly influenced by the thickness of the MRF core and CGRP-PMC top and bottom layers with the applied magnetic fields. Table 6.2 shows the

natural frequencies and damping ratios of the CGRP-PMC-MRF core sandwich beams for the first three modes subjected to the effect of 0 G, 200 G, 400 G, and 600 G magnetic flux densities. The results show that the natural frequencies and damping ratios of the CGRP-PMC core MRF sandwich beams increase with the increase in the applied magnetic flux densities. Similar results were reported by previous researches for MRF core aluminum sandwich beams (Lara et al. 2009)). It is observed that at 600 G magnetic flux density, the A3 CGRP-PMC-MRF core sandwich beam has higher damping ratio than the remaining CGRP-PMC-MRF core sandwich beams.

Table 6.2 The natural frequencies and damping ratios of the CGRP-PMC-MRF core sandwich beams with the influence of magnetic flux density

Beam No.	Magnetic flux density (gauss)	1st mode		2nd mode		3rd mode	
		Natural freq (Hz)	Damping ratio	Natural freq (Hz)	Damping ratio	Natural freq (Hz)	Damping ratio
A1	0	17.57	0.0058	99.29	0.0040	258.72	0.0025
	200	18.92	0.0251	100.01	0.0090	260.34	0.0157
	400	19.56	0.1012	100.86	0.0187	263.45	0.0190
	600	20.13	0.1726	101.95	0.0422	265.65	0.0306
A2	0	15.24	0.0193	88.48	0.0049	224.14	0.0052
	200	17.07	0.0520	90.27	0.0317	225.73	0.0166
	400	19.73	0.1544	90.74	0.0354	229.22	0.0282
	600	21.18	0.2347	91.83	0.0472	230.91	0.0385
A3	0	14.06	0.0322	78.49	0.0080	222.46	0.0105
	200	18.45	0.0694	84.85	0.0255	224.71	0.0219
	400	21.39	0.1879	86.56	0.0498	227.59	0.0335
	600	21.53	0.2839	89.64	0.0670	229.51	0.0464
A4	0	37.57	0.0042	186.16	0.0038	504.94	0.0021
	200	38.34	0.0180	187.37	0.0058	507.61	0.0109
	400	39.82	0.0571	188.85	0.0158	513.73	0.0188
	600	40.66	0.1216	190.93	0.0374	517.75	0.0264
A5	0	34.89	0.0152	178.15	0.0046	425.17	0.0049
	200	36.02	0.0453	180.91	0.0106	428	0.0114
	400	37.28	0.0764	181.94	0.0311	433.05	0.0200
	600	38.72	0.1712	183.15	0.0381	436.54	0.0319

	0	31.26	0.0246	170.02	0.0067	404.15	0.0089
A6	200	33.32	0.0521	173.30	0.0221	407.46	0.0180
	400	34.53	0.1762	175.84	0.0371	412.15	0.0261
	600	35.91	0.2081	177.63	0.0503	415.62	0.0356
	0	52.82	0.0037	313.76	0.0033	733.52	0.0011
A7	200	53.99	0.0178	315.66	0.0044	737.20	0.0053
	400	55.03	0.0225	317.95	0.0142	745.04	0.0091
	600	56.31	0.0451	320.91	0.0260	751.42	0.0125
	0	50.88	0.0089	303	0.0038	695.46	0.0026
A8	200	52.19	0.0216	306.37	0.0091	699.82	0.0086
	400	53.50	0.0250	308.83	0.0199	707.30	0.0142
	600	54.93	0.0525	310.55	0.0278	713.23	0.0183
	0	44.54	0.0138	264.89	0.0043	622.80	0.0030
A9	200	46.60	0.0230	268.98	0.0121	627.46	0.0090
	400	47.67	0.0711	271.36	0.0241	634.29	0.0146
	600	48.23	0.0783	273.28	0.0309	639.61	0.0195

Figures 6.3 – 6.5 show the influence of magnetic flux density on percentage increase in the natural frequency of CGRP-PMC-MRF core sandwich beams corresponding to the first, second and third mode. At 600 G magnetic flux density, the percentage increase in natural frequencies corresponding to the first mode is observed as 14.57%, 38.95%, 53.18%, 8.23%, 10.99%, 14.85%, 6.61%, 7.95 and 8.28% for A1, A2, A3, A4, A5, A6, A7, A8 and A9 CGRP-PMC-MRF core sandwich beams when compared to zero gauss magnetic flux density. It is observed that a similar percentage increase in natural frequencies is obtained for the second and third modes of CGRP-PMC-MRF core sandwich beams.
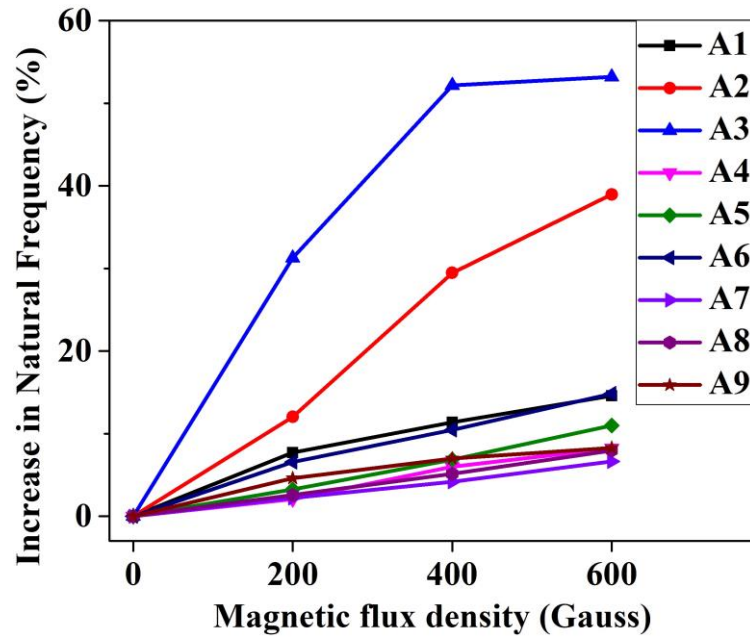
Figure 6.3 Influence of magnetic flux density on 1st mode percentage increase in natural frequency of CGRP-PMC-MRF core sandwich beams
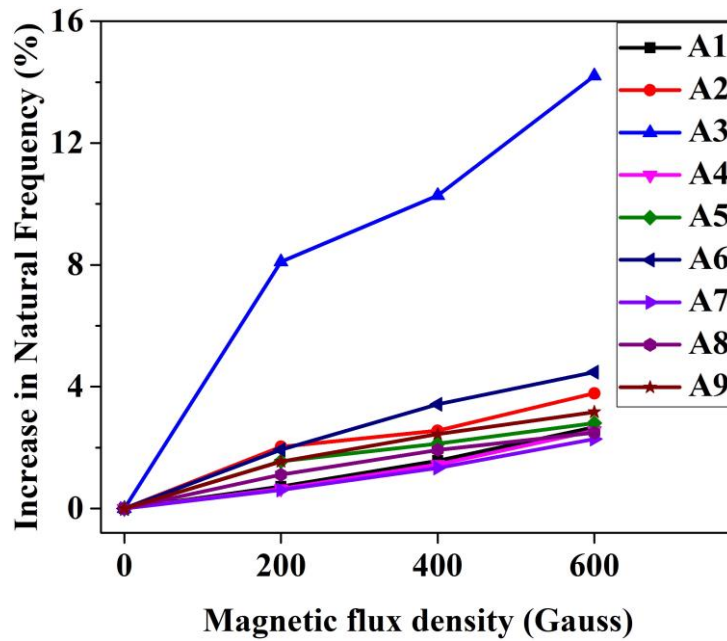
Figure 6.4 Influence of magnetic flux density on 2nd mode percentage increase in natural frequency of CGRP-PMC-MRF core sandwich beams
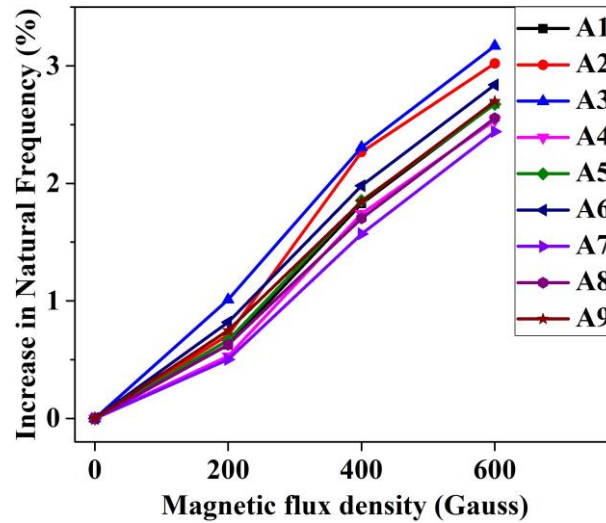
Figure 6.5 Influence of magnetic flux density on 3rd mode percentage increase in natural frequency of CGRP-PMC-MRF core sandwich beams

Based on the experimental study, it is observed that all the CGRP-PMC-MRF core sandwich beams exhibit an increase in the natural frequency with the increase in the applied magnetic flux density. Also, the results indicate that the increase in MRF core layer thickness decreases the natural frequency and increases the damping ratio of the CGRP-PMC-MRF core sandwich beams. However, increasing the CGRP-PMC top and bottom layer thickness increases the natural frequency and decreases the damping ratio of the CGRP-PMC-MRF core sandwich beams. Also, the A3 CGRP-PMC-MRF core sandwich beam has the highest increase in natural frequency percentage corresponding to all three modes with the influences of applied magnetic flux density.

6.4 FORCED VIBRATION CHARACTERIZATION

The experimental forced vibration analysis setup used to determine the frequency response function (FRF) curves of CGRP-PMC-MRF core sandwich beams is shown in figure 6.6. The vibration amplitude suppression behavior of the CGRP-PMC-MRF core sandwich beams with the influence of the applied magnetic field is analysed using forced vibration analysis. The experimental setup consists of 50 kgf electrodynamic shaker, digital switching power amplifier, function generator, accelerometer sensor, force transducer, NI 9234 DAQ and LabVIEW 2017 software. Using the function generator, the required electrodynamic shaker excitation

information is sent to the amplifier. The forced vibration analysis of CGRP-PMC-MRF core sandwich beams is performed by using a harmonic sine sweep base excitation. The electrodynamic shaker was excited by harmonic sine sweep from 10 Hz to 1000 Hz frequency at 25 seconds duration for four iterations and average FRF curves of CGRP-PMC-MRF core sandwich beams are determined. The accelerometer sensor measures the transverse vibration frequency response signals measured from CGRP-PMC-MRF core sandwich beams. The NI-9234 data acquisition (DAQ) collects the frequency response signals from the accelerometer sensor and are analyzed using LabVIEW software. The FRF curves of cantilever sandwich beams have been obtained at 25 mm from free end and evaluated over the frequency range of 10 Hz to 1000 Hz for 0 G, 200 G, 400 G, and 600 G magnetic flux density conditions.
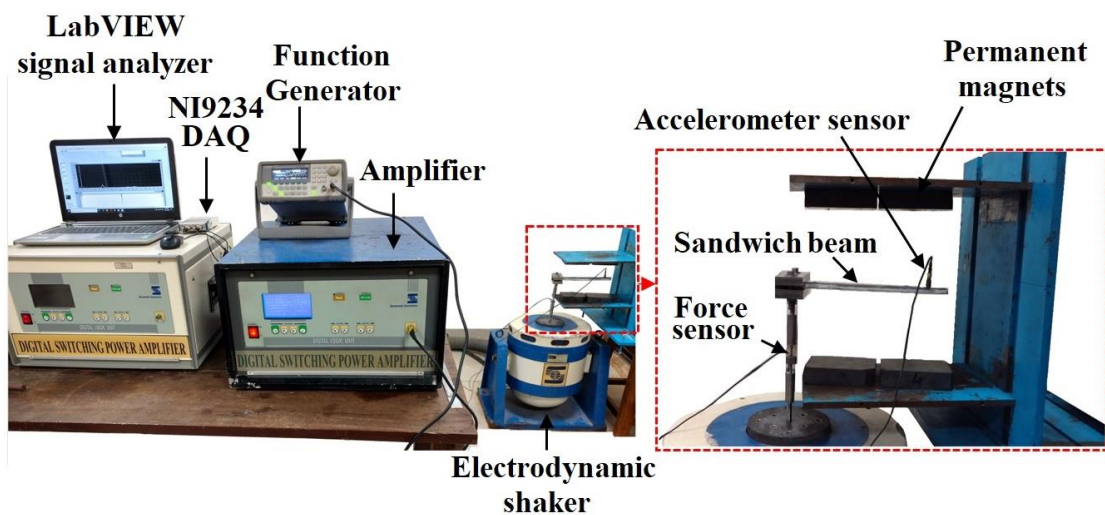
Figure 6.6 Forced vibration analysis experimental setup

The forced vibration analysis results of A1 – A9 CGRP-PMC-MRF core sandwich beams analyzed experimentally by using harmonic sine sweep base excitation are shown in figures 6.7 - 6.15. The results reveal that there is a successful suppression of amplitude obtained due to the influence of the external applied magnetic flux density.
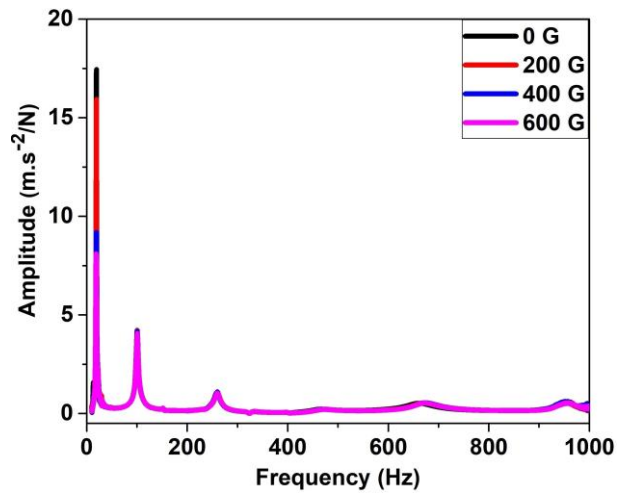
Figure 6.7 FRF curve for CGRP-PMC-MRF core sandwich beam A1 specimen
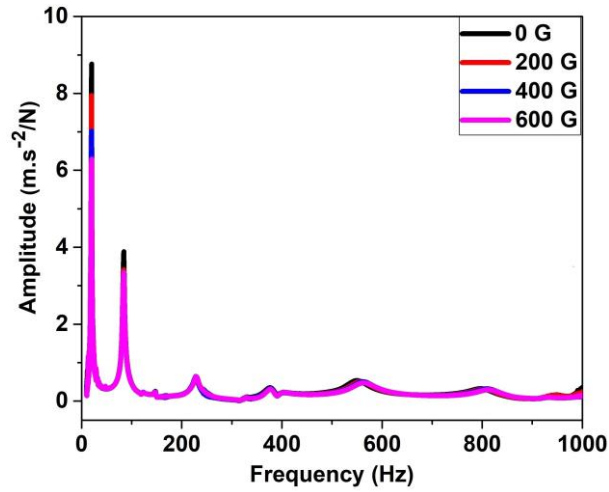
Figure 6.8 FRF curve for CGRP-PMC-MRF core sandwich beam A2 specimen
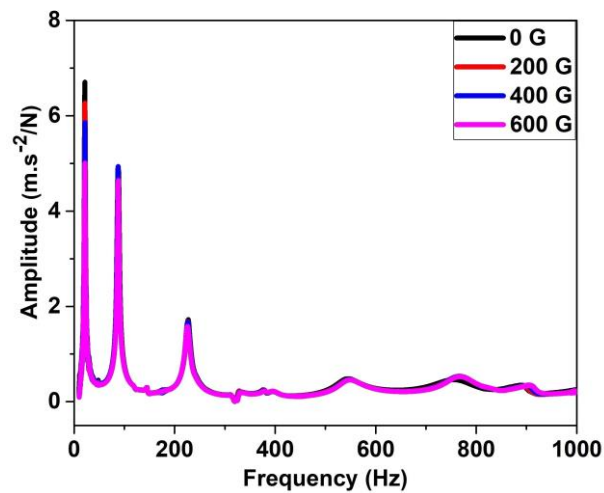
Figure 6.9 FRF curve for CGRP-PMC-MRF core sandwich beam A3 specimen
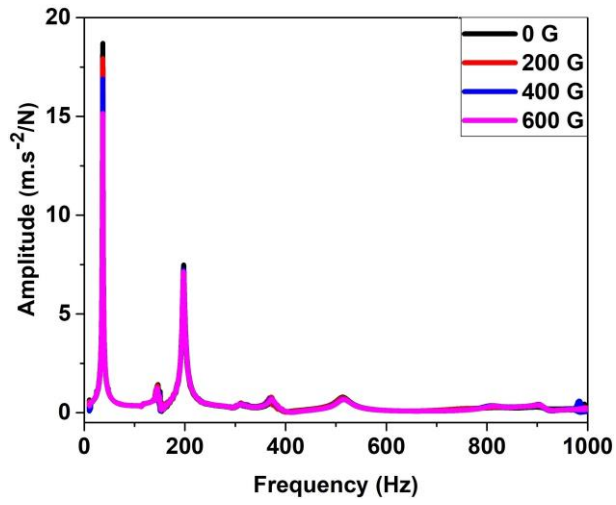
Figure 6.10 FRF curve for CGRP-PMC-MRF core sandwich beam A4 specimen
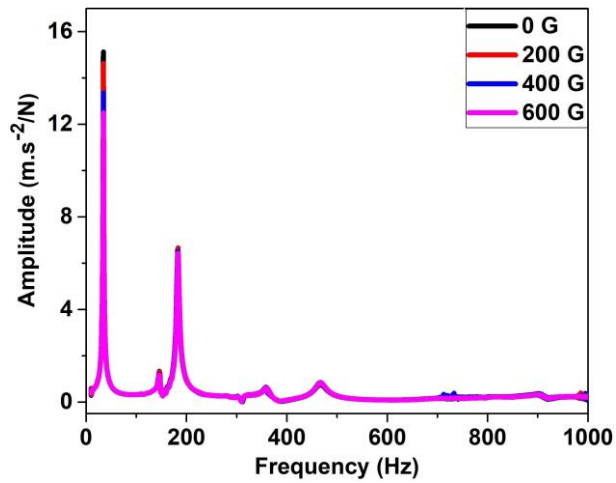
Figure 6.11 FRF curve for CGRP-PMC-MRF core sandwich beam A5 specimen
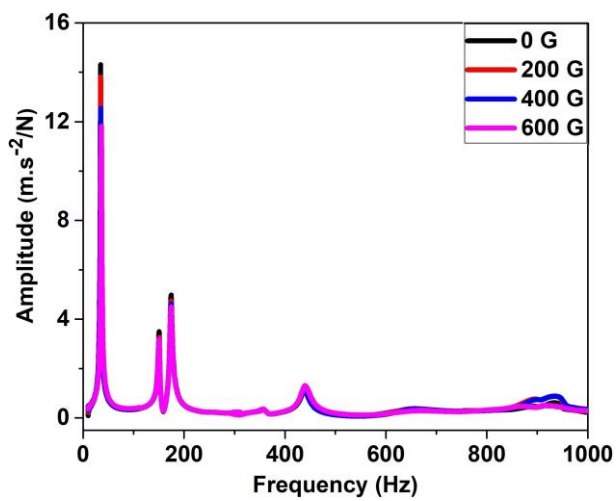
Figure 6.12 FRF curve for CGRP-PMC-MRF core sandwich beam A6 specimen
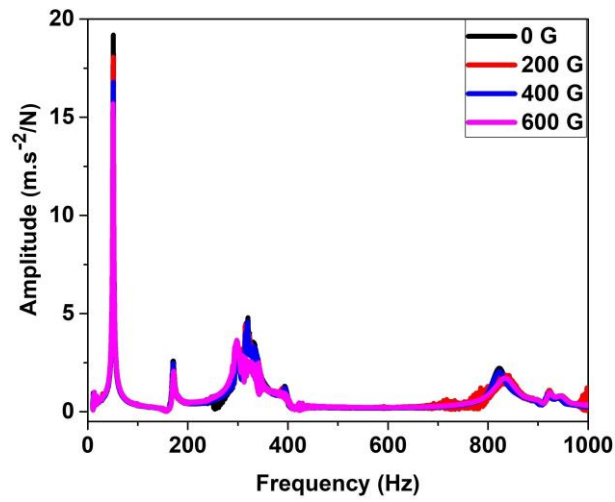
Figure 6.13 FRF curve for CGRP-PMC-MRF core sandwich beam A7 specimen
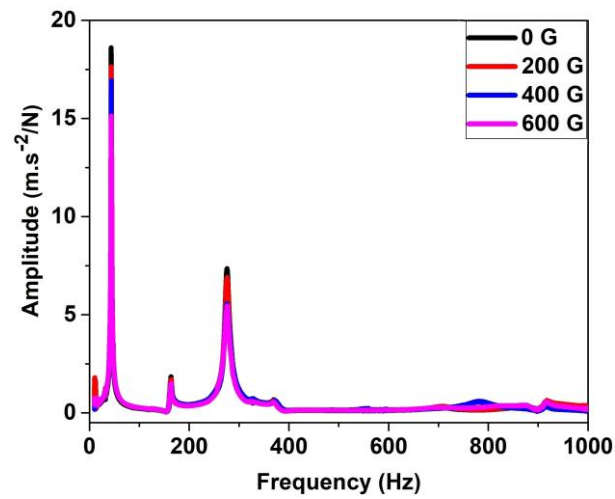
Figure 6.14 FRF curve for CGRP-PMC-MRF core sandwich beam A8 specimen
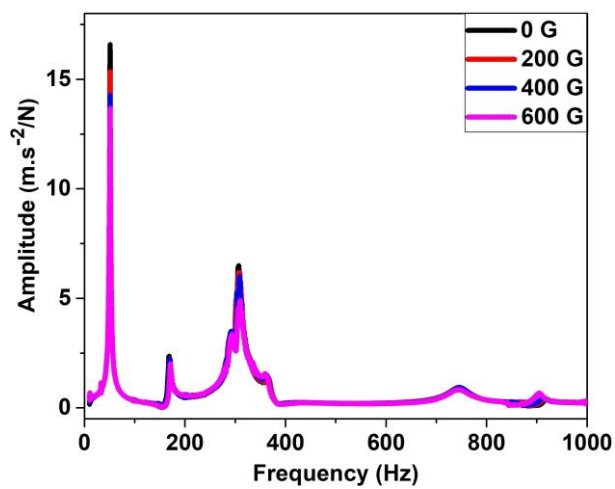
Figure 6.15 FRF curve for CGRP-PMC-MRF core sandwich beam A9 specimen

It is observed that the A3 CGRP-PMC-MRF core sandwich beam is having very less FRF magnitude when compared to the remaining CGRP-PMC-MRF core sandwich beams. However, all the CGRP-PMC-MRF core sandwich beams showed a considerable reduction in the frequency amplitude response with the influence of applied magnetic flux density. The CGRP-PMC material is a paramagnetic material, the MRF core activation is highly affected by the increase in the thickness of CGRP-PMC top and bottom layers. Hence, the damping properties of the CGRP-PMC-MRF core sandwich beams decreased with the increase in the thickness of the CGRP-PMC top and bottom layers.
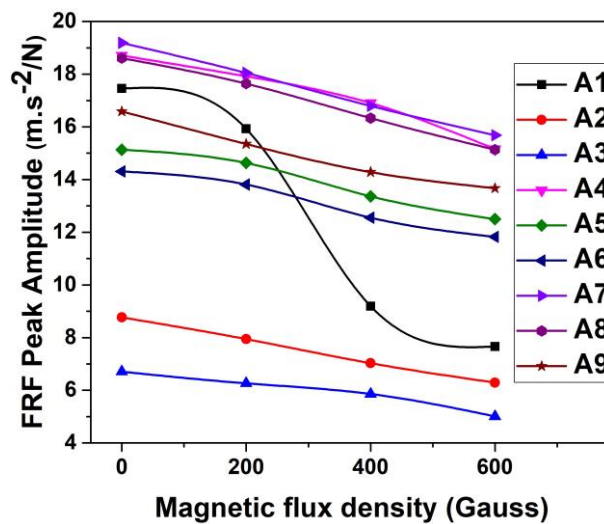
Figure 6.16 Influence of magnetic flux density on 1st mode FRF peak amplitude reduction

The first mode FRF curve peak amplitude values with respect to the influence of applied magnetic flux densities are shown in figure 6.16. The result shows that peak amplitude values for all the CGRP-PMC-MRF core sandwich beams reduced with increase in the applied magnetic flux density. At 600 G magnetic flux density the percentage reduction in peak amplitude is 56.10, 28.22, 25.34, 18.97, 18.67, 17.58, 18.27, 17.40 and 17.37% for A1, A2, A3, A4, A5, A6, A7, A8 and A9 CGRP-PMC-MRF core sandwich beams respectively. It is observed that the A1 CGRP-PMC-MRF core sandwich beam is having very high amplitude suppression with the influence of external applied magnetic flux densities. Based on the results obtained, the CGRP-PMC-MRF core sandwich beams having 2 mm thickness CGRP-PMC top and bottom

105

layers have effective vibration suppression than the 3.5 mm and 5 mm thickness CGRP-PMC top and bottom layers.

6.5 CONCLUSIONS

The semi-active vibration control performance of the CGRP-PMC-MRF core sandwich beams has been experimentally investigated and the following conclusions are found. The experimental free and forced vibration analysis revealed the tunability of the stiffness and damping properties of CGRP-PMC-MRF core sandwich beams. The natural frequencies of the CGRP-PMC-MRF core sandwich beams increased with an increase in the thickness of the top and bottom layers. Whereas, the damping ratio of the CGRP-PMC-MRF core sandwich beams decreased with an increase in the thickness of the top and bottom layers. However, the damping ratio of CGRP-PMC-MRF core sandwich beams increased with an increase in the thickness of the MRF core layer. Based on the free vibration results obtained, it is determined that A3 specimen (2 mm thickness top and bottom layers CGRP-PMC and 5 mm thickness MRF core) CGRP-PMC-MRF core sandwich beam has a higher change in natural frequencies and damping ratios than remaining sandwich beams. Hence, layer thickness combination like A3 CGRP-PMC-MRF core sandwich beam can be used for several applications. Furthermore, the forced vibration results revealed that the A3 CGRP-PMC-MRF core sandwich beam has lesser FRF peak amplitude than the remaining CGRP-PMC-MRF core sandwich beams. At 600 G magnetic flux density, A1 CGRP-PMC-MRF core sandwich beams have a higher percentage reduction in peak amplitude of 56.10%. However, the vibration amplitude suppression capabilities of CGRP-PMC-MRF core sandwich beams decreased due to increase in the thickness of the top and bottom CGRP-PMC layers. The CGRP-PMC-MRF core sandwich beam has the ability to control its natural frequency, damping ratio, and vibration amplitude responses. The CGRP-PMC-MRF core sandwich beams vibration controllable behavior may be used in walls and panels of aerospace and automotive structures.

6.6 SUMMARY

In this chapter, the dynamic analysis of CGRP-PMC-MRF core sandwich beams having varying thickness of the top, bottom and core layers sandwich beams are experimentally investigated. The free and forced vibration experimental characterizations are performed with and without the influence of external applied magnetic flux densities. The ability of CGRP-PMC-MRF core sandwich beams varying their dynamic properties with the influence of magnetic flux densities are analyzed in terms of natural frequency, damping ratio and FRF curves.

CHAPTER 7

CHARACTERIZATION OF METAL MATRIX COMPOSITE

7.1 INTRODUCTION

The Al6082 and Al7075 aluminum alloy reinforced with (0, 1, 2, 3, 4, 5, 7.5, 10, 15 and 20) different weight percentages of silicon carbide particles (SiC_p) MMCs have been fabricated through stir casting method. The microstructure, density, hardness, tensile strength, impact strength, natural frequencies and damping ratio of the MMCs were determined. The mechanical tests and free vibration analysis results revealed that the addition of SiC_p reinforcement enhanced the strength and stiffness of the aluminum alloy MMCs. Multi-attribute decision making (MADM) techniques like analytic hierarchy process (AHP), technique for order preference by similarity to ideal solution (TOPSIS) and preference ranking organization method for enrichment evaluation (PROMETHEE) methods were applied for determining the best fabricated MMCs. Based on MADM techniques, 15% SiC_p/Al7075 composite was selected as the best material and using response surface methodology (RSM) 13.66% SiC_p/Al7075 composite was found as the optimal MMC material.

7.2 CHARACTERIZATION OF MMC

The physical, mechanical and dynamic characterization procedure for MMC material is already been explained in chapter 3 methodology section 3.5.

7.2.1 Microstructural characterization

Microstructural investigations of MMC samples were carried out using scanning electron microscope (SEM) and energy dispersive spectroscopy (EDS) analysis (Make: Carl ZEISS FESEM instrument). The MMCs samples were polished in the grinder-polisher instrument (Make: METKON GRIPO 2V). The MMCs samples for SEM and EDS analysis were prepared through the standard process. Figure 7.1 shows the microstructure of the as-received SiC_p. The average size of SiC_p is observed as 30 microns.
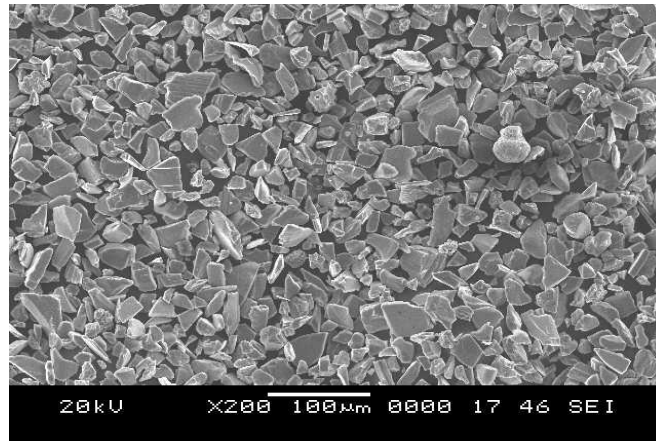
Figure 7.1 Microstructure of as-received SiC$_p$

The uniform distribution of SiC$_p$ in the matrix depends on the wettability of the SiC$_p$ with the molten metal and proper interfacial bonding between SiC$_p$ and aluminum alloys. The uniform distribution of SiC$_p$ in the aluminum alloy matrix yields enhanced mechanical property of the MMCs. Figure 7.2 shows the SEM microstructure of 20% SiC$_p$/Al6082 MMCs, the image reveals that the SiC$_p$ is non-homogeneously distributed in the Al6082 alloy. Small crack and porosity were observed in the matrix phase which decreases the strength of the MMCs.
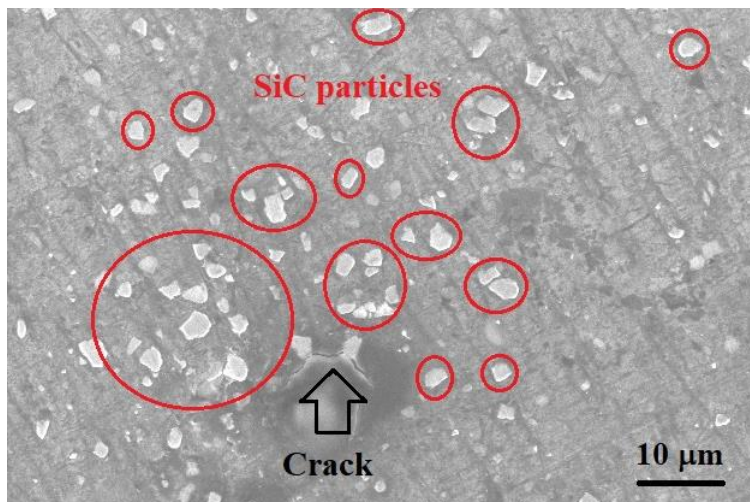
Figure 7.2 SEM micrograph of 20% SiC$_p$/Al6082 MMCs
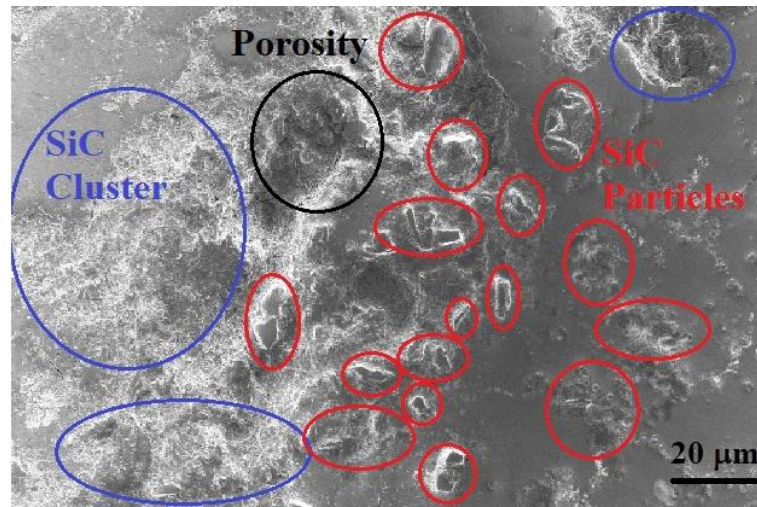
Figure 7.3 SEM micrograph of 20% SiC_p/Al7075 MMCs

The SEM microstructure of 20% SiC_p/Al7075 MMCs is shown in figure 7.3. The image reveals the clustering of SiC_p reinforcement. The clustering occurred due to magnesium and zinc segregation at the interface between the oxidized Al7075 alloy matrix and SiC_p reinforcement (Ahmed et al. (2010)). The possible interface chemical reactions in Al7075 alloy MMCs are $MgAl_2O_4$, $Al_2Mg_3Zn_3$ and $MgZn_2$. The $MgAl_2O_4$ reaction have undesirable effects on MMCs (Chen and Yan (2018)). The chemical reactions in Al7075 alloy MMCs are due to the Zinc element melting fast during homogenization and results in a chemical reaction between aluminum and magnesium elements.

The EDS elemental mapping of 5% SiC_p/Al6082 MMCs is shown in figure 7.4. The presence of aluminum (Al), magnesium (Mg), silicon (Si), carbon (C), iron (Fe) and oxide (O) elements was observed. Figure 7.5 shows the EDS elemental mapping of 5% SiC_p/Al7075 MMCs. The presence of aluminum (Al), zinc (Zn), magnesium (Mg), silicon (Si), carbon (C) and oxide (O) elements was observed. EDS analysis confirms the uniform distribution of chemical elements in MMCs.
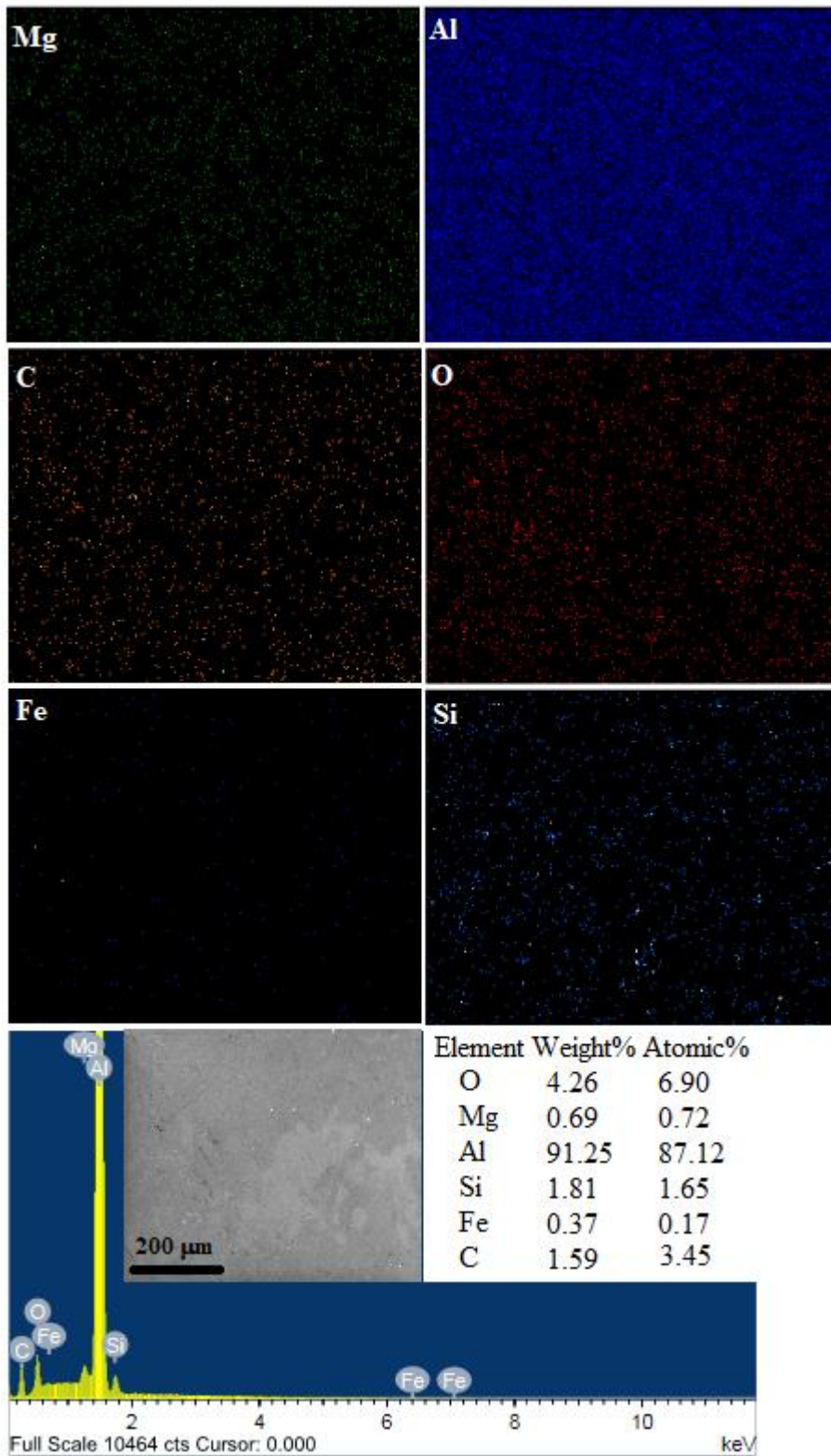
Figure 7.4 EDS elemental mapping of 5% SiC_p/Al6082 MMCs
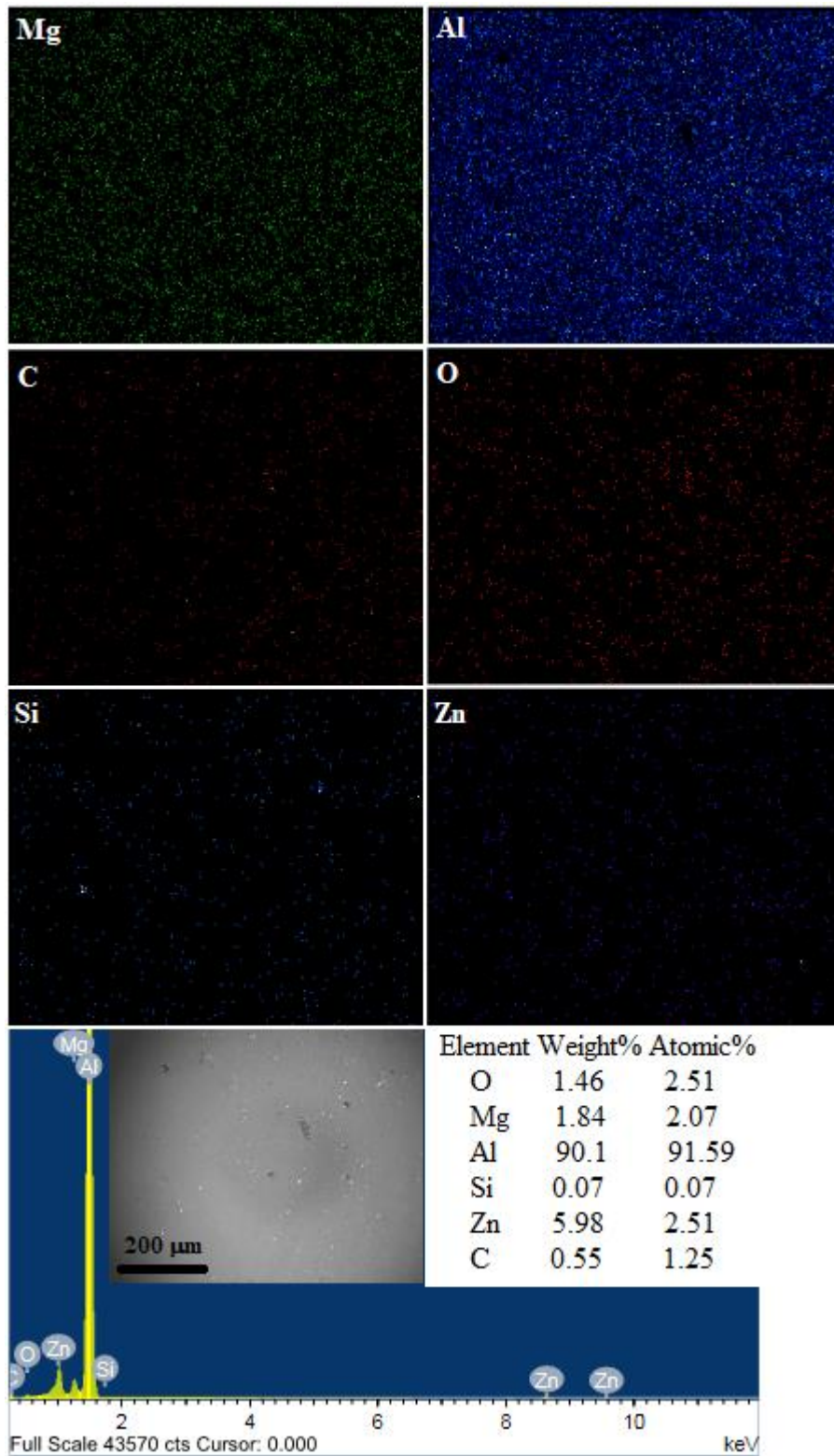
Figure 7.5 EDS elemental mapping of 5% SiC$_p$/Al7075 MMCs

7.2.2 Density

The densities of the as-received Al6082 and Al7075 alloy ingots are 2.71 g/cm^3 and 2.81 g/cm^3, provided by the suppliers. The densities of the Al6082 and Al7075 alloys reinforced with SiC$_p$ reinforcements MMCs are measured using density measurement kit apparatus and the results are shown in figure 7.6.
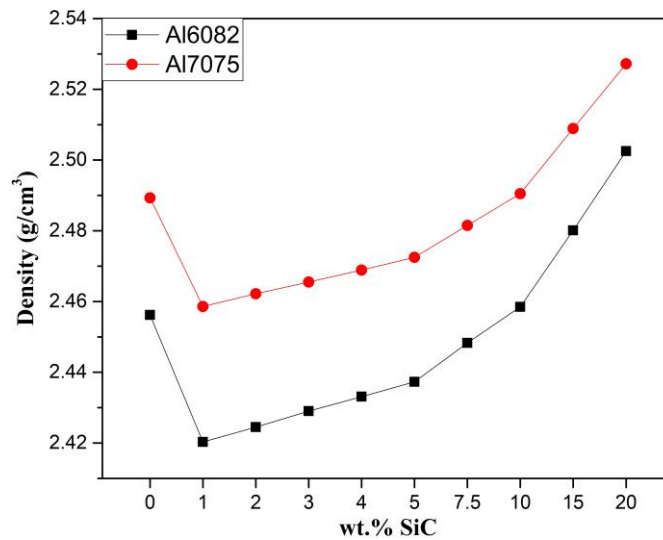
Figure 7.6 Density of MMCs

The density of the as-received Al6082 alloy ingot was 2.71 g/cm^3 but after casting the Al6082 alloy density decreased to 2.4562 g/cm^3. The density of the 1% SiC$_p$/Al6082 MMCs was observed as 2.4203 g/cm^3 whereas the as-cast Al6082 alloy was a bit higher. This is because, the stirring process, is not required in as-cast Al6082 alloy fabrication. However, for missing the SiC$_p$ reinforcement in the Al6082 alloy matrix, the mechanical stirrer was used. Hence, during the stirring process, the atmospheric oxygen might react and forms oxides in MMCs. Due to this reason, the density of the MMCs was observed to be less. The density of MMCs increased with the addition of 1% to 20% SiC$_p$ reinforcement, 20% SiC$_p$/Al6082 MMCs density was observed as 2.5025 g/cm^3. The presence of SiC$_p$ reinforcements has a major effect on the density of MMCs. Similarly, the density of the as-received Al7075 alloy ingot was 2.81 g/cm^3 but after casting the as-cast Al7075 alloy density was observed as 2.4893 g/cm^3. The density of 20% SiC$_p$/Al7075 MMCs was observed as 2.5272 g/cm^3 density. The density of MMCs increased with the addition of SiC$_p$ reinforcement from 1% to

114

20% SiC$_p$. However, the as-cast Al7075 alloy sample has high density compared to 7.5% SiC$_p$/Al7075 MMCs.

7.2.3 Hardness test

Figure 7.7 shows the test specimens of Al6082 as-cast alloy with indentation. The hardness value of MMCs increased as the percentage of SiC$_p$ reinforcement addition increased in the Al6082 and Al7075 alloy matrix. SiC$_p$ increases the hard and brittle phase of the alloy and increases the density at the particles–matrix interfaces. The hard and brittle SiC$_p$ reinforcement reduces ductility and offers high resistance to the plastic deformation which results in an increase in the hardness of MMCs.

50 μm
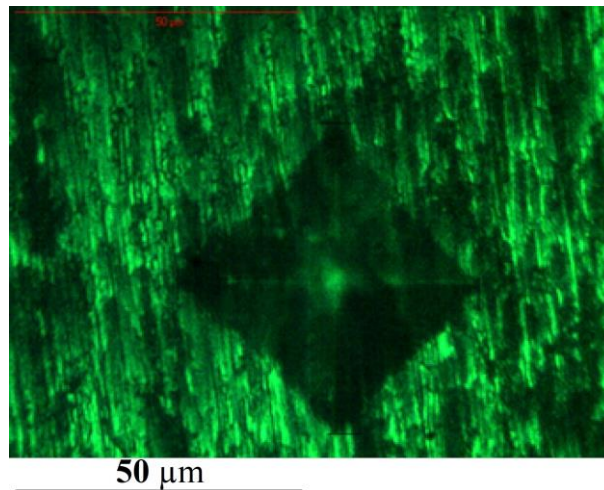
Figure 7.7 Hardness test of Al6082 as-cast alloy

The Vickers microhardness test results are shown in figure 7.8. The 20% SiC$_p$/Al6082 MMCs has hardness value of 76.41 HV, which is 1.33 times higher than as-cast Al6082 alloy. However, 20% SiC$_p$/Al7075 MMCs had the highest hardness value of 97.69 HV, which is 1.25 times higher than as-cast Al7075 alloy.
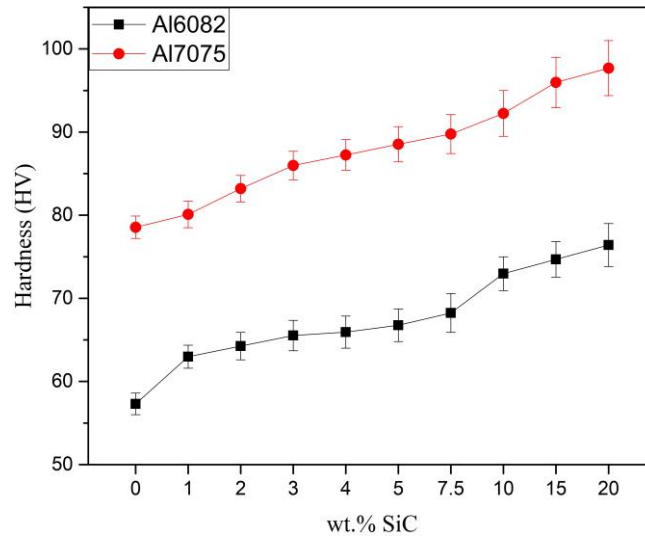
Figure 7.8 Hardness of MMCs

7.2.4 Tensile test

The MMCs showed increased tensile strength due to increase in the load-bearing capacity of the matrix by transferring the tensile load to SiC_p reinforcement. Figure 7.9 shows the tensile test specimens of as-cast Al6082 alloy.

Figure 7.9 Tensile test specimens of as-cast Al6082 alloy

The strengthening of MMCs was achieved by the addition of hard ceramic SiC_p reinforcement which strengthens the grain boundaries of the aluminum alloy matrix and helps to achieve higher strength (Hasan et al. (2004), Myriounis et al. (2010), and Shah and Hasan (2015)).The UTS results of the Al6082 and Al7075 alloy reinforced with SiC_p reinforcements MMCs are shown in figure 7.10. The yield strength, UTS and tensile modulus improved with the addition of SiC_p. The strength and brittle behavior of MMCs increased and ductility reduced with the addition of SiC_p. Considering the Al6082 matrix with different wt% SiC_p, 10% SiC_p/Al6082 MMCs had the UTS of 221 MPa. However, it was found that 15% SiC_p/Al7075 MMCs has the highest UTS of 275.287 MPa, which is 1.8 times higher than as-cast Al7075 alloy. Further 20% SiC_p/Al7075 MMCs showed reduction in UTS when compared to the 15% SiC_p/Al7075 MMCs. Due to the clustering of SiC_p in 20% SiC_p/Al7075 MMCs may result in reduced UTS.
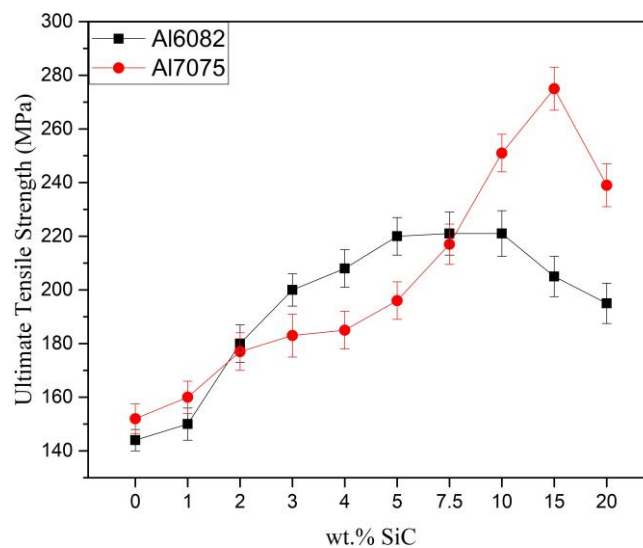
Figure 7.10 Ultimate tensile strength of MMCs

7.2.5 Charpy impact test

The impact test specimens of Al6082 as-cast alloy are shown in figure 7.11. The impact energy of the Al6082 and Al7075 alloy reinforced with different wt% of SiC_p reinforcements MMCs are shown in figure 7.12.

Figure 7.11 Impact test specimens of Al6082 as-cast alloy

The brittle properties of the SiC$_p$ have an important effect on the impact energy. 15% SiC$_p$/Al7075 MMCs has the highest impact energy of 8 J, which is 1.6 times higher than as-cast Al7075 alloy. Agglomeration of SiC$_p$ reinforcement in the Al7075 matrix reduces the impact energy of 20% SiC$_p$/Al7075 MMCs. From the obtained results, it was found that the SiC$_p$ reinforced Al7075 alloy MMCs had higher impact energy than SiC$_p$ reinforced Al6082 alloy MMCs.
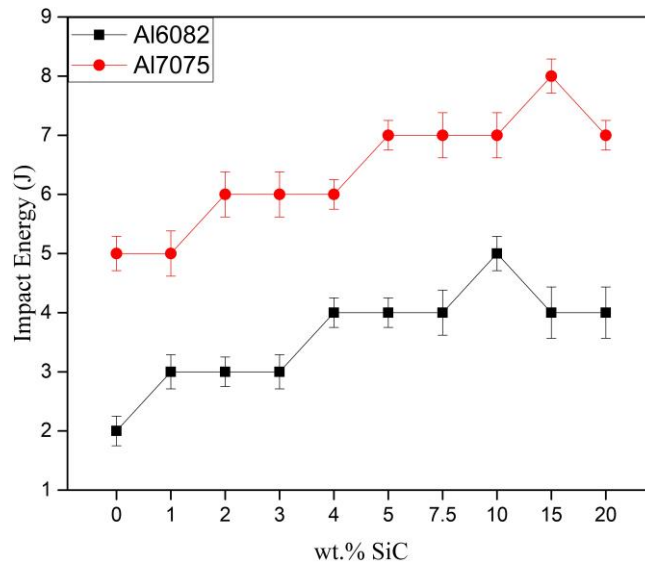
Figure 7.12 Impact energy of MMCs

The physical and mechanical properties of the Al6082 and Al7075 alloy reinforced with different wt% of SiC$_p$ reinforcements MMCs are shown in Tables 7.1 and 7.2.

Table 7.1 Material Properties of Al6082 matrix reinforced with SiC_p reinforcement.

No.	MMCs	Density		Impact energy	Tensile stress	Tensile modulus	VHN
		Theoreti-cal	Actual				
		(g/cm^3)	(g/cm^3)	J	MPa	MPa	
S1	Al6082	2.71	2.4562	2	144	16883	57.30
S2	1% SiC_p/Al6082	2.7142	2.4203	3	150	18033	62.98
S3	2% SiC_p/Al6082	2.7184	2.4245	3	180	15734	64.25
S4	3% SiC_p/Al6082	2.7227	2.4290	3	200	19232	65.53
S5	4% SiC_p/Al6082	2.7269	2.4331	4	208	19332	65.93
S6	5% SiC_p/Al6082	2.7312	2.4373	4	220	20636	66.76
S7	7.5% SiC_p/Al6082	2.7420	2.4483	4	221	19815	68.24
S8	10% SiC_p/Al6082	2.7528	2.4585	5	221	18970	72.97
S9	15% SiC_p/Al6082	2.7748	2.4801	4	205	19527	74.69
S10	20% SiC_p/Al6082	2.7971	2.5025	4	195	16620	76.41

Table 7.2 Material Properties of Al7075 matrix reinforced with SiC_p reinforcement.

No.	MMCs	Density		Impact energy	Tensile stress	Tensile modulus	VHN
		Theoreti-cal	Actual				
		(g/cm^3)	(g/cm^3)	J	MPa	MPa	
S11	Al7075	2.81	2.4893	5	152	18470	78.55
S12	1% SiC_p/Al7075	2.8135	2.4586	5	160.297	13176.8	80.10
S13	2% SiC_p/Al7075	2.8170	2.4622	6	177.448	15324.6	83.19
S14	3% SiC_p/Al7075	2.8205	2.4655	6	183.413	15067	85.98
S15	4% SiC_p/Al7075	2.8240	2.4689	6	185.237	14902	87.25
S16	5% SiC_p/Al7075	2.8276	2.4725	7	195.522	18533.9	88.53
S17	7.5% SiC_p/Al7075	2.8365	2.4815	7	216.778	15081.9	89.76
S18	10% SiC_p/Al7075	2.8454	2.4905	7	250.901	15715.2	92.24
S19	15% SiC_p/Al7075	2.8635	2.5089	8	275.287	15449.9	95.97
S20	20% SiC_p/Al7075	2.8818	2.5272	7	239.812	13829.2	97.69

7.2.6 Free vibration analysis

The dynamic behavior of the SiC$_p$ reinforced Al6082 and Al7075 MMCs was determined using free vibration analysis. The natural frequency and damping ratio corresponding to the first three modes were determined experimentally for the fabricated MMCs beam. The rectangular specimen of size 200 mm × 20 mm × 2 mm was fixed to a rigid fixture. The required dimensions of MMCs were machined using the WEDM method. Figure 7.13 shows the different wt% SiC$_p$ reinforced Al6082 and Al7075 alloy MMCs beams used for conducting the transverse free vibration analyses. Fixed free cantilever beam condition was considered for the study. MMCs beams were excited with the help of impact hammer. The natural frequency was measured from the peak of frequency response function plots. The damping factor of the MMCs beam was determined using half power bandwidth method.
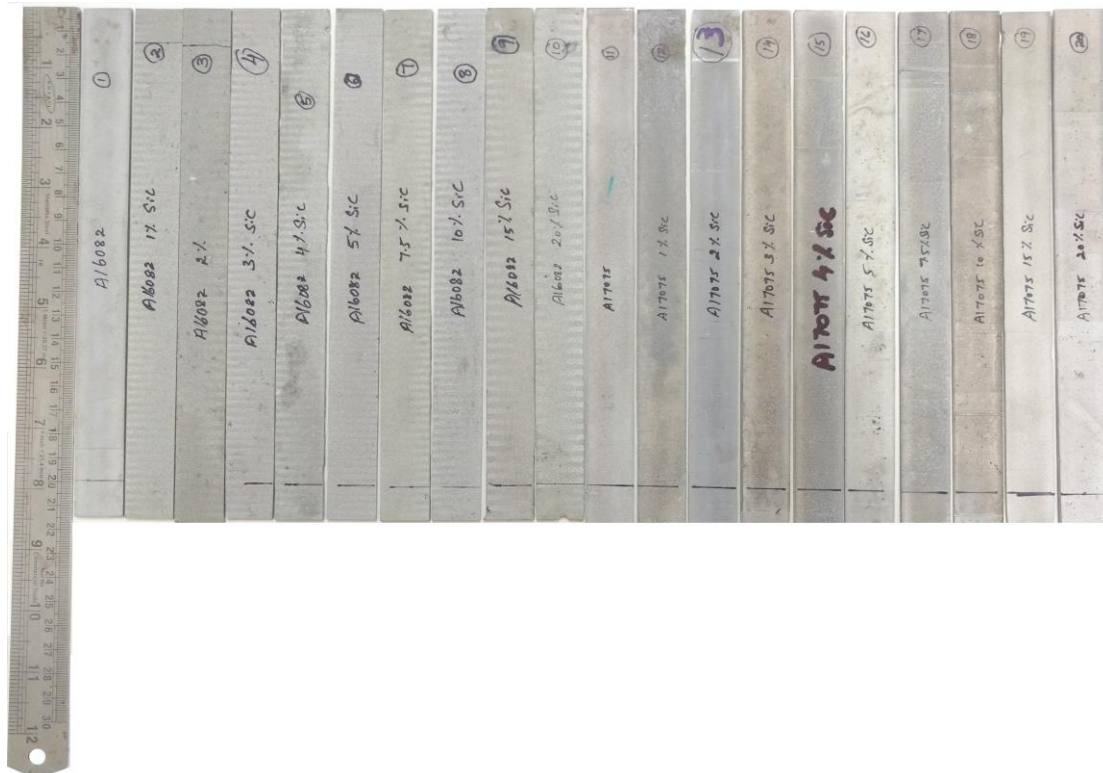
Figure 7.13 Different wt% of SiC$_p$ reinforced Al6082 and Al7075 alloy MMCs beam samples
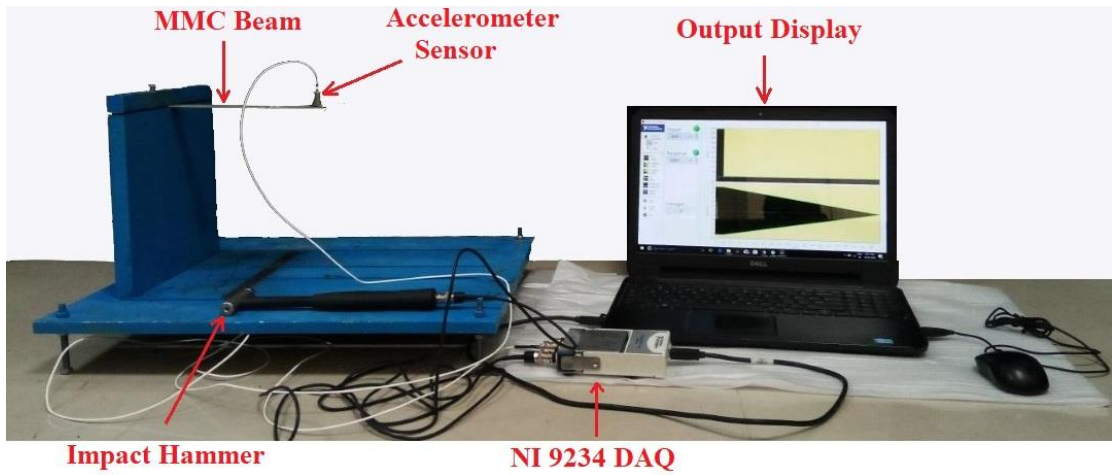
Figure 7.14 Free vibration analysis experimental setup

Table 7.3 Experimental free vibration analysis of MMCs

Material	1st mode		2nd mode		3rd mode	
	Natural freq. (Hz)	Damping ratio	Natural freq. (Hz)	Damping ratio	Natural freq. (Hz)	Damping ratio
Al6082	19.456	0.02027	176.640	0.02015	352.768	0.24608
1% SiC$_p$/Al6082	17.408	0.02123	164.864	0.00962	406.016	0.00627
2% SiC$_p$/Al6082	17.920	0.04608	173.568	0.03839	454.656	0.06912
3% SiC$_p$/Al6082	17.920	0.02716	168.960	0.02807	373.760	0.10999
4% SiC$_p$/Al6082	17.920	0.02230	164.352	0.02301	366.080	0.09881
5% SiC$_p$/Al6082	17.920	0.02598	193.024	0.08728	599.040	0.02814
7.5% SiC$_p$/Al6082	17.920	0.02442	167.936	0.02365	650.752	0.06477
10% SiC$_p$/Al6082	18.432	0.02305	166.400	0.03215	634.880	0.06318
15% SiC$_p$/Al6082	18.432	0.02332	167.424	0.02390	637.952	0.07417
20% SiC$_p$/Al6082	18.432	0.02931	173.568	0.01530	388.096	0.20483
Al7075	20.992	0.02846	208.896	0.05898	420.864	0.03854
1% SiC$_p$/Al7075	18.944	0.02009	170.496	0.01732	374.272	0.12712
2% SiC$_p$/Al7075	18.944	0.02841	169.984	0.00739	417.280	0.17711
3% SiC$_p$/Al7075	19.968	0.04503	179.200	0.01205	457.728	0.05049
4% SiC$_p$/Al7075	18.432	0.02889	171.008	0.00948	438.272	0.06320
5% SiC$_p$/Al7075	18.432	0.04082	169.984	0.00769	424.960	0.06599
7.5% SiC$_p$/Al7075	19.968	0.03563	198.656	0.01405	595.968	0.07902
10% SiC$_p$/Al7075	20.480	0.02341	179.200	0.02809	409.088	0.10326
15% SiC$_p$/Al7075	22.528	0.04999	195.072	0.01852	513.536	0.15287
20% SiC$_p$/Al7075	22.016	0.02466	204.288	0.01293	432.128	0.17437

The experimental free vibration analysis setup of the MMCs beam is shown in figure 7.14. Table 7.3 shows the experimentally determined first three mode natural frequencies and the damping ratio of MMCs respectively. From the obtained results for the first mode, it was found that the as-cast Al6082 alloy had a higher natural frequency than 1 to 20 wt% SiC_p reinforced Al6082 MMCs. Also, the as-cast Al7075 alloy had a higher natural frequency than 1 to 5 wt% SiC_p reinforced Al7075 MMCs. Further addition of 7.5 to 20 wt%. SiC_p in Al7075 alloy MMCs enhanced the natural frequency from 19.6968 Hz to 22.016 Hz. The highest natural frequency was observed in 15% SiC_p/Al7075 MMCs that could happen as a result of precise interface bonding between matrix and reinforcement. Similarly, for the second mode, as-cast Al6082 and as-cast Al7075 alloy had higher natural frequency than 1 to 20 wt% SiC_p reinforced Al6082 and Al7075 MMCs. However, in higher modes, the natural frequency of SiC_p reinforced Al6082 and Al7075 MMCs are higher than as-cast Al6082 and Al7075 alloy.

Based on the damping ratio for the first mode, SiC_p reinforced Al6082 MMCs showed a higher damping ratio than as-cast Al6082 alloy. The nonuniform damping ratio was observed with different wt% SiC_p reinforced Al7075 MMCs. However, 15% SiC_p/Al7075 MMCs had the highest damping ratio of 0.04999. Considering the second mode, 5% SiC_p/Al6082 MMCs had the highest damping ratio of 0.08728 and in third mode 20% SiC_p/Al7075 MMCs had the highest damping ratio of 0.17437. Increase in the damping ratio of SiC_p reinforced Al6082 and Al7075 MMCs indicates that the peak amplitude decreased with the addition of SiC_p reinforcement. Also, increased damping ratio leads to improvement in the fatigue life of the material.

The natural frequency of the material is directly proportional to the stiffness and inversely proportional to the mass of the material. Hence, it was found that the natural frequency of as-cast alloy was higher than SiC_p reinforced MMCs. However, the SiC_p reinforced MMCs had improved damping ratio than as-cast alloy. Further for the study, the fundamental first mode damping ratio values of MMCs samples are selected as an attribute in MADM techniques.

7.3 MADM

The optimal MMCs sample depending on their physical, mechanical and dynamic properties was determined by using AHP and TOPSIS and PROMETHEE techniques. After the determination of the weights of various attributes utilizing the AHP method, the MADM techniques were connected to the MMCs selection problem. The experimentally observed density, impact energy, UTS, hardness, and damping ratio of MMCs were considered as attributes for the optimal material selection. The steps involved in these techniques were discussed in chapter 3 methodology section 3.6.

7.3.1 Analytical hierarchy process (AHP)

The AHP method is the simplest method, applied to estimate the weights of the attributes. AHP method is mainly focused on determining the hierarchical structure, comparative judgment of the attributes and the alternatives and consistency check.

Step 1: Hierarchical structure, number of alternatives and attributes

The decision hierarchy structure for the selection of optimum MMCs sample is shown in figure 7.15. The objectives, attributes, and alternatives are arranged in the hierarchy structure which appears similar to a family tree. In this study, 20 alternatives and five attributes were chosen. Al6082 and Al7075 alloy reinforced with different wt% SiC_p MMCs were considered as alternatives. The density, impact energy, UTS, hardness, and damping ratio properties of MMCs were considered as attributes.

Table 7.4 shows the experimental data of MMCs. The main objective is to determine the optimal MMCs considering their physical, mechanical and dynamic properties. In the given attributes, for density low value is preferred whereas, for mechanical and dynamic properties like impact energy, UTS, hardness and damping ratio, high values are more preferred.
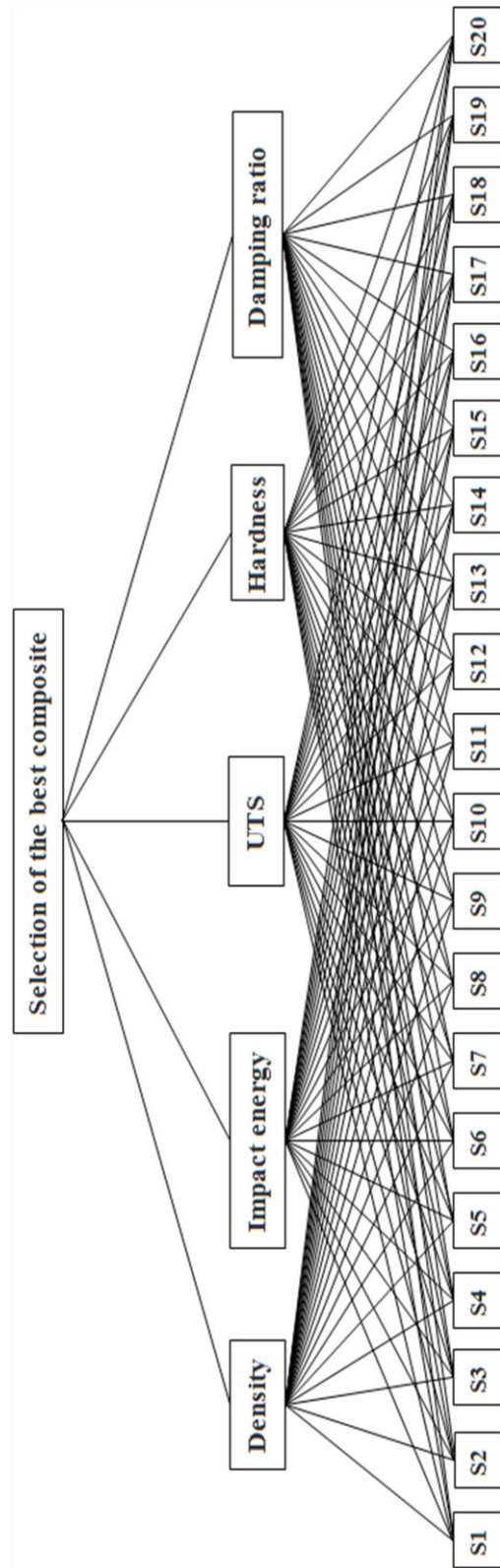
Figure 7.15 Decision hierarchy structure

Table 7.4 Data of MMCs

Sample No.	Alternatives	Attributes				
	MMCs	Density	Impact energy	UTS	Hardness	Damping ratio
S1	Al6082	2.4562	2	144	57.30	0.02027
S2	1% SiC$_p$/Al6082	2.4203	3	150	62.98	0.02123
S3	2% SiC$_p$/Al6082	2.4245	3	180	64.25	0.04608
S4	3% SiC$_p$/Al6082	2.4290	3	200	65.53	0.02716
S5	4% SiC$_p$/Al6082	2.4331	4	208	65.93	0.02230
S6	5% SiC$_p$/Al6082	2.4373	4	220	66.76	0.02598
S7	7.5% SiC$_p$/Al6082	2.4483	4	221	68.24	0.02442
S8	10% SiC$_p$/Al6082	2.4585	5	221	72.97	0.02305
S9	15% SiC$_p$/Al6082	2.4801	4	205	74.69	0.02332
S10	20% SiC$_p$/Al6082	2.5025	4	195	76.41	0.02931
S11	Al7075	2.4893	5	152	78.55	0.02846
S12	1% SiC$_p$/Al7075	2.4586	5	160	80.10	0.02009
S13	2% SiC$_p$/Al7075	2.4622	6	177	83.19	0.02841
S14	3% SiC$_p$/Al7075	2.4655	6	183	85.98	0.04503
S15	4% SiC$_p$/Al7075	2.4689	6	185	87.25	0.02889
S16	5% SiC$_p$/Al7075	2.4725	7	196	88.53	0.04082
S17	7.5% SiC$_p$/Al7075	2.4815	7	217	89.76	0.03563
S18	10% SiC$_p$/Al7075	2.4905	7	251	92.24	0.02341
S19	15% SiC$_p$/Al7075	2.5089	8	275	95.97	0.04999
S20	20% SiC$_p$/Al7075	2.5272	7	240	97.69	0.02466

Step 2: Normalization matrix

The normalization matrix is done depending on the maximum or minimum value of the attributes based on the preference. In the case of density attribute, minimum alternative value is chosen and all alternative value should divide the minimum alternative value for normalization. For all the other attributes maximum alternative value is chosen and all alternative values should be divided by the maximum alternative value for normalization.

Normalization matrix

$$\begin{array}{ccccc} \text{Density} & \text{Impact} & \text{UTS} & \text{Hardness} & \text{Damping} \\ \begin{bmatrix} 0.9853 & 0.25 & 0.5236 & 0.5865 & 0.40548 \\ 1 & 0.375 & 0.5454 & 0.6446 & 0.42468 \\ 0.9982 & 0.375 & 0.6545 & 0.6576 & 0.92178 \\ 0.9964 & 0.375 & 0.7272 & 0.6707 & 0.54331 \\ 0.9947 & 0.5 & 0.7563 & 0.6748 & 0.44609 \\ 0.9930 & 0.5 & 0.8 & 0.6833 & 0.51970 \\ 0.9885 & 0.5 & 0.8036 & 0.6985 & 0.48850 \\ 0.9844 & 0.625 & 0.8036 & 0.7469 & 0.46109 \\ 0.9758 & 0.5 & 0.7454 & 0.7645 & 0.46649 \\ 0.9671 & 0.5 & 0.7090 & 0.7821 & 0.58632 \\ 0.9722 & 0.625 & 0.5527 & 0.8040 & 0.56931 \\ 0.9844 & 0.625 & 0.5818 & 0.8199 & 0.40188 \\ 0.9829 & 0.75 & 0.6436 & 0.8515 & 0.56831 \\ 0.9816 & 0.75 & 0.6654 & 0.8801 & 0.90078 \\ 0.9803 & 0.75 & 0.6727 & 0.8931 & 0.57792 \\ 0.9788 & 0.875 & 0.7127 & 0.9062 & 0.81656 \\ 0.9753 & 0.875 & 0.7891 & 0.9188 & 0.71274 \\ 0.9718 & 0.875 & 0.9127 & 0.9442 & 0.46829 \\ 0.9646 & 1 & 1 & 0.9823 & 1 \\ 0.9577 & 0.875 & 0.8727 & 1 & 0.49330 \end{bmatrix} \end{array}$$

Step 3: Determining the relative importance matrix (Decision maker)

The relative importance matrix is assigned based on the importance given for the selected attributes. The damping ratio is considered the most important factor when compared to other attributes, followed by UTS, density, hardness, and impact energy. This decision matrix is constructed depending on the wide application of MMCs.

Relative importance matrix

$$\begin{array}{cccccc} \text{Attributes} & \text{Density} & \text{Impact} & \text{UTS} & \text{Hardness} & \text{Damping} \\ \text{Density} & \begin{bmatrix} 1 & 3 & 1/4 & 2 & 1/5 \\ \text{Impact} & 1/3 & 1 & 1/3 & 1/2 & 1/4 \\ \text{UTS} & 4 & 3 & 1 & 3 & 1/2 \\ \text{Hardness} & 1/2 & 2 & 1/3 & 1 & 1/3 \\ \text{Damping} & 5 & 4 & 2 & 3 & 1 \end{bmatrix} \end{array}$$

Step 4: Geometric mean

The geometric mean for each attribute was calculated based on equation (3.14). The geometric mean values are 0.786003, 0.425142, 1.782602, 0.644394, 2.605171 for density, impact energy, UTS, hardness and damping ratio respectively.

Step 5: Determining normalized weights w_j

The normalized weights of each attribute were calculated based on the equation (3.15). The obtained normalized weights are 0.12589, 0.06809, 0.28552, 0.10321 and 0.41727 for density, impact energy, UTS, hardness and damping ratio respectively.

Step 6: Consistency check

The RI value corresponding to five attributes is 1.11 (Rao (2007)). After solving equations (3.16) and (3.17), the CR value was calculated as 0.07032 which is less than 0.1 and hence the weights determined are allowable.

Step 6: Determination of Score and Rank

The scores of MMCs using SAW and WPM methods were derived based on equation (3.18) and (3.19). Obtained scores and ranks were shown in Table 7.5.

Table. 7.5 Scores in SAW and WPM

Sl. No.	MMC	SAW		WPM	
		Score	Rank	Score	Rank
1	Al6082	0.52033	20	0.49032	20
2	1% SiC$_p$/Al6082	0.55092	19	0.52597	19
3	2% SiC$_p$/Al6082	0.79062	5	0.76702	5
4	3% SiC$_p$/Al6082	0.65458	14	0.63512	14
5	4% SiC$_p$/Al6082	0.63104	17	0.60350	17
6	5% SiC$_p$/Al6082	0.67488	11	0.65430	11
7	7.5% SiC$_p$/Al6082	0.66389	13	0.63952	12
8	10% SiC$_p$/Al6082	0.66545	12	0.63792	13
9	15% SiC$_p$/Al6082	0.64332	16	0.61876	16
10	20% SiC$_p$/Al6082	0.68365	9	0.67187	9
11	Al7075	0.64333	15	0.62977	15
12	1% SiC$_p$/Al7075	0.58494	18	0.55461	18
13	2% SiC$_p$/Al7075	0.68363	10	0.67036	10
14	3% SiC$_p$/Al7075	0.83137	2	0.82284	2
15	4% SiC$_p$/Al7075	0.69990	8	0.68678	8
16	5% SiC$_p$/Al7075	0.82059	3	0.81612	3
17	7.5% SiC$_p$/Al7075	0.79992	4	0.79460	4
18	10% SiC$_p$/Al7075	0.73540	7	0.69680	7
19	15% SiC$_p$/Al7075	0.99374	1	0.99366	1
20	20% SiC$_p$/Al7075	0.73839	6	0.70591	6

Based on the obtained rank in the SAW and WPM method, 15% $SiC_p/Al7075$ MMC is selected as the best MMCs.

7.3.2 TOPSIS

The procedure for solving the TOPSIS method is explained in chapter 3 methodology section 3.6.2. The MMCs samples having a higher relative closeness coefficient is selected as the best MMCs. The steps followed to identify the optimum MMCs sample are given as follows.

Step 1: Determination of Normalization decision matrix

The normalization decision matrix is determined based on equation (3.20).

Normalization decision matrix

Density	Impact	UTS	Hardness	Damping
0.22273	0.08497	0.15956	0.16302	0.14745
0.21947	0.12746	0.16620	0.17918	0.15443
0.21985	0.12746	0.19945	0.18280	0.33519
0.22026	0.12746	0.22161	0.18644	0.19756
0.22063	0.16994	0.23047	0.18758	0.16221
0.22101	0.16994	0.24377	0.18994	0.18898
0.22201	0.16994	0.24487	0.19415	0.17763
0.22293	0.21243	0.24487	0.20760	0.16767
0.22489	0.16994	0.22715	0.21250	0.16963
0.22692	0.16994	0.21607	0.21739	0.21320
0.22573	0.21243	0.16842	0.22348	0.20702
0.22294	0.21243	0.17728	0.22789	0.14614
0.22327	0.25492	0.19612	0.23668	0.20666
0.22357	0.25492	0.20277	0.24462	0.32755
0.22388	0.25492	0.20499	0.24823	0.21015
0.22420	0.29740	0.21717	0.25187	0.29693
0.22502	0.29740	0.24044	0.25537	0.25917
0.22584	0.29740	0.27812	0.26243	0.17029
0.22751	0.33989	0.30471	0.27304	0.36363
0.22916	0.29740	0.26593	0.27793	0.17938

Step 2: Determination of the weighted normalized matrix

Weights of each attribute, calculated from equation (3.15) obtained from the AHP method were used for this study. Weighted normalized matrix calculated based on equation (3.21).

Weighted normalized matrix

	Density	Impact	UTS	Hardness	Damping
	0.02804	0.00579	0.04556	0.01683	0.06152
	0.02763	0.00868	0.04745	0.01849	0.06444
	0.02768	0.00868	0.05695	0.01887	0.13986
	0.02773	0.00868	0.06327	0.01924	0.08244
	0.02778	0.01157	0.06580	0.01936	0.06769
	0.02782	0.01157	0.06960	0.01960	0.07886
	0.02795	0.01157	0.06992	0.02004	0.07412
	0.02807	0.01446	0.06992	0.02143	0.06996
	0.02831	0.01157	0.06485	0.02193	0.07078
	0.02857	0.01157	0.06169	0.02244	0.08896
	0.02842	0.01446	0.04809	0.02307	0.08638
	0.02807	0.01446	0.05062	0.02352	0.06098
	0.02811	0.01736	0.05600	0.02443	0.08623
	0.02815	0.01736	0.05789	0.02525	0.13668
	0.02819	0.01736	0.05853	0.02562	0.08769
	0.02823	0.02025	0.06201	0.02600	0.12390
	0.02833	0.02025	0.06865	0.02636	0.10815
	0.02843	0.02025	0.07941	0.02709	0.07106
	0.02864	0.02314	0.08700	0.02818	0.15173
	0.02885	0.02025	0.07593	0.02869	0.07485

Step 3: Determination of ideal best and ideal worst solutions

The ideal best and ideal worst solutions for all the five attributes were determined based on equation (3.22).

$$V_1^+ = 0.02763 \quad V_1^- = 0.02885$$

$$V_2^+ = 0.02314 \quad V_2^- = 0.00579$$

$$V_3^+ = 0.08700 \quad V_3^- = 0.04556$$

$$V_4^+ = 0.02869 \quad V_4^- = 0.01683$$

$$V_5^+ = 0.15173 \quad V_5^- = 0.06098$$

Step 4: Calculation of separation measures and relative closeness coefficient

The distance of positive (S_i^+) and negative (S_i^-) separation measures were determined based on equation (3.23). The relative closeness coefficient (C_i) for each MMCs alternatives was determined based on equation (3.24). The obtained ranks of MMCs were shown in Table 7.6.

Table 7.6 Positive and negative ideal reference points, relative closeness coefficient and Rank of MMCs

Sample No.	Sl. No	MMC	S_i^+	S_i^-	C_i	Rank
S1	1	Al6082	0.10147	0.00098	0.00954	20
S2	2	1% SiC$_p$/Al6082	0.09745	0.00531	0.05169	19
S3	3	2% SiC$_p$/Al6082	0.03674	0.07979	0.68472	3
S4	4	3% SiC$_p$/Al6082	0.07525	0.02810	0.27191	12
S5	5	4% SiC$_p$/Al6082	0.08794	0.02227	0.20207	17
S6	6	5% SiC$_p$/Al6082	0.07636	0.03066	0.28649	11
S7	7	7.5% SiC$_p$/Al6082	0.08077	0.02847	0.26064	14
S8	8	10% SiC$_p$/Al6082	0.08430	0.02777	0.24780	15
S9	9	15% SiC$_p$/Al6082	0.08499	0.02299	0.21288	16
S10	10	20% SiC$_p$/Al6082	0.06895	0.03329	0.32563	8
S11	11	Al7075	0.07676	0.02768	0.26504	13
S12	12	1% SiC$_p$/Al7075	0.09830	0.01210	0.10959	18
S13	13	2% SiC$_p$/Al7075	0.07282	0.03064	0.29616	10
S14	14	3% SiC$_p$/Al7075	0.03346	0.07802	0.69989	2
S15	15	4% SiC$_p$/Al7075	0.07040	0.03307	0.31960	9
S16	16	5% SiC$_p$/Al7075	0.03762	0.06726	0.64129	4
S17	17	7.5% SiC$_p$/Al7075	0.04744	0.05530	0.53826	5
S18	18	10% SiC$_p$/Al7075	0.08110	0.03952	0.32765	7
S19	19	15% SiC$_p$/Al7075	0.00113	0.10190	0.98903	1
S20	20	20% SiC$_p$/Al7075	0.07774	0.03827	0.32989	6

The ranking order of MMCs obtained using TOPSIS method are as follows: S19 > S14 > S3 > S16 > S17 > S20 > S18 > S10 > S15 > S13 > S6 > S4 > S11 > S7 > S8 > S9 > S5 > S12 > S2 > S1. The sample S19, 15% SiC$_p$/Al7075 MMCs had been inferred as the optimum sample compared to other MMCs alternatives. The last rank of the alternative was found to be sample S1, Al6082 as-cast alloy.

7.3.3 PROMETHEE

The PROMETHEE method is used for the selection of suitable MMCs samples. MMCs data is identified with respect to their weights and maximisation. Table 7.7 shows the alternatives and criteria arranged. Here, "maximise the criteria" is considered and weights for the criteria were selected from the AHP method for the study. Table 7.18 shows the specific preference values of C1 (Density) criteria. Similarly, preference calculations were done for C2 (Impact Strength), C3 (UTS), C4 (Hardness) and C5

(Damping ratio). Corresponding to all the preferences C1, C2, C3, C4 and C5, the final matrix was determined and is shown in Table 7.9. The leaving flow, entering flow and net flow were determined based on equation (3.29) to (3.31) and are shown in Table 7.10. The Rank of MMCs sample is given based on the highest net flow value.

Table 7.7 Alternatives with respect to criterion and corresponding weights

Alternatives (MMC)	Attributes (Criteria)				
	C_1	C_2	C_3	C_4	C_5
Al6082	2.4562	2	144	57.30	0.02027
1% SiC$_p$/Al6082	2.4203	3	150	62.98	0.02123
2% SiC$_p$/Al6082	2.4245	3	180	64.25	0.04608
3% SiC$_p$/Al6082	2.4290	3	200	65.53	0.02716
4% SiC$_p$/Al6082	2.4331	4	208	65.93	0.02230
5% SiC$_p$/Al6082	2.4373	4	220	66.76	0.02598
7.5% SiC$_p$/Al6082	2.4483	4	221	68.24	0.02442
10% SiC$_p$/Al6082	2.4585	5	221	72.97	0.02305
15% SiC$_p$/Al6082	2.4801	4	205	74.69	0.02332
20% SiC$_p$/Al6082	2.5025	4	195	76.41	0.02931
Al7075	2.4893	5	152	78.55	0.02846
1% SiC$_p$/Al7075	2.4586	5	160	80.10	0.02009
2% SiC$_p$/Al7075	2.4622	6	177	83.19	0.02841
3% SiC$_p$/Al7075	2.4655	6	183	85.98	0.04503
4% SiC$_p$/Al7075	2.4689	6	185	87.25	0.02889
5% SiC$_p$/Al7075	2.4725	7	196	88.53	0.04082
7.5% SiC$_p$/Al7075	2.4815	7	217	89.76	0.03563
10% SiC$_p$/Al7075	2.4905	7	251	92.24	0.02341
15% SiC$_p$/Al7075	2.5089	8	275	95.97	0.04999
20% SiC$_p$/Al7075	2.5272	7	240	97.69	0.02466
Maximise	No	Yes	Yes	Yes	Yes
Weights	0.12589	0.06809	0.28552	0.10321	0.41727

Table 7.8 Preference values P resulting from the pairwise comparisons of the 20 alternative MMCs with respect to criterion C1 (density)

C1	a1	a2	a3	a4	a5	a6	a7	a8	a9	a10	a11	a12	a13	a14	a15	a16	a17	a18	a19	a20
a1	-	0	0	0	0	0	0	1	1	1	1	1	1	1	1	1	1	1	1	1
a2	1	-	1	1	1	1	1	1	1	1	1	1	1	1	1	1	1	1	1	1
a3	1	0	-	1	1	1	1	1	1	1	1	1	1	1	1	1	1	1	1	1
a4	1	0	0	-	1	1	1	1	1	1	1	1	1	1	1	1	1	1	1	1
a5	1	0	0	0	-	1	1	1	1	1	1	1	1	1	1	1	1	1	1	1
a6	1	0	0	0	0	-	1	1	1	1	1	1	1	1	1	1	1	1	1	1
a7	1	0	0	0	0	0	-	1	1	1	1	1	1	1	1	1	1	1	1	1
a8	0	0	0	0	0	0	0	-	1	1	1	1	1	1	1	1	1	1	1	1
a9	0	0	0	0	0	0	0	0	-	1	1	0	0	0	0	0	1	1	1	1
a10	0	0	0	0	0	0	0	0	0	-	0	0	0	0	0	0	0	0	1	1
a11	0	0	0	0	0	0	0	0	0	1	-	0	0	0	0	0	0	1	1	1
a12	0	0	0	0	0	0	0	0	1	1	1	-	1	1	1	1	1	1	1	1
a13	0	0	0	0	0	0	0	0	1	1	1	0	-	1	1	1	1	1	1	1
a14	0	0	0	0	0	0	0	0	1	1	1	0	0	-	1	1	1	1	1	1
a15	0	0	0	0	0	0	0	0	1	1	1	0	0	0	-	1	1	1	1	1
a16	0	0	0	0	0	0	0	0	1	1	1	0	0	0	0	-	1	1	1	1
a17	0	0	0	0	0	0	0	0	0	1	1	0	0	0	0	0	-	1	1	1
a18	0	0	0	0	0	0	0	0	0	1	0	0	0	0	0	0	0	-	1	1
a19	0	0	0	0	0	0	0	0	0	0	0	0	0	0	0	0	0	0	-	1
a20	0	0	0	0	0	0	0	0	0	0	0	0	0	0	0	0	0	0	0	-

Table 7.9 Final preference matrix

	a1	a2	a3	a4	a5	a6	a7	a8	a9	a10	a11	a12	a13	a14	a15	a16	a17	a18	a19	a20
a1	-	0	0	0	0	0	0	0.12589	0.12589	0.12589	0.12589	0.54316	0.12589	0.12589	0.12589	0.12589	0.12589	0.12589	0.12589	0.12589
a2	0.99998	-	0.19398	0.19398	0.12589	0.12589	0.12589	0.12589	0.12589	0.12589	0.12589	0.54316	0.12589	0.12589	0.12589	0.12589	0.12589	0.12589	0.12589	0.12589
a3	0.99998	0.80600	-	0.61125	0.54316	0.54316	0.54316	0.54316	0.54316	0.54316	0.82868	0.82868	0.82868	0.54316	0.54316	0.54316	0.54316	0.54316	0.12589	0.54316
a4	0.99998	0.80600	0.38873	-	0.54316	0.54316	0.54316	0.54316	0.54316	0.41141	0.41141	0.82868	0.41141	0.41141	0.41141	0.41141	0.12589	0.54316	0.12589	0.54316
a5	0.99998	0.87409	0.45682	0.45682	-	0.19398	0.19398	0.12589	0.47950	0.47950	0.41141	0.82868	0.41141	0.41141	0.41141	0.41141	0.12589	0.12589	0.12589	0.12589
a6	0.99998	0.87409	0.45682	0.45682	0.80600	-	0.61125	0.54316	0.89677	0.47950	0.41141	0.82868	0.41141	0.41141	0.41141	0.41141	0.41141	0.54316	0.12589	0.54316
a7	0.99998	0.87409	0.45682	0.45682	0.80600	0.38873	-	0.82868	0.89677	0.47950	0.41141	0.82868	0.41141	0.41141	0.41141	0.41141	0.41141	0.54316	0.12589	0.12589
a8	0.87409	0.87409	0.45682	0.45682	0.87409	0.45682	0.17130	-	0.47950	0.47950	0.47950	0.89677	0.41141	0.41141	0.41141	0.41141	0.41141	0.12589	0.12589	0.12589
a9	0.87409	0.87409	0.45682	0.45682	0.52048	0.10321	0.10321	0.52048	-	0.47950	0.41141	0.70279	0.28552	0.28552	0.28552	0.28552	0.12589	0.12589	0.12589	0.12589
a10	0.87409	0.87409	0.45682	0.58857	0.52048	0.52048	0.52048	0.52048	0.52048	-	0.70279	0.70279	0.70279	0.28552	0.70279	0	0	0.41727	0.12589	0.54316
a11	0.87409	0.87409	0.17130	0.58857	0.58857	0.58857	0.58857	0.52048	0.58857	0.29719	-	0.48536	0.41727	0	0	0	0	0.54316	0.12589	0.54316
a12	0.45682	0.45682	0.17130	0.17130	0.17130	0.17130	0.17130	0.10321	0.29719	0.29719	0.51462	-	0.12589	0.12589	0.12589	0.12589	0.12589	0.12589	0.12589	0.12589
a13	0.87409	0.87409	0.17130	0.58857	0.58857	0.58857	0.58857	0.58857	0.71446	0.29719	0.58271	0.87409	-	0.19398	0.19398	0.12589	0.12589	0.54316	0.12589	0.54316
a14	0.87409	0.87409	0.45682	0.58857	0.58857	0.58857	0.58857	0.58857	0.71446	0.71446	0.99998	0.87409	0.80600	-	0.61125	0.54316	0.54316	0.54316	0.12589	0.54316
a15	0.87409	0.87409	0.45682	0.58857	0.58857	0.58857	0.58857	0.58857	0.71446	0.29719	0.99998	0.87409	0.80600	0.38873	-	0.12589	0.12589	0.54316	0.12589	0.54316
a16	0.87409	0.87409	0.45682	0.58857	0.58857	0.58857	0.58857	0.58857	0.71446	0.99998	0.99998	0.87409	0.87409	0.45682	0.87409	-	0.61125	0.61125	0.12589	0.61125
a17	0.87409	0.87409	0.45682	0.87409	0.87409	0.58857	0.58857	0.58857	0.87409	0.99998	0.99998	0.87409	0.87409	0.45682	0.87409	0.38873	-	0.61125	0.12589	0.61125
a18	0.87409	0.87409	0.45682	0.45682	0.87409	0.45682	0.45682	0.87409	0.87409	0.58271	0.45682	0.87409	0.45682	0.45682	0.45682	0.38873	0.38873	-	0.12589	0.47950
a19	0.87409	0.87409	0.87409	0.87409	0.87409	0.87409	0.87409	0.87409	0.87409	0.87409	0.87409	0.87409	0.87409	0.87409	0.87409	0.87409	0.87409	0.87409	-	0.89677
a20	0.87409	0.87409	0.45682	0.45682	0.87409	0.45682	0.87409	0.87409	0.87409	0.45682	0.45682	0.87409	0.45682	0.45682	0.45682	0.38873	0.38873	0.52048	0.10321	-

Table 7.10 Leaving flow, entering flow, net flow and Rank

Sample No.	Sl. No	MMC	$\phi^+(a)$	$\phi^-(a)$	$\phi(a)$	Rank
S1	1	Al6082	2.05384	16.94578	-14.89194	20
S2	2	1% SiC$_p$/Al6082	3.81945	15.18017	-11.36072	19
S3	3	2% SiC$_p$/Al6082	11.54708	7.45254	4.09454	5
S4	4	3% SiC$_p$/Al6082	9.54575	9.45387	0.09188	12
S5	5	4% SiC$_p$/Al6082	7.64985	11.34977	-3.69992	16
S6	6	5% SiC$_p$/Al6082	10.63374	8.36588	2.26786	9
S7	7	7.5% SiC$_p$/Al6082	10.27947	8.72015	1.55932	10
S8	8	10% SiC$_p$/Al6082	8.93402	10.06560	-1.13158	14
S9	9	15% SiC$_p$/Al6082	7.14854	11.85108	-4.70254	17
S10	10	20% SiC$_p$/Al6082	9.57897	9.42065	0.15832	11
S11	11	Al7075	7.79484	11.20478	-3.40994	15
S12	12	1% SiC$_p$/Al7075	3.98947	15.01015	-11.02068	18
S13	13	2% SiC$_p$/Al7075	9.18273	9.81689	-0.63416	13
S14	14	3% SiC$_p$/Al7075	12.16662	6.83300	5.33362	4
S15	15	4% SiC$_p$/Al7075	10.69229	8.30733	2.38496	8
S16	16	5% SiC$_p$/Al7075	12.90100	6.09862	6.80238	3
S17	17	7.5% SiC$_p$/Al7075	13.40915	5.59047	7.81868	2
S18	18	10% SiC$_p$/Al7075	10.86466	8.13496	2.72970	7
S19	19	15% SiC$_p$/Al7075	16.63039	2.36923	14.26116	1
S20	20	20% SiC$_p$/Al7075	11.17434	7.82528	3.34906	6

Based on the obtained rank in Table 7.10, it is observed that the 15% SiC$_p$/Al7075 gives better strength and damping ability compared to other alternatives. The last rank of MMCs was found to be Al6082 alloy. The strength and stiffness of MMCs improved due to the addition of SiC$_p$. The best range (Rank 1) 15% SiC$_p$/Al7075 MMCs and least range (Rank 20) Al6082 as-cast alloy matches in all the MADM methods. Based on the obtained rank in TOPSIS and PROMETHEE method, the ranks are plotted and shown in figure 7.16. Based on the obtained result, it can be inferred that 15% SiC$_p$/Al7075 is the best MMCs specimen. The AHP, SAW, WPM, TOPSIS and PROMETHEE methods had been very useful in the selection of MMCs. Also, these MADM methods are simple, systematic and easy to understand by using the concept of statistics.
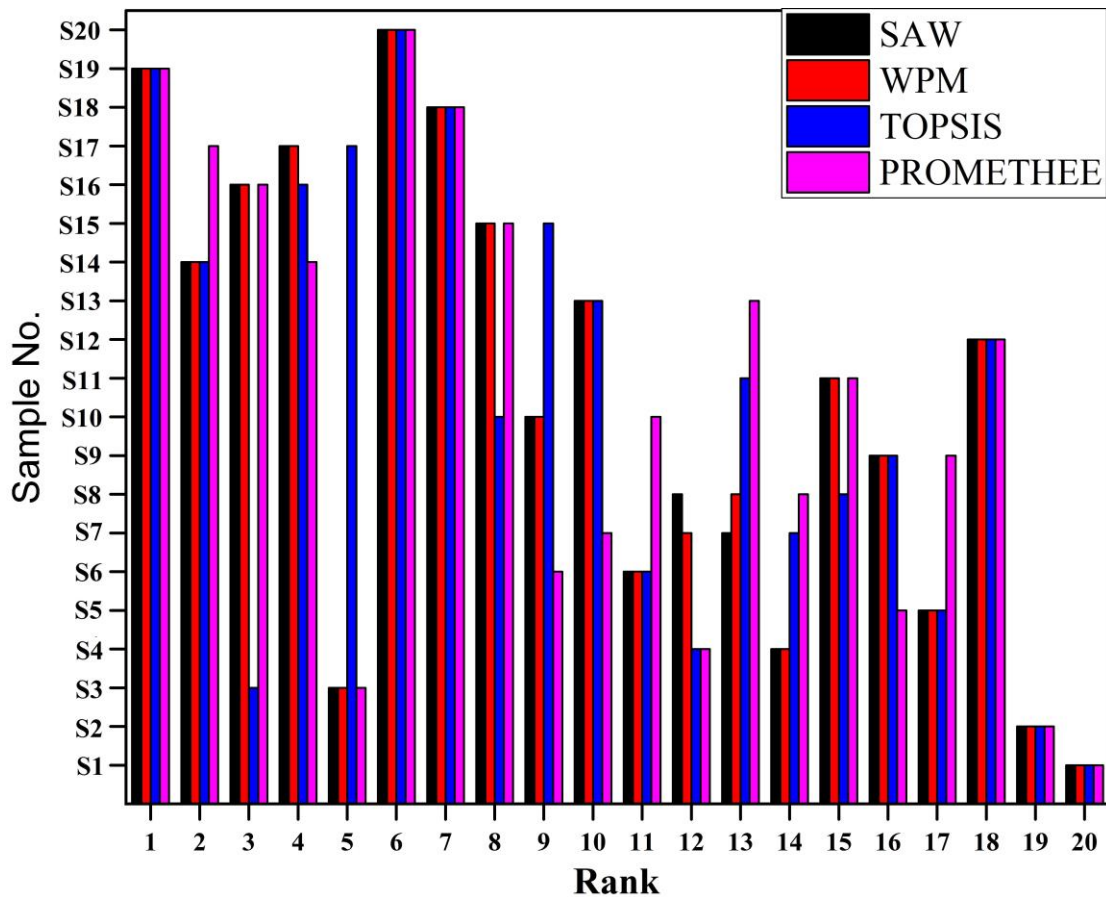
Figure 7.16 MMCs rank

7.3.4 Response surface methodology

The main objective of the RSM is to figure out the significant independent parameters, which influence the response (density, impact energy, UTS, hardness and natural frequency) output parameter. The variation of responses to the independent parameters such as aluminum alloy matrix and SiC_p reinforcement are plotted in the 3D response curve. The three steps involved in solving RSM are as follows. In the first step, the user-defined design was selected for the RSM with two factors at three levels. The user-defined analysis was carried out for Al6082 alloy and SiC_p factors with 800 (-1), 900 (0), 1000 (1) and 0 (-1), 100 (0), 200 (1) levels. Similarly, the same analysis was carried out for Al7075 alloy and SiC_p factors. The experimentally determined response parameters of MMCs at the stipulated conditions are carried out for nine runs.

In the second step, the quadratic model was selected for the analysis. The motive of using this quadratic model in this study was to examine the independent factor space

135

and to locate the region where the response approaches optimal value for the desired goal. The significant model prediction was obtained for all the responses in the ANOVA. Hence, the analysis was verified with respect to the significant model prediction. In the last step, the 3D response surface curves were plotted as a function of aluminum alloy and SiC_p.

The 3D response surface curve of density, impact energy, UTS, hardness and natural frequency are shown in figures 7.17-7.21. Based on the figures, it can be seen that the responses of both Al6082 alloy and Al7075 alloy reinforced SiC_p appear almost similar. However, the response magnitude of the SiC_p reinforced Al7075 alloy was higher than that of SiC_p reinforced Al6082 alloy. The density response curve indicates that increment in wt% of SiC_p and decrement in the aluminum alloy will result in an increased density of MMCs. The impact energy and UTS response curves indicate that both responses enhanced with an increment in wt% of SiC_p and decrement in aluminum alloy up to a certain level and further increment in wt% of SiC_p and decrement in the aluminum alloy the impact energy and UTS responses tend to decrease. The hardness and natural frequency response curves indicate that both these responses improved with an increment in wt% of SiC_p reinforcement.
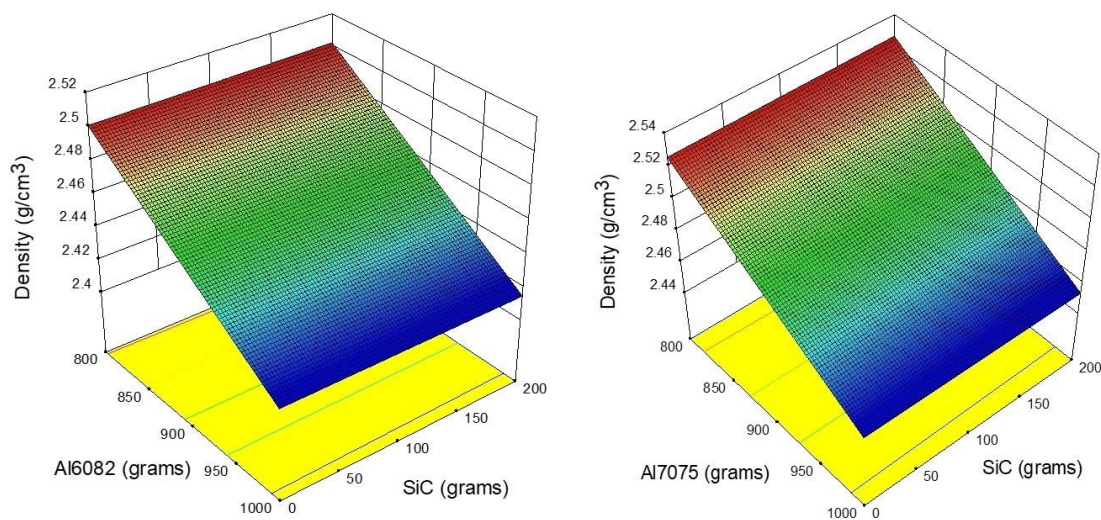
Figure 7.17 3D response surface curve of density

136
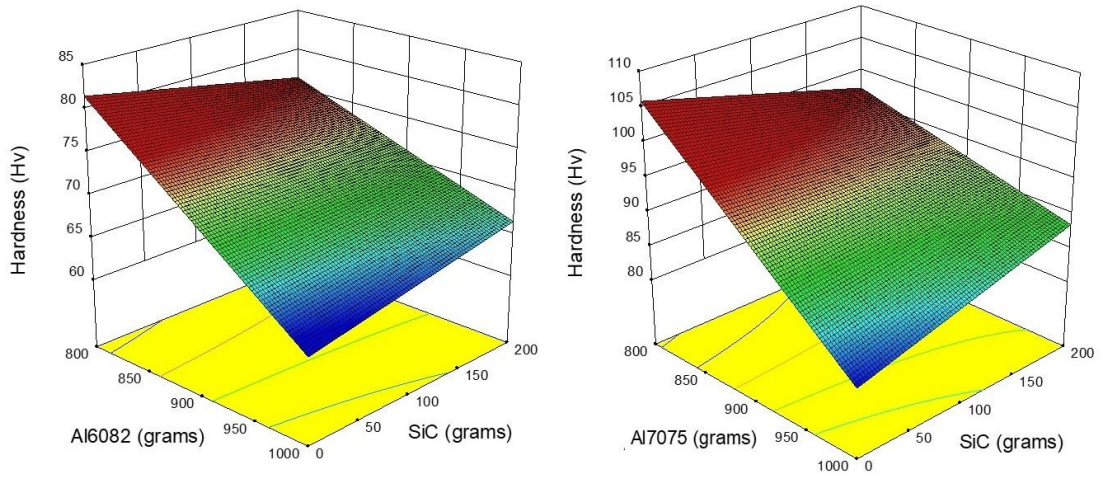
Figure 7.18 3D response surface curve of hardness
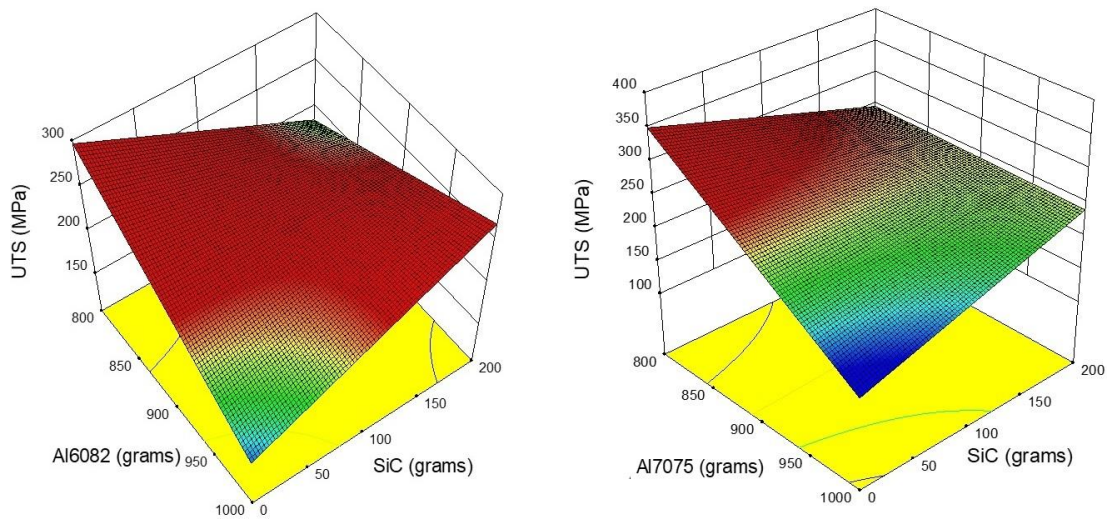
Figure 7.19 3D response surface curve of UTS
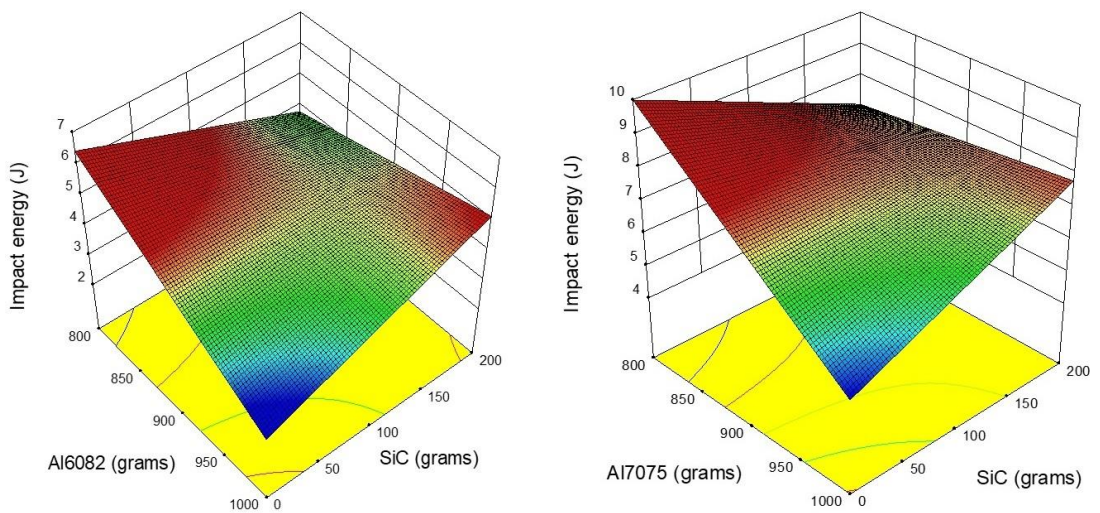
Figure 7.20 3D response surface curve of impact energy

137
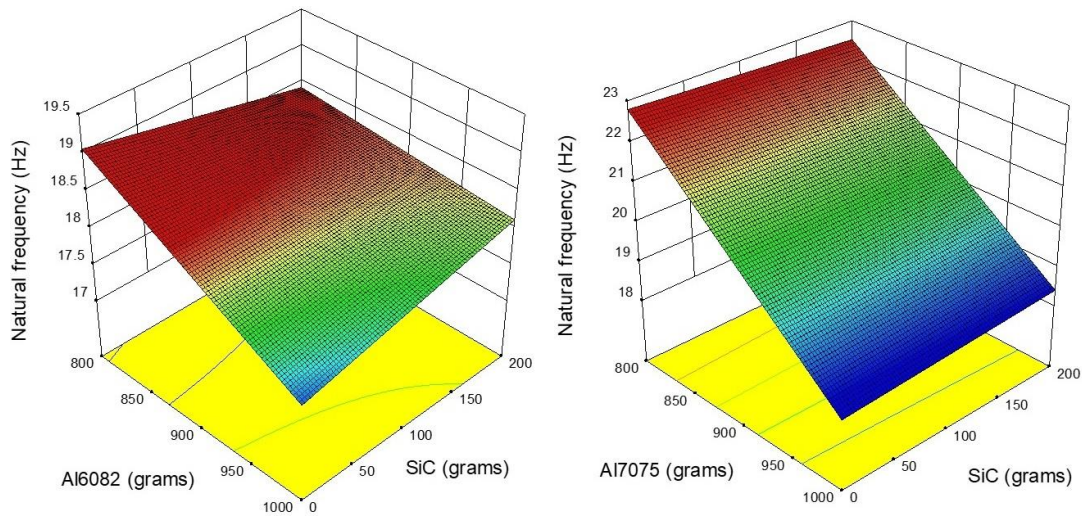
Figure 7.21 3D response surface curve of natural frequency

Numerical optimization was carried out to determine the optimum solution. The main goal of optimization is to minimize the density and to maximize the impact energy, UTS, hardness, and natural frequency. Table 7.11 shows the optimum solutions factors and responses corresponding to the physical, mechanical and dynamic properties of MMCs. 12.62% SiC_p/Al6082 and 13.66% SiC_p/Al7075 were identified as the optimum solution for different wt% SiC_p reinforced Al6082 alloy and SiC_p reinforced Al7075 alloy MMCs.

Table 7.11 Optimal solutions

MMCs	Aluminum alloy (g)	SiC_p (g)	Density (g/cm^3)	Impact energy (J)	UTS (MPa)	Hardness (Hv)	Natural frequency (Hz)
12.62% SiC_p/Al6082	873.8 (Al6082)	126.2	2.470	5	245.35	74.155	18.488
13.66% SiC_p/Al7075	863.4 (Al7075)	136.6	2.503	8.379	283.38	97.690	21.316

7.4 CONCLUSIONS

In this study, samples of Al6082 and Al7075 alloy with different weight fractions of (0, 1, 2, 3, 4, 5, 7.5, 10, 15 and 20 wt%) SiC_p reinforced MMCs were successfully fabricated through stir casting method. The microstructure, physical, mechanical and dynamic properties like density, hardness, impact energy, tensile

strength, natural frequency, damping ratio and optimum selection of MMCs were determined. The microstructure analysis revealed the non-homogeneous distribution of SiC_p reinforcement in aluminum alloy MMCs. The density and hardness of MMCs increased with the increase in the addition of SiC_p. The impact energy of MMCs increased with the addition of SiC_p reinforcement and reduced for higher weight percentage of SiC_p due to the clustering of reinforcement. The tensile strength enhanced up to 10 wt% addition of SiC_p reinforcement in Al6082 alloy MMCs and 15 wt% addition of SiC_p reinforcement in Al7075 alloy MMCs. 15% SiC_p/Al7075 MMCs obtained the maximum tensile strength of 275 MPa. Using free vibration analysis, it was observed that the natural frequency and damping ratio of MMCs improved with the addition of SiC_p reinforcement. By using AHP, TOPSIS and PROMETHEE multi-attribute decision-making techniques, 15% SiC_p/Al7075 MMCs was identified as the best MMCs sample among all other fabricated MMCs considering their physical, mechanical and dynamic properties. However, 13.66% SiC_p/Al7075 MMCs was identified as the optimum MMCs using RSM optimization. Hence, considering the strength and stiffness of 13.66% SiC/Al7075 MMCs, it will be most suitable for aerospace, aircraft, automobiles, landing gear cylinders, marine, military, fittings, and transportation equipment applications.

7.5 SUMMARY

In this chapter, the fabrication of different wt% SiC_p reinforced Al6082 and Al7075 MMCs carried out using the stir-casting technique is presented. The density, hardness, tensile and impact test properties have been evaluated through material characterization. Experimental free vibration analysis was carried out to determine the natural frequency and damping ratio of the MMCs materials. MADM techniques such as AHP, SAW, WPM, TOPSIS and PROMETHEE methods are used to determine the optimal MMCs materials. Based on MADM techniques 15% SiC_p/Al7075 MMCs is selected as the optimal MMCs material. Based on response surface methodology it was determined that 12.62% SiC_p/Al6082 MMCs and 13.66% SiC_p/Al7075 MMCs were identified as the optimum solutions for different wt% SiC_p reinforced Al6082 alloy and SiC_p reinforced Al7075 alloy MMCs.

CHAPTER 8

DYNAMIC ANALYSIS OF MMC-MRF CORE SANDWICH BEAMS

8.1 INTRODUCTION

The dynamic analysis of MMC-MRF core sandwich beams having 0, 5, 10, 15 and 20 wt% SiC_p reinforced Al6082 MMC as top and bottom layers and with MRF as the core was experimentally analyzed. The dynamic properties of these sandwich beams were subjected to 0, 200, 400 and 600 gauss magnetic flux densities and analyzed for their response to free and forced vibration analysis. The first three modes, natural frequencies and damping ratios of the sandwich beams are determined through free vibration analysis using DEWESoft modal analysis software. The frequency amplitude response of the sandwich beams was determined under forced vibration using LabVIEW software. The effect of various parameters such as magnetic flux density and addition of different wt% SiC_p reinforced Al6082 MMC top and bottom layers on the natural frequencies, damping ratio and vibration amplitude suppressions of the MMC-MRF core sandwich beams are investigated.

8.2 FABRICATION OF MMC-MRF CORE SANDWICH BEAMS

The Al6082 aluminum alloy reinforced with 0, 5, 10, 15 and 20 wt% of SiC_p were fabricated via stir casting method and used as top and bottom layers of sandwich beams. The MMCs fabrication procedure is explained in section 3.7. Also, the MRF preparation procedure is mentioned in section 3.3. Using WEDM, 220 mm x 20 mm x 2 mm MMC beams were machined and used as top and bottom layers of sandwich beams. Table 8.1 shows the matrix and reinforcement wt% of MMCs and dimensions of MMC-MRF core sandwich beams. Figure 8.1 illustrates the schematic and photograph of MMC-MRF core sandwich beams.

Table 8.1 Al6082 matrix and SiC$_p$ reinforcement wt% of MMCs and dimensions of MMC-MRF core sandwich beams

Sandwich Beams	Top and Bottom MMC Layers					MRF core layer		
	Al6082 wt%	SiC$_p$ wt%	Length (mm)	Width (mm)	Thickness (mm)	Length (mm)	Width (mm)	Thickness (mm)
B1	100	0	220	20	2	200	20	2
B2	95	5	220	20	2	200	20	2
B3	90	10	220	20	2	200	20	2
B4	85	15	220	20	2	200	20	2
B5	80	20	220	20	2	200	20	2
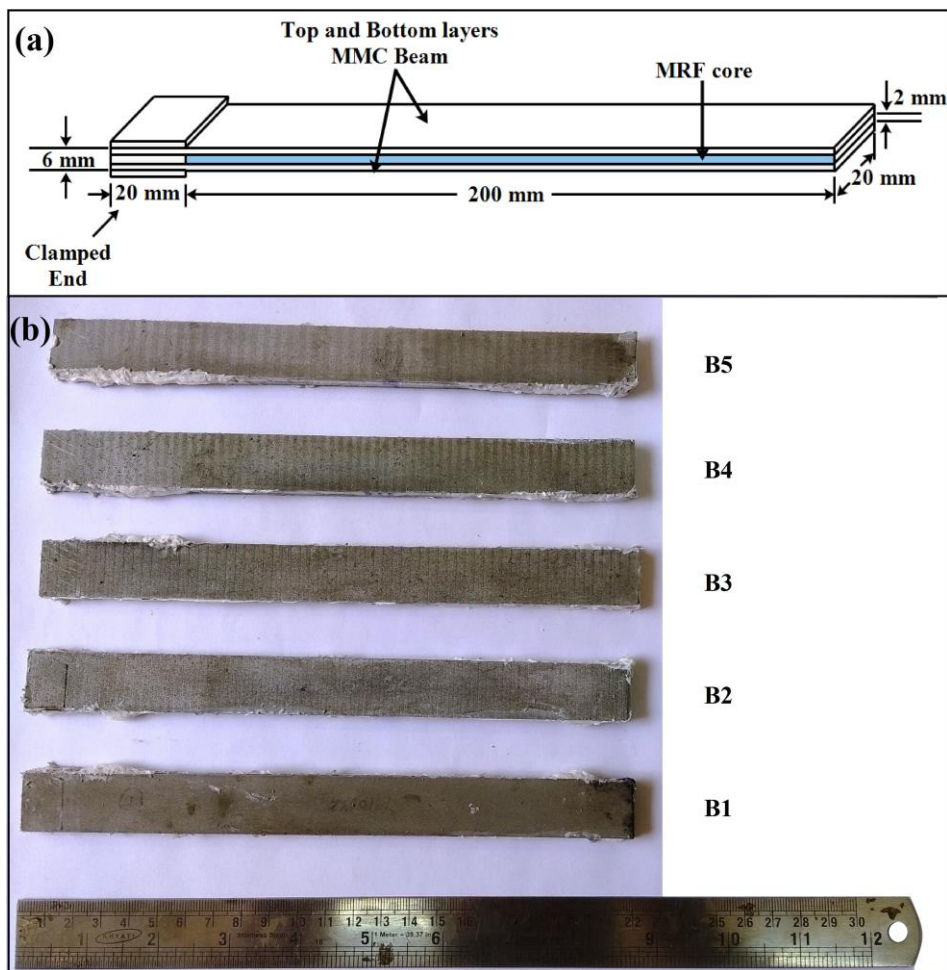
Figure 8.1 B1, B2, B3, B4 and B5 MMC-MRF core sandwich beams (a) Schematic view and (b) Photograph view

142

The procedure for the fabrication of the MMC-MRF core sandwich beam is as follows. The top and bottom MMC layers are fixed using Araldite adhesive having a 2 mm gap between them. The 2 mm gap between the top and bottom MMC layers was covered using silicone sealant. The applied silicone sealant is kept to cure for 24 hours. A small gap (opening) is made in the silicone sealant layer for filling the MRF. The prepared MRF is filled inside the silicone sealant layer between the top and bottom MMC layers and the voids in the core are removed. After filling MRF in the hollow MMC sandwich beam the gap in the middle core is sealed using silicone sealant. Five MMC-MRF core sandwich beams named B1, B2, B3, B4 and B5 were prepared. Further, experimental free vibration characteristics and forced vibration characteristics of fabricated sandwich beams were performed.

8.3 FREE VIBRATION CHARACTERIZATION

The free vibration modal analysis using impulse hammer excitation was carried out based on the ASTM E756-05 standard. The natural frequency and damping ratio of the MRF core enclosed SiC_p reinforced Al6082 MMCs sandwich beams were determined. The effective overall dimensions of the MMC-MRF core sandwich beams are 200 mm $\times$ 20 mm $\times$ 6 mm. The accelerometer sensor is placed at 175 mm from the fixed end.

Figure 8.2 Free vibration analysis experimental setup

Figure 8.3 Free vibration modal analysis of B1 MMC-MRF core sandwich beam at 0 G magnetic flux density (a) First mode, (b) Second mode, and (c) Third mode

The experimental free vibration setup used for determining the natural frequency and damping ratios of sandwich beams subjected to the influence of the external non-homogeneous magnetic field is shown in figure 8.2. The experimental setup consists of a modal analysis DEWESoft software with the data acquisition system (Make: DEWETRON), gaussmeter, accelerometer sensor, four permanent magnets (ferrite iron magnets) and fixture for holding the sandwich beams.

The first three modes, natural frequency and damping ratios of sandwich beams were determined. Figure 8.3 shows the snapshot display of 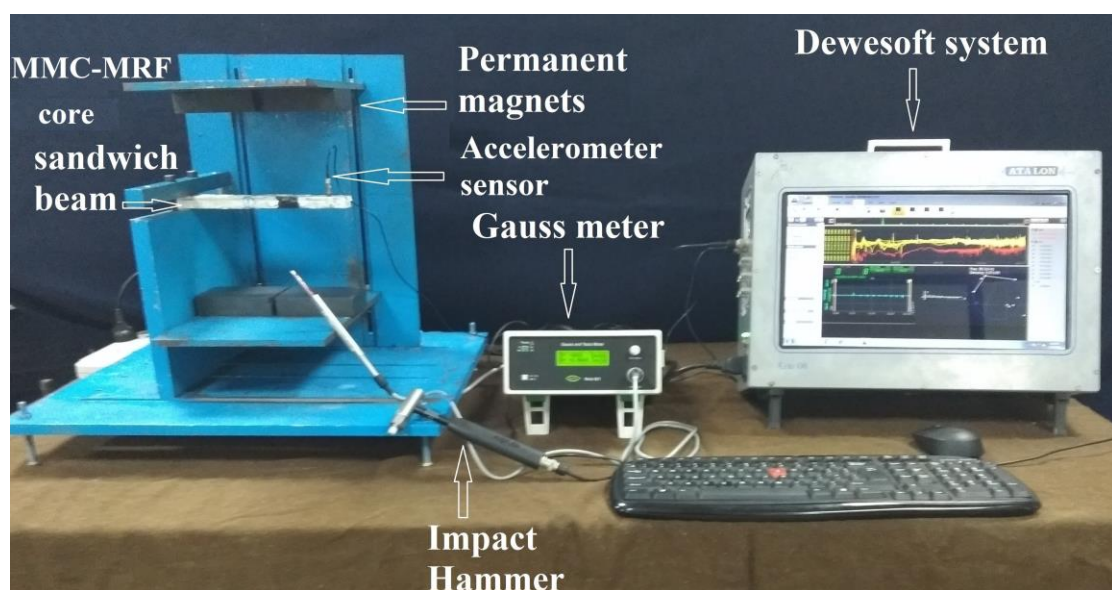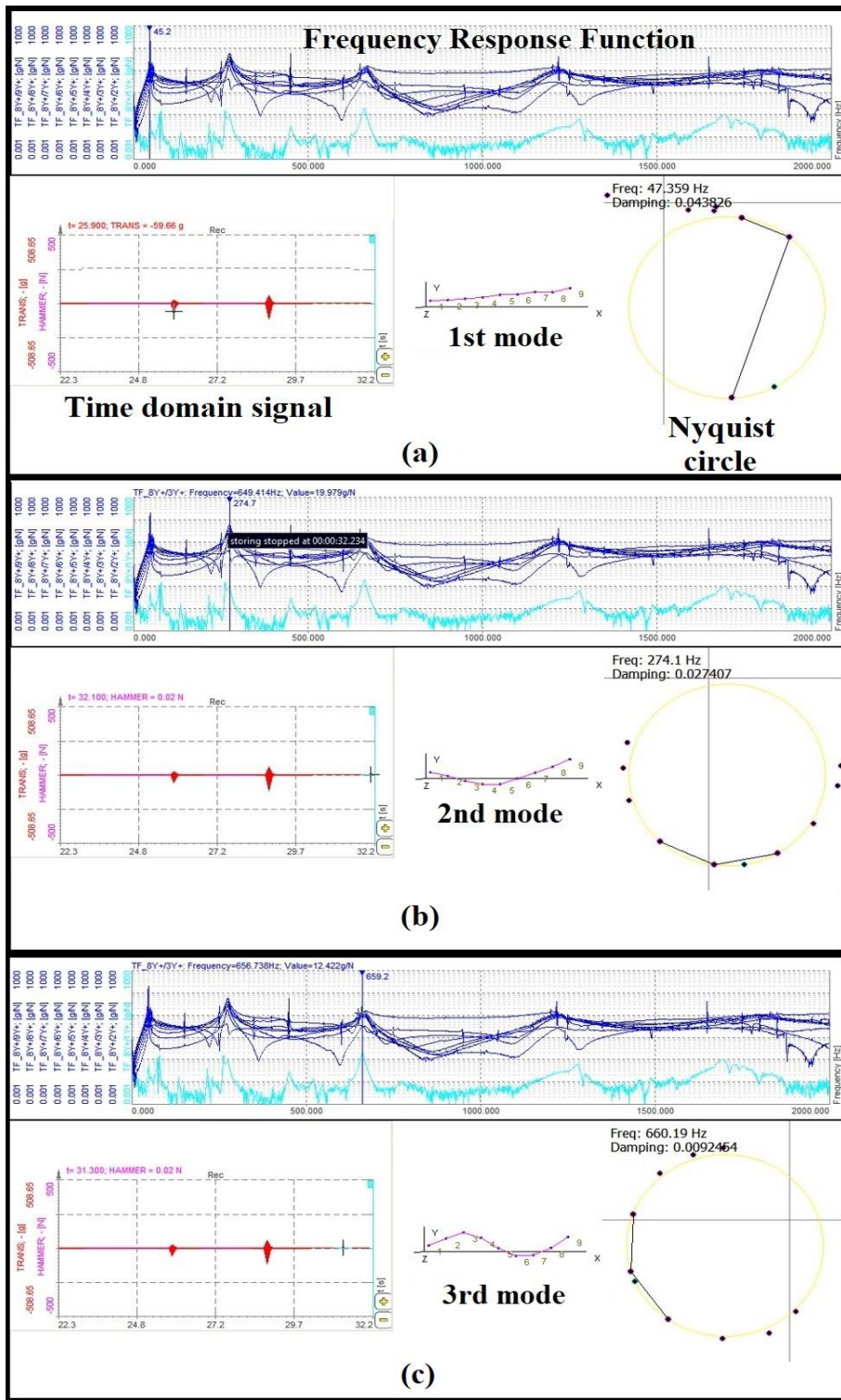free vibration modal analysis using DEWESoft software for the first three modes of B1 MMC-MRF core sandwich beam sample at zero magnetic flux density. The frequency response function curves generated while impacting with impulse hammer helps to determine the resonant frequency of the sandwich beams. The damping ratio was determined based on the circle fit method from the Nyquist circle plot.

The natural frequencies and damping ratios of five different wt% SiC_p reinforced sandwich beams corresponding to the influence of 0, 200, 400, and 600 gauss magnetic flux densities are shown in Table 8.2. The result reveals that the increase in the external applied magnetic field will increase the natural frequency and the damping ratio of the sandwich beams. Hence, from the results obtained, it was observed that the stiffness of the sandwich beams increased with the increase in the applied magnetic field. It is also noticed that the increase in wt% of SiC_p in Al6082 alloy MMCs will also increase the natural frequency of the sandwich beams. The increase in natural frequencies and damping ratio is attributed to two criteria. The first criteria is because of the addition of SiC_p in Al6082 alloy makes a stiff top and bottom layers of the sandwich beam. The second criteria is, because of the effect of the magnetic field, the MRF core becomes stiffer and hence the overall stiffness of the sandwich beam is increased. It is observed that in the first mode, the sandwich beam B1 had higher natural frequencies than the remaining sandwich beams. It is due to the presence of oxides and porosities in the MMC layers may reduce the natural frequencies of the remaining sandwich beam (Umashankar et al. (2009)).

145

Table 8.2 The natural frequencies and damping ratios of the Al6082 alloy MMC-MRF core sandwich beams with the influence of magnetic flux density

Beam No.	Magnetic flux density (gauss)	1st mode		2nd mode		3rd mode	
		Natural freq (Hz)	Damping ratio	Natural freq (Hz)	Damping ratio	Natural freq (Hz)	Damping ratio
B1	0	47.36	0.0438	274.10	0.0274	660.19	0.0092
	200	49.27	0.0537	276.31	0.0418	663.64	0.0167
	400	49.71	0.0644	277.18	0.0539	666.86	0.0322
	600	50.18	0.0767	278.5	0.0585	673.81	0.0379
B2	0	44.83	0.0403	248.04	0.0191	594.87	0.0129
	200	46.17	0.0487	253.14	0.0279	594.94	0.0198
	400	46.36	0.0633	253.45	0.0316	604.38	0.0486
	600	47.43	0.0728	253.30	0.0365	610.5	0.0505
B3	0	46.31	0.0289	255.62	0.0156	622.06	0.0095
	200	47.45	0.0391	256.92	0.0198	631.63	0.0209
	400	47.94	0.0485	257.73	0.0253	643.76	0.0316
	600	48.86	0.0615	259.13	0.0283	645.33	0.0403
B4	0	47.58	0.0184	258.05	0.0141	614.17	0.0068
	200	48.08	0.0282	258.68	0.0161	623.61	0.0137
	400	48.60	0.0355	259.41	0.0197	627.43	0.0214
	600	49.72	0.0444	262.29	0.0231	647.94	0.0283
B5	0	48.16	0.0157	260.13	0.0130	627.43	0.0148
	200	49.17	0.0265	260.58	0.0182	632.34	0.0152
	400	49.64	0.0349	264.16	0.0221	638.91	0.0177
	600	50.09	0.0411	268.03	0.0281	641.09	0.0244

The percentage increase in natural frequencies corresponding to the first, second and third mode of MMC-MRF core sandwich beams at 600 G magnetic flux density is shown in figure 8.4. Considering fundamental first mode for B1, B2, B3, B4 and B5 sandwich beams, 5.95%, 5.79%, 5.50%, 4.49% and 4% increase in natural frequencies were obtained. Hence, it is observed that the increase in SiC_p wt% will decrease the percentage increase in natural frequencies. It happens because the SiC particles act as barriers in the sandwich beams in permitting the magnetic effect to the MRF core. The result reveals that at 600 G magnetic field conditions, the percentage increase in natural frequencies for the B5 MMC-MRF core sandwich beam is lesser compared to the other

samples in first and third mode. Considering the second mode, the B5 MMC-MRF core sandwich beam has a high percentage increase in natural frequencies than other samples.
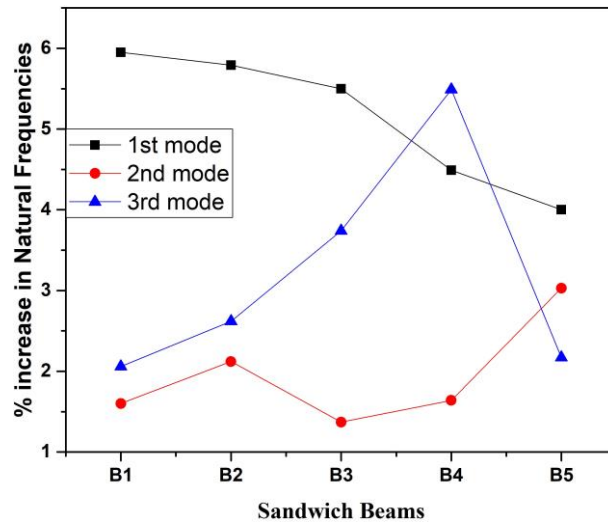
Figure 8.4 Percentage increase in natural frequencies of MMC-MRF core sandwich beams at 600 G magnetic flux density

Based on the analysis, it is observed that the damping ratio of the MMC-MRF core sandwich beam decreased due to the reinforcement of SiC_p. However, the damping ratios of sandwich beams increased with increase in the applied magnetic flux density. The result reveals that B1, B2, B3, B4 and B5 MMC-MRF core sandwich beams have 1.75, 1.8, 2.04, 2.41 and 2.61 times increase in damping ratio in the first mode at 600 G magnetic flux density. Hence, considering the first mode B5 MMC-MRF core sandwich beam have excellent damping properties compared to other sandwich beams. Also, in second and third modes, all the MMC-MRF core sandwich beams had more than 2 times increase in damping ratios at 600 G magnetic flux density.

8.4 FORCED VIBRATION CHARACTERIZATION

The forced vibration test was conducted with electrodynamic base excitation as per the ASTM E756-05 standard. Figure 8.5 shows the experimental forced vibration analysis setup used to determine the excitation frequency amplitude response of the sandwich beams with and without the influence of the magnetic field. The experimental setup consists of 50 kgf electrodynamic shaker, digital switching power amplifier,

function generator, uniaxial accelerometer sensor, force sensor, NI 9234 DAQ and LabVIEW 2017 software. The acceleration response of the sandwich beam was measured using the accelerometer sensor through NI-9234 data acquisition.

1 - LabVIEW software, output Display
2 - NI 9234 DAQ, 3 - Function Generator
4 - Power Amplifier
5 - Accelerometer sensor
6 - Permanent Magnet
7 - Force sensor
8 - Electrodynamic shaker
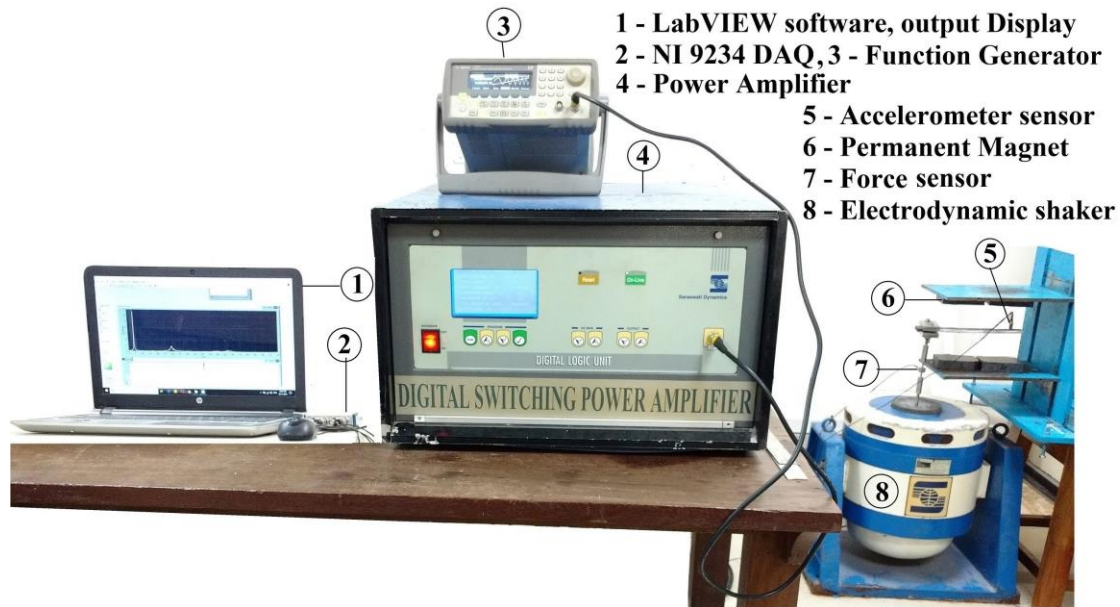
Figure 8.5 Forced vibration analysis experimental setup

The forced vibration analysis of SiC_p reinforced Al6082 MMCs top and bottom layer with middle MRF core sandwich beams are performed by using a harmonic sine sweep base excitation. The amplitude response of the cantilever sandwich beams has been obtained at 25 mm from free end and evaluated over the frequency range of 1–700 Hz for 0 G, 200 G, 400 G and 600 G magnetic flux density conditions. The transverse vibration natural frequencies and acceleration responses of the sandwich beam samples obtained experimentally were analyzed.

The transverse vibration frequency response of sandwich cantilever beam samples are shown in figures 8.6 - 8.10. The experiment results reveal that the natural frequencies increased with an increase in the applied magnetic flux density and the acceleration response amplitudes decreased with an increase in the magnetic flux density. An increase in the magnetic flux density from 0 to 600 gauss yields a significant suppression in the resonant natural frequency amplitudes. Hence, natural frequency peak amplitude reduction control is achieved in MMC-MRF core sandwich beams.

148
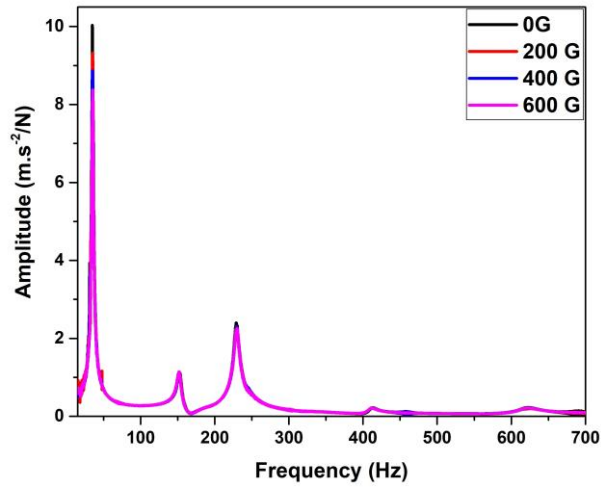
Figure 8.6 FRF curve for MMC-MRF core sandwich beam B1 specimen
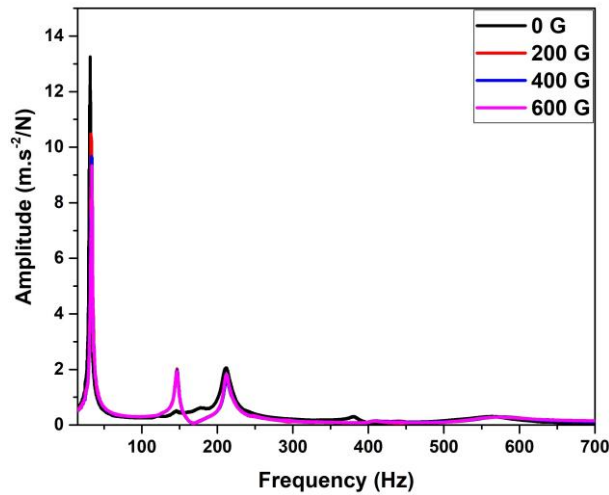
Figure 8.7 FRF curve for MMC-MRF core sandwich beam B2 specimen
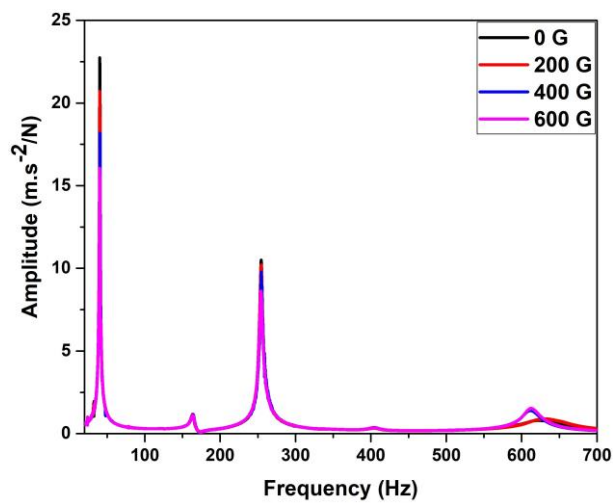
Figure 8.8 FRF curve for MMC-MRF core sandwich beam B3 specimen
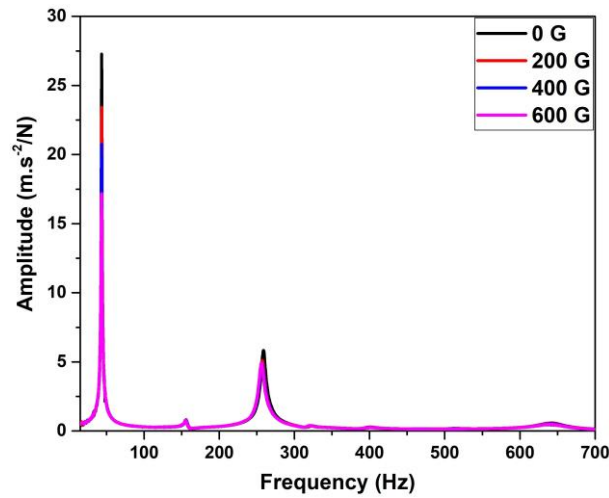
Figure 8.9 FRF curve for MMC-MRF core sandwich beam B4 specimen
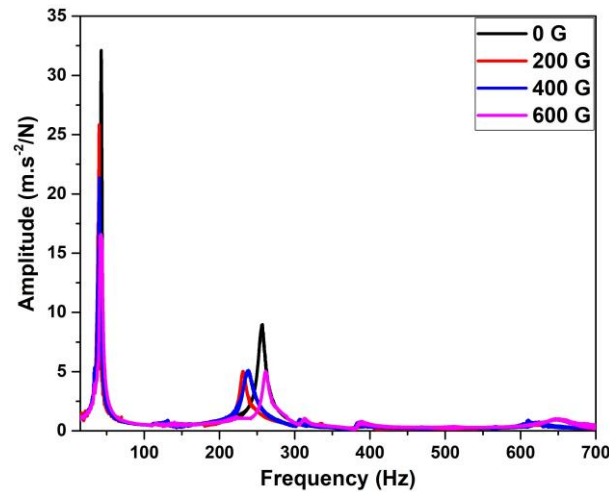
Figure 8.10 FRF curve for MMC-MRF core sandwich beam B5 specimen

The percentage of vibration amplitude suppression for the fundamental first mode excitation under the influence of magnetic flux density for the Al6082 alloy MMC-MRF core sandwich beams is shown in figure 8.11. It is observed that at 0 G, 200 G, 400 G and 600 G, the B5 MMC-MRF core sandwich beam yields a substantial reduction in the peak amplitudes of 0%, 19.55%, 33.40%, and 48.34% respectively. Hence, from the forced vibration analysis the result reveals that vibration amplitude at first resonance natural frequency can be suppressed up to 48.34% for the B5 MMC-MRF core sandwich beam at 600 G magnetic flux density.
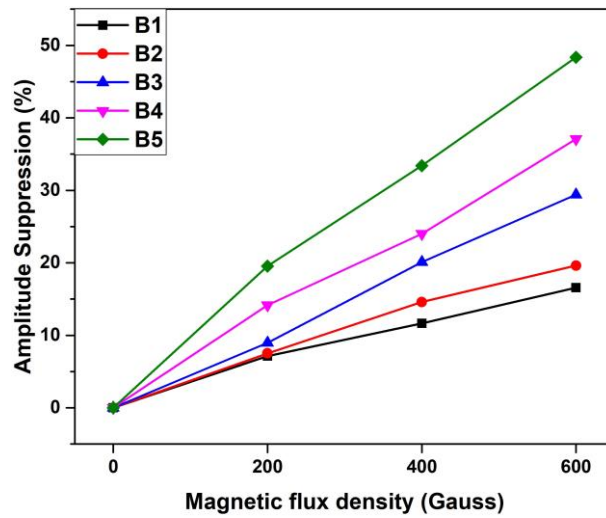
Figure 8.11 Percentage of vibration amplitude suppression of Al6082 alloy MMC-MRF core sandwich beams for the first mode excitation by the influence of magnetic field

8.5 CONCLUSIONS

In this study, an experimental investigation to analyze the dynamic characteristics of novel SiC_p reinforced Al6082 MMC-MRF core sandwich beams is presented. Initially, the different wt% SiC_p reinforced Al6082 MMC samples were fabricated through the stir casting method. Both physical and mechanical characterizations were carried out for MMCs and the beam samples were machined using WEDM. The MRF is prepared with 30% volume CI_p and 70% volume silicone oil.

The free vibration characterization result revealed that the natural frequency and the damping ratio of MMC-MRF core sandwich beams increased with increase in the external applied magnetic flux density. Furthermore, it has also been determined that the increase in wt% of SiC_p reinforced Al6082 MMCs will also increase the natural frequency but decrease the damping ratio of the sandwich beams. Significant increase in natural frequency and damping ratio was observed for all MMC-MRF core sandwich beam samples at 600 G magnetic flux density. From forced vibration characterization it was found that the vibration amplitude can be suppressed up to 48.34% for the B5 MMC-MRF core sandwich beam at 600 G magnetic flux density. The experimental

151

forced vibration result shows that the different wt% SiC_p reinforced Al6082 MMC-MRF core sandwich beams have effective vibration control capabilities. Hence, SiC_p reinforced Al6082 MMC-MRF core sandwich beams can be used as an alternative for conventional solid structures.

8.6 SUMMARY

In this chapter, the dynamic analysis of MMC-MRF core sandwich beams having 0, 5, 10, 15 and 20 wt% SiC_p reinforced Al6082 MMC top and bottom layers sandwich beams with MRF core were experimentally analyzed. The free and forced experimental characterizations are performed with and without the influence of external applied magnetic flux densities. The ability of MMC-MRF core sandwich beams varying their dynamic properties with the influence of magnetic flux densities are analyzed.

CHAPTER 9

CONCLUSIONS AND FUTURE WORK

9.1 CONCLUSIONS

In this research work, the physical, mechanical and dynamic properties of the two-layer, four-layer, six-layered CGRP-PMCs and different wt% SiC_p reinforced Al6082 and Al7075 alloy MMCs are experimentally determined. Further, the vibration suppression capabilities of CGRP-PMC-MRF core sandwich beams and MMC-MRF core sandwich beams were investigated with reference to objectives listed in section 2.8, the foremost contributions from this dissertation research are follows.

9.1.1 Polymer matrix composite

The CGRP-PMC is prepared by hand layup method. The physical, mechanical and dynamic characterization of polyester resin based two-layer, four-layer and six-layered CGRP-PMC materials have been determined. In material characterization, the tensile, flexural, impact, ILSS, fracture toughness properties have been determined. The results have revealed that the four-layered CGRP-PMC material has high impact strength, ILSS and fracture toughness compared to two-layer and six-layered CGRP-PMC material. It is observed that for better mechanical characteristics of CGRP-PMC, proper interaction between matrix and reinforcement is required. Six-layered CGRP-PMC material has the highest UTS and flexural strength than two-layer and four-layered CGRP-PMC. The strain percentage of six-layered CGRP-PMC is less compared to two-layer and four-layered CGRP-PMC. Hence, based on material characterization, the tensile and flexural properties are higher in six-layered CGRP-PMC. The experimental free vibration analysis results revealed that six-layered CGRP-PMC had high natural frequencies than two-layer and four-layered CGRP-PMC. Hence, it is determined that the stiffness of CGRP-PMC increases with an increase in the number of layers of CSM glass fiber reinforcement.

Based on MADM techniques it is found that six-layered CGRP-PMC material has better physical. mechanical and dynamic properties than two-layer and four-layered CGRP-PMC. The rank of samples obtained is similar in all MADM (SAW, WPM, TOPSIS and PROMETHEE) methods.

9.1.2 Metal matrix composite

The Al6082 and Al7075 alloys reinforced with (0, 1, 2, 3, 4, 5, 7.5, 10, 15, 20 wt%) SiC_p reinforcement MMCs were fabricated by stir casting method. The microstructure, physical, mechanical and dynamic properties like density, hardness, impact energy, tensile strength, natural frequency, and damping ratio were determined. The optimum MMCs were determined using MADM techniques. The microstructure analysis revealed the non-homogeneous distribution of SiC_p reinforcement in aluminum alloy MMCs. The density and hardness of MMCs increased with the increase in the addition of SiC_p. The impact energy of MMCs increased with the addition of SiC_p reinforcement and reduced for higher wt% of SiC_p due to the clustering of reinforcement. The tensile strength enhanced up to 10 wt% addition of SiC_p reinforcement in Al6082 alloy MMCs and 15 wt% addition of SiC_p reinforcement in Al7075 alloy MMCs. 15% SiC_p/Al7075 MMCs obtained the maximum tensile strength of 275 MPa. The natural frequency and damping ratio of MMCs improved with the addition of SiC_p reinforcement. By using AHP, TOPSIS and PROMETHEE MADM techniques, 15% SiC_p/Al7075 MMCs was identified as the best MMCs specimen among all other fabricated MMCs considering their physical, mechanical and dynamic properties. Also, by using RSM optimization 13.66% SiC_p/Al7075 MMCs was identified as the optimum MMCs.

9.1.3 Magnetorheological fluid

The MRF is prepared with 30% volume CI_p, 70% volume silicone oil and two grams grease for 100 ml MRF. The microstructure, particle size distribution, magnetization and sedimentation ratio of CI_p were determined. Being 5.27 µm as average particle size, CI_p has a high saturation magnetization of 2.1497 emu and the MRF showed good sedimentation stability where particles settled completely after 28

days. The oscillatory frequency sweep rheological characterization of the MRF with and without the magnetic field was analyzed. The Viscosity and shear stress of MRF increases with increase in magnetic flux density and saturated at 0.63 T. It was found that the complex shear modulus, storage modulus, loss modulus, complex viscosity and shear stress rheological properties of MRF increases with the increase in applied magnetic flux density. Whereas, the loss factor of MRF decreased with the increase in the applied magnetic flux density. Also, the complex viscosity of MRF decreased with increasing oscillating frequency.

9.1.4 CGRP-PMC-MRF core sandwich beams

The semi-active vibration control performance of the CGRP-PMC-MRF core sandwich beams has been experimentally investigated and the following conclusions are made. The experimental free and forced vibration analysis revealed the tunability of the stiffness and damping properties of CGRP-PMC-MRF core sandwich beams. The natural frequencies of the CGRP-PMC-MRF core sandwich beams increased with an increase in the thickness of the top and bottom layers. Whereas, the damping ratio of the CGRP-PMC-MRF core sandwich beams decreased with an increase in the thickness of the top and bottom layers. However, the damping ratio of CGRP-PMC-MRF core sandwich beams increased with an increase in the thickness of the MRF core layer. Based on the free vibration results obtained, it is determined that 2 mm thickness top and bottom layers CGRP-PMC bonded with 5 mm thickness MRF core CGRP-PMC-MRF core sandwich beam has a higher change in natural frequencies and damping ratios than remaining sandwich beams. Furthermore, the forced vibration results revealed that the 2 mm thickness top and bottom layers CGRP-PMC bonded with 5 mm thickness MRF core CGRP-PMC-MRF core sandwich beam has lesser FRF peak amplitude than the remaining CGRP-PMC-MRF core sandwich beams. At 600 G magnetic flux density, 2 mm thickness top and bottom layers CGRP-PMC bonded with 2 mm thickness MRF core CGRP-PMC-MRF core sandwich beam has a higher percentage reduction in peak amplitude of 56.10%. However, the vibration amplitude suppression capabilities of CGRP-PMC-MRF core sandwich beams decreased due to increase in the thickness of the CGRP-PMC top and bottom layers. The CGRP-PMC-MRF core sandwich beam has the ability to control its natural frequency, damping ratio

and vibration amplitude responses and can be effectively used as an alternative for conventional solid structures. The CGRP-PMC-MRF core beams vibration controllable behavior can be used in walls and panels of aerospace and automotive structures.

9.1.5 MMC-MRF core sandwich beams

The dynamic characterization of MMC-MRF core sandwich beams has been experimentally analyzed. The vibration suppression behavior of a different wt% SiC_p reinforced Al6082 alloy MMCs bonded with MRF core sandwich beams were determined.

The free vibration analysis results reveal that the natural frequency and the damping ratio of MMC-MRF core sandwich beams increased by increasing the strength of the external applied magnetic field. Furthermore, it has also been determined that the increase in wt% of SiC_p reinforced Al6082 MMCs will also increase the natural frequency but decrease the damping ratio of the MMC-MRF core sandwich beams. Significant increase in natural frequency and damping ratio was observed for all the MMC-MRF core sandwich beam samples at 600 G magnetic flux density.

The forced vibration analysis results reveal that the transverse vibration frequency amplitude response of the MMC-MRF core sandwich beam could be considerably reduced using the applied magnetic field. Based on the results, the maximum amplitude reduction of 48.34% is achieved for the MRF core with $20\% SiC_p$/Al6082 MMCs sandwich beam at 600 G magnetic flux density. Hence, the MMC-MRF core sandwich beam can be effectively used in the vibration control of adaptive structures.

9.2 SCOPE FOR FUTURE WORK

In the present work, the dynamic analysis of MRF core with CGRP-PMC and different wt% SiC_p reinforced Al6082 MMC face layers sandwich beams were performed experimentally. Further, this study can be extended as given below.

- To investigate the dynamic response of different wt% SiC_p reinforced Al7075 MMC-MRF core sandwich beams.

- To investigate the dynamic response of MRF core sandwich beams by varying the matrix and reinforcement of PMC and MMC face layers.
- To investigate the dynamic characteristics of partially treated MRF core enclosed between PMC and MMC face layers.
- To investigate the dynamic analysis of the MRF core enclosed between the PMC and MMC sandwich beams with the influence of a homogeneous magnetic field using electromagnet.

REFERENCES

Acharya, S., Saini T.R.S. and Kumar, H., (2019). "Determination of optimal magnetorheological fluid particle loading and size for shear mode monotube damper." *J. Braz. Soc. Mech. Sci. Eng.*, 41(392), 1-15.

Ahamed, R., Choi, S.B. and Ferdaus M.M. (2018). "A state of art on magneto-rheological materials and their potential applications." *J. Intell. Mater. Syst. Struct.* 29, 2051–2095.

Ahmed, A., Neely, A.J., Shankar, K., Nolan, P., Moricca, S. and Eddowes, T. (2010). "Synthesis, tensile testing, and microstructural characterization of nanometric SiC particulate-reinforced Al 7075 matrix composites." *Metall. Mater. Trans. A*, *41*(6), 1582-1591.

Aigbodion, V.S. and Hassan, S.B. (2007). "Effects of silicon carbide reinforcement on microstructure and properties of cast Al–Si–Fe/SiC particulate composites." *Mater. Sci. Eng., 447*(1-2), 355-360.

Allien, V., Kumar, H. and Desai, V. (2016). "An investigation on characteristics and free vibration analysis of laminated chopped glass fiber reinforced polyester resin composite." *ARPN J. Eng. Appl. Sci.,* 11(18), 11016-11022.

Allien, V.J., Kumar, H. and Desai, V. (2019). "Dynamic analysis and optimization of SiC reinforced Al6082 and Al7075 MMCs." *Mater. Res. Express*, 6, 056528.

Arifin, A.M.T., Abdullah, S., Rafiquzzaman, M., Zulkifli, R., Wahab, D.A. and Arifin, A.K. (2014). "Investigation of the behaviour of a chopped strand mat/woven roving/foam-Klegecell composite lamination structure during Charpy testing." *Mater. Des.*, 59, 475-485.

Asgari, M. and Kouchakzadeh, M.A. (2016). "Aeroelastic characteristics of magnetorheological fluid sandwich beams in supersonic airflow." *Compos. Struct.,* 143, 93-102.

Ashtiani, M., Hashemabadi, S.H. and Ghaffari, A. (2015). "A review on the magnetorheological fluid preparation and stabilization." *J. Magn. Magn. Mater.,* 374, 716-730.

ASM International. Handbook Committee, and ASM International. Alloy Phase Diagram Committee. (1990). "Metals Handbook: Properties and selection." (Vol. 2). ASM international.

ASTM, E. 23b. (2016). "Standard Test Methods for Notched Bar Impact Testing of Metallic Materials." *ASTM International*, United States.

ASTM. E92-82. (2003). "Standard test methods for Vickers hardness of metallic materials." *ASTM International*, United States.

ASTM. E8/E8M-16a. (2004). "Standard Test Methods for Tension Testing of Metallic Materials." *ASTM International*, United States.

ASTM. E756-05. (2010). "Standard Test Methods for Measuring Vibration-Damping Properties of Materials." *ASTM International*, United States.

ASTM D3039/ D3039M-14. (2014). "Standard Test Method for Tensile Properties of Polymer Matrix Composite Materials." *ASTM International*, United States.

ASTM D790-10. (2010). "Standard Test Methods for Flexural Properties of Unreinforced and Reinforced Plastics and Electrical Insulating Materials." *ASTM International*, United States.

ASTM D5045-99. (2007). "Standard Test Methods for Plane-Strain Fracture Toughness and Strain Energy Release Rate of Plastic Materials." *ASTM International*, United States.

ASTM D2344/D2344M – 13. (2013). "Standard Test Method for Short-Beam Strength of Polymer Matrix Composite Materials and Their Laminates." *ASTM International*, United States.

Ates, H. (2007). "Prediction of gas metal arc welding parameters based on artificial neural networks." *Mater. Des.*, 28(7), 2015-2023.

Azdast, T., Doniavi, P., Esmaili, A. (2018). "Selecting optimal molding and material conditions of reinforced polymeric nanocomposites with MWCNT using a multi criteria decision making model." *Int. Polym. Proc.,* 33, 688-694.

Baltacıoglu, A.K., Akgoz, B. and Civalek, O. (2010). "Nonlinear static response of laminated composite plates by discrete singular convolution method." *Compos. Struct.,* 93, 153–161.

Baradeswaran, A. and Perumal, A.E. (2014). "Wear and mechanical characteristics of Al 7075/graphite composites." *Composites Part B: Eng.*, 56, 472-476.

Bhowmik, C., Gangwar, S., Bhowmik, S. and Ray, A. (2018). "Optimum selection of energy-efficient material: A MCDM-based distance approach." *Soft computing applications*, Springer, Singapore, 59-79.

Bhuyan, R.K., Routara, B.C. and Parida, A.K. (2015). "An approach for optimization the process parameter by using TOPSIS Method of Al–24% SiC metal matrix composite during EDM." *Mater. Today: Proc., 2*(4-5), 3116-3124.

Birman, V. and Kardomateas, G.A. (2018). Review of current trends in research and applications of sandwich structures. *Composites Part B: Engineering*, 142, 221-240.

Brans, J.P. and Vincke, P. (1985). "Note—A Preference Ranking Organisation Method: (The PROMETHEE Method for Multiple Criteria Decision-Making)." *Manage. Sci.,* 31(6), 647-656.

Brans, J.P., Vincke, P. and Mareschal, B. (1986). "How to select and how to rank projects: The PROMETHEE method." *Eur. J. Oper. Res.,* 24(2), 228-238.

Butt, J., Hewavidana, Y., Mohaghegh, V., Sadeghi-Esfahlani, S. and Shirvani, H. (2019). "Hybrid manufacturing and experimental testing of glass fiber enhanced thermoplastic composites." *J. Manuf. Mater. Process.,* 3(4), 1-16.

Çalışkan, H. (2013). "Selection of boron based tribological hard coatings using multi-criteria." Mater. Des., 50, 742–749.

Çalışkan, H., Kurşuncu, B., Kurbanoğlu, C. and Güven, Ş.Y. (2013). "Material selection for the tool holder working under hard milling conditions using different multi criteria decision making methods." *Mater. Des.*, 45, 473-479.

Carfagni, M., Lenzi, E. and Pierini, M. (1998). "The loss factor as a measure of mechanical damping." *SPIE Proceedings Series*, 1, 580–584.

Carlson, J.D. and Jolly, M.R. (2000). "MR fluid, foam and elastomer devices." *Mechatronics*, 10(4), 555-569.

Carlson, J. D., Catanzarite, D.M. and St. Clair, K.A. (1996). "Commercial magneto-rheological fluid devices." *Int. J. Mod. Phys. B*, 10(23n24), 2857-2865.

Chandradass, J., Kumar, M.R. and Velmurugan, R. (2007). 'Effect of nanoclay addition on vibration properties of glass fibre reinforced vinyl ester composites." *Mater. Lett.,* 61(22), 4385-4388.

Chen, X. H. and Yan, H. (2018). "Fabrication of Al7075–Al_2O_3np-based metal matrix composites with a high solid fraction for thixoforming." *J. Mater. Res.,* 33(24), 4349-4361.

Cheng, H., Zhang, X., Liu, G., Ma, W. and Wereley, N.M. (2016). "Measuring the sedimentation rate in a magnetorheological fluid column via thermal conductivity monitoring." *Smart mat. Struct.*, 25(5), 055007.

Cheng, H., Wang, M., Liu, C. and Wereley, N.M. (2018). "Improving sedimentation stability of magnetorheological fluids using an organic molecular particle coating." *Smart mat. Struct.*, 27(7), 075030.

Choi, Y., Sprecher, A.F. and Conrad, H. (1990). "Vibration characteristics of a composite beam containing an electrorheological fluid." *J. Intel. Mater. Syst. Str.,* 1(1): 91-104.

Chuaqui, T.R.C., Roque, C.M.C. and Ribeiro, P. (2018). "Active vibration control of piezoelectric smart beams with radial basis function generated finite difference collocation method." *J. Intel. Mater. Sys. Struct.*, 29, 2728–2743.

Civalek, O. (2004). "Application of differential quadrature (DQ) and harmonic differential quadrature (HDQ) for buckling analysis of thin isotropic plates and elastic columns." *Eng. Struct.*, 26, 171–186.

Dağdeviren, M. (2008). "Decision making in equipment selection: an integrated approach with AHP and PROMETHEE." *J. Intell. Manuf.*, *19*(4), 397-406.

Devaneyan, S.P., Ganesh, R. and Senthilvelan, T. (2017). "On the mechanical properties of hybrid aluminium 7075 matrix composite material reinforced with SiC and TiC produced by powder metallurgy method." *Indian J. Mater. Sci.*, 2017(3067257), 1-6.

Du, Y., Zhang, P., Wang, Y., Zhang, J., Yao, S. and Li, C. (2013). "The uniform distribution of SiC particles in an a356-sicp composite produced by the tilt-blade mechanical stirring." *Acta Metall. Sin. (Engl. Lett.)*, 26, 69–74.

Ebrahimi, F. and Farazmandnia, N. (2017). "Thermo-mechanical vibration analysis of sandwich beams with functionally graded carbon nanotube-reinforced composite face sheets based on a higher-order shear deformation beam theory." *Mech. Adv. Mater. Struct.* 24, 820–829.

El-Sabbagh, A., Soliman, M., Taha, M. and Palkowski, H. (2012). Hot rolling behaviour of stir-cast Al 6061 and Al 6082 alloys–SiC fine particulates reinforced composites. *J. Mater. Process. Tech.*, 212(2), 497-508.

El-Tayeb, N.S.M., Yousif, B.F. and Yap, T.C. (2006). Tribological studies of polyester reinforced with CSM 450-R-glass fiber sliding against smooth stainless steel counter face. *Wear*, 261(3-4), 443-452.

El-Tayeb, N.S.M. and Yousif, B.F. (2007). "Evaluation of glass fiber reinforced polyester composite for multi-pass abrasive wear applications." *Wear*, 262(9-10), 1140-1151.

Ezatpour, H.R., Parizi, M.T., Sajjadi, S.A., Ebrahimi, G.R. and Chaichi, A. (2016). "Microstructure, mechanical analysis and optimal selection of 7075 aluminum alloy based composite reinforced with alumina nanoparticles." *Mater. Chem. Phys.,* 178, 119-127.

Fan, Z., Santare, M.H., Advani, S.G. (2008). "Interlaminar shear strength of glass fiber reinforced epoxy composites enhanced with multi-walled carbon nanotubes." *Compos. Pt. A,* 39, 540–554.

Feiz, A., and Khosravi, H. (2019). "Multiscale composites based on a nanoclay-enhanced matrix and E-glass chopped strand mat." *J. Reinf. Plast. Compos.*, 38(13), 591-600.

Franz, T., Nurick, G.N. and Perry, M.J. (2002). "Experimental investigation into the response of chopped-strand mat glass fibre laminates to blast loading." *Int. J. impact Eng.*, 27(6), 639-667.

Ganapathi, M., Patel, B.P., Boisse, P. and Polit, O. (1999). "Flexural loss factors of sandwich and laminated composite beams using linear and nonlinear dynamic analysis." *Compos. Part, B, Eng.,* 30(3), 245-256.

Genc, S. and Phule, P.P. (2002). "Rheological properties of magnetorheological fluids." *Smart Mater. Struct.*, 11, 140-146.

Gurubasavaraju, T.M., Kumar, H. and Arun, M. (2017). "Evaluation of optimal parameters of MR fluids for damper application using particle swarm and response surface optimisation." *J. Braz. Soc. Mech. Sci. Eng.,* 39, 3683-3694.

Han, Y. and Elliott, J. (2007). "Molecular dynamics simulations of the elastic properties of polymer/carbon nanotube composites." *Comp. Mater. Sci.,* 39, 315-323.

Hasan, S.T., Beynon, J.H. and Faulkner, R.G. (2004). "Role of segregation and precipitates on interfacial strengthening mechanisms in SiC reinforced aluminium alloy when subjected to thermomechanical processing." *J. Mater. Process. Tech.*, 153, 758-764.

Hashim, J., Looney, L. and Hashmi, M.S.J. (1999). "Metal matrix composites: production by the stir casting method." *J. Mater. Process. Technol.,* 92, 1-7.

Heckadka, S.S., Nayak, S.Y., Narang, K. and Pant, K.V. (2015). "Chopped strand/plain weave E-glass as reinforcement in vacuum bagged epoxy composites." *J. Mater.*, 957043, 1-7.

Howson, W.P. and Zare, A. (2005). "Exact dynamic stiffness matrix for flexural vibration of three-layered sandwich beams." *J. Sound Vib.*, 282, 753–767.

Hu, G., Guo, M., Li, W., Du, H. and Alici, G. (2011). "Experimental investigation of the vibration characteristics of a magnetorheological elastomer sandwich beam under non-homogeneous small magnetic fields." *Smart mat. Struct.*, 20(12), 127001.

Hwang, C.L. and Yoon, K. (1981). "Methods for multiple attribute decision making." *Springer*, Berlin, Heidelberg.

Inegbenebor, A.O., Bolu, C.A., Babalola, P.O., Inegbenebor, A.I. and Fayomi, O.S.I. (2016). "Influence of the grit size of silicon carbide particles on the mechanical and electrical properties of stir casting aluminum matrix composite material." *Silicon*, 8 573–578.

Inegbenebor, A.O., Bolu, C.A., Babalola, P.O., Inegbenebor, A.I. and Fayomi, O.S.I. (2018). "Aluminum Silicon Carbide Particulate Metal Matrix Composite Development Via Stir Casting Processing." *Silicon*, 10, 343-347.

Jahan, A., Ismail, M.Y., Sapuan, S.M. and Mustapha, F. (2010). "Material screening and choosing methods - A review." *Mater. Des.,* 31, 696–705.

Jolly, M.R., Bender, J.W. and Carlson, J.D. (1999). "Properties and applications of commercial magnetorheological fluids." *J. Intell. Mater. Syst. Struct.,* 10(1), 5-13.

Jolly, M.R., Carlson, J.D. and Munoz, B.C. (1996). "A model of the behaviour of magnetorheological materials." *Smart Mater. Struct.,* 5(5), 607.

Japka, J. E. (1988). "Microstructure and properties of carbonyl iron powder." *J. Metals*, *40*(8), 18-21.

Kafi, A.A., Abedin, M.Z., Beg, M.D.H., Pickering, K.L. and Khan M.A. (2006). "Study on the mechanical properties of jute/glass fiber-reinforced unsaturated polyester hybrid composites: effect of surface modification by ultraviolet radiation." *J. Reinf. Plast. Compos.*, 25(6), 575-588.

Kaliszewski, I. and Podkopaev, D. (2016). "Simple additive weighting—A metamodel for multiple criteria decision analysis methods." *Expert Syst. Appl.,* 54, 155-161.

Khorshidi, R., Hassani, A., Rauof, A.H. and Emamy, M. (2012). "Selection of an optimal refinement condition to achieve maximum tensile properties of Al–15% Mg2Si composite based on TOPSIS method." *Mater. Des.,* 46, 442-450.

Khorshidi, R. and Hassani, A. (2013). "Comparative analysis between TOPSIS and PSI methods of materials selection to achieve a desirable combination of strength and workability in Al/SiC composite." *Mater. Des.*, 52, 999-1010.

Kluczek, A. and Gladysz, B. (2015). "Analytical hierarchy process/technique for order preference by similarity to ideal solution-based approach to the generation of environmental improvement options for painting process e Results from an industrial case study." *J. Clean. Prod.,* 101, 360-367.

Kozlowska, J., Boczkowska, A., Czulak, A., Przybyszewski, B., Holeczek, K., Stanik, R. and Gude, M. (2016). "Novel MRE/CFRP sandwich structures for adaptive vibration control." *Smart Mater. Struct.*, 25(3), 035025.

Kumar, G.V., Rao, C.S.P., Selvaraj, N. and Bhagyashekar, M.S. (2010). "Studies on Al6061-SiC and Al7075-Al$_2$O$_3$ metal matrix composites." *J. Miner. Met. Mater. Eng.*, 9(1), 43-55.

Kumar, K.K.A., Viswanath, A., Rajan, T.P.D., Pillai, U.T.S. and Pai, B.C. (2014). "Physical, mechanical, and tribological attributes of stir-cast AZ91/SiC$_p$ composite." *Acta Metall. Sin. (Engl. Lett.),* 27, 295–305.

Kumar, K.K., Krishna, Y. and Bangarubabu, P. (2015). "Damping in beams using viscoelastic layers." *Proc IMechE, Proc. Inst. Mech. Eng. Pt. L J. Mater. Des. Appl.,* 229(2), 117-125.

Kumar, K.K., Krishna, Y. and Bangarubabu, P. (2015). "Estimation of loss factors of a constrained layer plate using viscoelastic layer." *Proc. Inst. Mech. Eng. Pt. L J. Mater. Des. Appl.,* 229(6), 481-492.

Kumar, R. and Chauhan, S. (2015). "Study on surface roughness measurement for turning of Al 7075/10/SiC$_p$ and Al 7075 hybrid composites by using response surface methodology (RSM) and artificial neural networking (ANN)." *Measurement*, 65, 166-180.

Kumbhar, B.K., Patil, S.R. and Sawant, S.M. (2015). "Synthesis and characterization of magneto-rheological (MR) fluids for MR brake application." *Eng. Sci. Technol. Int. J.*, 18(3), 432-438.

Lara-Prieto, V., Parkin, R., Jackson, M., Silberschmidt, V. and Zbigniew, K. (2009). "Vibration characteristics of MR cantilever sandwich beams: experimental study." *Smart Mater. Struct.*, 19(1), 015005.

Li, H., Li, H. and Tzou, H. (2015). "Frequency control of beams and cylindrical shells with light-activated shape memory polymers." *J. Vib. Acoust.,* 137(1), 011006.

Li, W.H., Chen, G. and Yeo, S.H. (1999). "Viscoelastic properties of MR fluids." *Smart Mater. Struct.*, 8(4), 460.

Manjunath, G.K., Kumar, P.G.V. and Bhat, U.K. (2017). "Tensile properties and tensile fracture characteristics of cast al–zn–mg alloys processed by equal channel angular pressing." *Trans. Indian Inst. Met.* 70, 833–842.

Mangera, T., Kienhöfer, F., Carlson, K.J., Conning, M., Brown, A. and Govender, G. (2018). "Optimal material selection for the construction of a paediatric prosthetic knee." *Proc. Inst. Mech. Eng. Pt. L J. Mater. Des. Appl.,* 232, 137–147.

Manoharan, R., Vasudevan, R. and Jeevanantham, A.K. (2014). "Dynamic characterization of a laminated composite magnetorheological fluid sandwich plate." *Smart Mater. Struct.*, 23(2), 025022.

Mirzaei, M. and Kiani, Y. (2016). "Nonlinear free vibration of temperature-dependent sandwich beams with carbon nanotube-reinforced face sheets." *Acta Mech.*, 227, 1869-1884.

Mobasherpour, I., Tofigh, A. A. and Ebrahimi, M. (2013). Effect of nano-size Al2O3 reinforcement on the mechanical behavior of synthesis 7075 aluminum alloy composites by mechanical alloying. *Mater. chem. phys.*, 138(2-3), 535-541.

Modrea, A., Teodorescu. F. and Rosu, D. (2015). "Tensile tests on four layers CSM600 glass fibers-reinforced Polylite 440-M888 polyester resin." *Procedia Technology*. 19, 284-290.

Moreno, M.C.S. and Vicente, J.L.M (2015). "In- plane shear failure properties of a chopped glass-reinforced polyester by means of traction–compression biaxial testing." *Compos. Struct.,* 122: 440–444.

Mousavi-Nasab, S.H. and Sotoudeh-Anvari, A. (2017). "A comprehensive MCDM-based approach using TOPSIS, COPRAS and DEA as an auxiliary tool for material selection problems." *Mater. Des.,* 121, 237-253.

Myriounis, D. P., Hasan, S. T. and Matikas, T. E. (2010). "Predicting Interfacial Strengthening Behaviour of Particulate-Reinforced MMC—A Micro-mechanistic Approach." Compos. Interfaces, 17(4), 347-355.

Naji, J., Zabihollah, A. and Behzad, M. (2018). "Vibration characteristics of laminated composite beams with magnetorheological layer using layer wise theory." *Mech. Adv. Mater. Struct.,* 25, 202-211.

Nayak, B., Dwivedy, S.K. and Murthy, K.S.R.K. (2011). "Dynamic analysis of magnetorheological elastomer-based sandwich beam with conductive skins under various boundary conditions." *J. Sound. Vib.*, 330, 1837-1859.

Nayak, B., Dwivedy, S.K. and Murthy, K.S.R.K. (2013). Dynamic stability of magnetorheological elastomer based adaptive sandwich beam with conductive skins using FEM and the harmonic balance method. *Int. J. Mech. Sci.,* 77, 205–216.

Okafor, A. C., Singh, N., Enemuoh, U. E. and Rao, S. V. (2005). Design, analysis and performance of adhesively bonded composite patch repair of cracked aluminum aircraft panels. *Compos. Struct.*, 71(2), 258-270.)

Ozden, S., Ekici, R. and Nair, F. (2007). "Investigation of impact behaviour of aluminium based SiC particle reinforced metal–matrix composites." *Compos. Pt. A. Appl. Sci. Manuf.,* 38(2), 484-494.

Prakash, C. and Barua, M.K. (2015). "Integration of AHP-TOPSIS method for prioritizing the solutions of reverse logistics adoption to overcome its barriers under fuzzy environment." *J. Manuf. Syst.,* 37, 599-615.

Prasad, M.S.S., Venkatesha, C.S. and Jayaraju, T. (2011). Experimental methods of determining fracture toughness of fiber reinforced polymer composites under various loading conditions. *J. Miner. Mater. Character. Eng.*, 10(13), 1263-1275.

Premalatha, S.E., Chokkalingam, R. and Mahendran, M. (2012). "Magneto mechanical properties of iron based MR fluids." *American J. Polymer Sci.*, 2(4), 50-55.

Rabinow, J. (1948). "The magnetic fluid clutch." *Electrical Eng.*, 67(12), 1167-1167.

Rajamohan, V. and Ramamoorthy, M. (2012). "Dynamic characterization of non-homogeneous magnetorheological fluids based multi-layer beam." *Appl. Mech. Mater.,* 110, 105-112.

Rajamohan, V., Rakheja, S. and Sedaghati, R. (2010). "Vibration analysis of a partially treated multi-layer beam with magnetorheological fluid." *J. Sound Vib.*, *329*(17), 3451-3469.

Rajamohan, V., Sedaghati, R. and Rakheja, S. (2009). "Vibration analysis of a multi-layer beam containing magnetorheological fluid." *Smart Mater. Struct.*, 19(1), 015013.

Rajamohan, V., Sedaghati, R. and Rakheja, S. (2010). "Optimum design of a multilayer beam partially treated with magnetorheological fluid." *Smart Mater. Struct.*, 19(6), 065002.

Rajamohan, V., Sedaghati, R. and Rakheja, S. (2011). "Optimal vibration control of beams with total and partial MR-fluid treatments." *Smart Mater. Struct.*, 20(11), 115016.

Rajamohan, V., Sundararaman, V. and Govindarajan, B. (2013). "Finite element vibration analysis of a magnetorheological fluid sandwich beam." *Procedia Eng.*, 64, 603-612.

Rajesh, M. and Pitchaimani, J. (2016). "Dynamic mechanical analysis and free vibration behavior of intra-ply woven natural fiber hybrid polymer composite." *J. Reinf. Plast. Compos.,* 35(3), 228-242.

Rajini, N., Jappes, J.W., Rajakarunakaran, S. and Jeyaraj, P. (2012). "Mechanical and free vibration properties of montmorillonite clay dispersed with naturally woven coconut sheath composite." *J. Reinf. Plast. Compos.,* 31(20), 1364-1376.

Ramesh, M., Palanikumar, K. and Reddy, K.H. (2013). "Mechanical property evaluation of sisal–jute–glass fiber reinforced polyester composites." *Compos. Part B: Eng.,* 48, 1-9.

Ramji, M., Srilakshmi, R, and Prakash, M.B. (2013). Towards optimization of patch shape on the performance of bonded composite repair using FEM. *Compos. Part B: Eng.,* 45(1), 710-720.

Rao, R.V. (2006). "Machinability evaluation of work materials using a combined multiple attribute decision-making method." *Int. J. Adv. Manuf. Technol.*, 28(3-4), 221-227.

Rao, R.V. (2007). "Decision making in the manufacturing environment: using graph theory and fuzzy multiple attribute decision making methods." *Springer Science and Business Media*. Springer-Verlag, London.

Rao, R.V. (2008). "A decision making methodology for material selection using an improved compromise ranking method." *Mater. Des.,* 29(10), 1949-1954.

Rao, R.V. and Patel, B.K. (2010). "A subjective and objective integrated multiple attribute decision making method for material selection." *Mater. Des.,* 31(10), 4738-4747.

Rao, R.V. and Patel, B.K. (2010). "Decision making in the manufacturing environment using an improved PROMETHEE method" *Int. J. Prod. Res.* 48, 4665-4682.

Romaszko, M. (2013). "Free vibration control of a cantilever MR fluid based sandwich beam." *In Proceedings of the 14th International Carpathian Control Conference (ICCC),* Rytro, Poland, 311-314.

Saaty, T.L. (1980). "The analytic hierarchy process: planning, priority setting, resources allocation." *McGraw*, New York, 281.

Saaty, T.L. (1990). "How to Make a Decision: The Analytic Hierarchy Process." *Eur. J. Oper. Res.,* 48, 9-26.

Saadatmand, M. and Mohandesi, J.A. (2015) "Optimization of mechanical and wear properties of functionally graded Al6061/SiC nanocomposites produced by friction stir processing (FSP)." *Acta Metall. Sin. (Engl. Lett.),* 28, 584-590.

Sajjadi, S.A., Ezatpour, H.R. and Parizi M.T. (2012). "Comparison of microstructure and mechanical properties of A356 aluminum alloy/Al$_2$O$_3$ composites fabricated by stir and compo-casting processes." *Mater. Des.,* 34, 106-111.

Sapiński, B. and Snamina, J. (2009). "Modeling of an adaptive beam with MR fluid." *In Solid State Phenomena,* 147, 831-838.

Sapiński, B., Snamina, J. and Romaszko, M. (2010). "Identification of model parameters of a sandwich beam incorporating magnetorheological fluid." *Vib. Phys. Syst.*, 24, 349-354.

Shah, S. A. and Hasan, S. T. (2015). "An empirical method of calculating interfacial strength in a second phase reinforced alloy." *Advances Mater. Process. Tech.,* 1(3-4), 316-326.

Shanian, A. and Savadogo, O. (2006). "TOPSIS multiple-criteria decision support analysis for material selection of metallic bipolar plates for polymer electrolyte fuel cell." *J. Power Sources*, 159(2), 1095-1104.

Sharma, P., Sharma, S. and Khanduja, D. (2015). "A study on microstructure of aluminium matrix composites." *J. Asian Ceram. Soc.*, 3(3), 240-244.

Sharma, P., Sharma, S. and Khanduja, D. (2015). "Production and some properties of Si3N4 reinforced aluminium alloy composites." *J. Asian Ceram. Soc.*, 3(3), 352-359.

Shin, S.E. and Bae, D.H. (2015). "Deformation behavior of aluminum alloy matrix composites reinforced with few-layer graphene." *Composites Part A*, 78, 42-47.

Shokrieh, M.M., Saeedi, A., Chitsazzadeh. M. (2014). "Evaluating the effects of multi-walled carbon nanotubes on the mechanical properties of chopped strand mat polyester composites." *Mater. Des.,* 56, 274-279.

Spaggiari, A., Castagnetti, D., Golinelli, N., Dragoni, E. and Mammano, G.S. (2019). "Smart materials: properties, design and mechatronic applications." *Proc. Inst. Mech. Eng. Pt. L J. Mater. Des. Appl.,* 233(4): 734-762.

Talebitooti, M. and Fadaee, M. (2019). "Effects of carbon nanotube reinforcements on vibration suppression of magnetorheological fluid sandwich beam." *J. Intell. Mater. Syst. Str.,* 30(7), 1053-1069.

Thimmarayan, R. and Thanigaiyarasu, G. (2010). "Effect of particle size, forging and ageing on the mechanical fatigue characteristics of Al6082/SiC$_p$ metal matrix composites." *Int. J. Adv. Manuf. Tech.*, *48*(5-8), 625-632.

Umashankar, K.S., Abhinav, A., Gangadharan, K.V. and Vijay, D. (2009). "Damping behaviour of cast and sintered aluminium." *ARPN J. Eng. Appl. Sci.,* 4(6), 66-71.

Vishwakarma, D.K., Kumar, N. and Padap, A.K. (2017). "Modelling and optimization of aging parameters for thermal properties of Al 6082 alloy using response surface methodology." *Mater. Res. Express.* 4, 046502.

Vo-Duy, T., Ho-Huu, V. and Nguyen-Thoi, T. (2018). "Free vibration analysis of laminated FG-CNT reinforced composite beams using finite element method." *Front. Struct. Civ. Eng*., 13(2), 324-336.

Wang, J. and Meng, G. (2001). "Magnetorheological fluid devices: principles, characteristics and applications in mechanical engineering." *Proc. Inst. Mech. Eng. Pt. L J. Mater. Des. Appl.,* 215, 165-174.

Wang, P., Zhu, Z. and Wang, Y. (2016). "A novel hybrid MCDM model combining the SAW, TOPSIS and GRA methods based on experimental design." *Inf. Sci.,* 345, 27-45.

Węgrzynowski, M. (2014). 'Magnetorheological damper control in an energy-harvesting vibration reduction system." *Proc., 15th Int. Carpathian Control Conference (ICCC),* Velke Karlovice, Poland, 679-683.

Wei, K., Meng, G. and Zhou, S. (2007). "Vibration suppression of rotating flexible beams using ER fluids: experimental work." *Proc., 10th Int. Conference, Electrorheological Fluids and Magnetorheological Suspensions*, Lake Tahoe, USA, 584-590.

Wei, M., Sun, L. and Hu, G. (2017). "Dynamic properties of an axially moving sandwich beam with magnetorheological fluid core." *Adv. Mech. Eng.,* 9(2), 1-9.

Wu, H., Kitipornchai, S. and Yang, J. (2015). "Free vibration and buckling analysis of sandwich beams with functionally graded carbon nanotube-reinforced composite face sheets." *Int. J. Struct. Stab. Dy.,* 15, 1540011.

Xue, Y., Jiang, B., Bourgeois, L., Dai, P., Mitome, M., Zhang, C., ... and Tsuchiya, K. (2015). "Aluminum matrix composites reinforced with multi-walled boron nitride nanotubes fabricated by a high-pressure torsion technique." *Mater. Des.*, 88, 451-460.

Yaghobizadeh, O., Baharvandi, H.R., Ahmadi, A.R. and Aghaei, E. (2018). "Development of the Properties of Al/SiC Nano-Composite Fabricated by Stir Cast Method by Means of Coating SiC Particles with Al." *Silicon,* 10, 643-649.

Yalcintas, M. and Coulter, J.P. (1995). "Electrorheological material based adaptive beams subjected to various boundary conditions." *J. Intell. Mater. Syst. Struct.*, 6(5), 700-717.

Yalcintas, M. and Dai, H. (2003). "Vibration suppression capabilities of magnetorheological materials based adaptive structures." *Smart Mater. Struct.*, 13(1), 1-11.

Yazdani, M. and Payam, A.F. (2015). "A comparative study on material selection of microelectromechanical systems electrostatic actuators using Ashby, VIKOR and TOPSIS," *Mater. Des.*, 65, 328-334.

Yeh, Z.F. and Shih, Y.S. (2006). "Dynamic stability of a sandwich beam with magnetorheological core." *Mech. Based Des. Struc.* 34, 181-200.

Yeh, J.Y., Chen, L.W. and Wang, C.C. (2004). "Dynamic stability of a sandwich beam with a constrained layer and electrorheological fluid core." *Compos. Struct.*, 64(1), 47-54.

Zafarani, H.R., Hassani, A. and Bagherpour, E. (2014). "Achieving a desirable combination of strength and workability in Al/SiC composites by AHP selection method." *J. Alloys Compd.*, 589, 295-300.

PUBLICATIONS

INTERNATIONAL JOURNALS

1. Vipin Allien J, Hemantha Kumar and Vijay Desai "Dynamic analysis and optimization of SiC reinforced Al6082 and Al7075 MMCs" Materials Research Express, Vol. 6, No. 056528, pp. 1-20. January 2019. Publisher: IOP Publishing, https://doi.org/10.1088/2053-1591/ab038e. (SCIE Index, Impact factor: 1.929).

2. Vipin Allien J, Hemantha Kumar and Vijay Desai "Semi-active vibration control of SiC reinforced Al6082 MMC sandwich beam with magnetorheological fluid core" Journal of Materials: Design and Applications, pp. 1-17. Publisher: SAGE, DOI: 10.1177/1464420719890374. November 2019. (SCIE Index, Impact factor: 2.014).

3. Vipin Allien J, Hemantha Kumar and Vijay Desai "Semi-active vibration control of MRF core PMC cantilever sandwich beams: Experimental study" Journal of Materials: Design and Applications, pp. 1-12. January 2020. Publisher: SAGE, DOI: 10.1177/1464420720903078. (SCIE Index, Impact factor: 2.014).

4. Vipin Allien, Hemantha Kumar and Vijay Desai "Free vibration analysis and selection of composite for high strength and stiffness using multi attribute decision making" International Journal of Materials Research, pp. 1-8. February 2020. Publisher: HANSER Publications, https://doi.org/10.3139/146.111879. (SCI Index, Impact factor: 0.653).

5. Vipin Allien, Hemantha Kumar and Vijay Desai "An investigation on characteristics and free vibration analysis of laminated chopped glass fiber reinforced polyester resin composite" Journal of Engineering and Applied Sciences, Vol. 11, No. 18, pp. 11016-11022, Publisher: Asian Research Publishing Network, September 2016. (Scopus Index).

INTERNATIONAL CONFERENCE

1. Vipin Allien J, Hemantha Kumar and Vijay Desai "Semi-active vibration control of partially treated magnetorheological fluid sandwich composite beams" 13th International Conference on Vibration Problems (ICOVP-2017), IIT Guwahati, 29 November - 2 December 2017.

BIODATA

Name   :   VIPIN ALLIEN J

Date of Birth   :   02-07-1989

Mobile No.   :   +91 9164714432, +91 9865234071

Email   :   vipinallien@gmail.com

Qualification   :   B.E. (Mechanical Engg.), M.E. (Engineering Design)

Journal Publications   :   5

No. of Conference Publications :   1